CFD Modelling Of Wind Flow Over Complex And Rough Terrain.

by

John Walshe

A Doctoral Thesis

Submitted in partial fulfilment of the requirements

for the award of

Doctor of Philosophy of Loughborough University

2003

CFD Modelling of Wind Flow Over Complex and Rough Terrain.

John Walshe, 2003

Abstract:

A model has been developed using the general-purpose Navier-Stokes solver CFX4 to simulate Atmospheric Boundary Layer flow over complex terrain. This model has been validated against the measured data from the Askervein Hill experiment, and has been shown to perform well. The CFD model is also compared to the WAsP linear model of wind flow over topography, and a significant improvement is noted for flow over complex topography. Boundary conditions, gridding issues and sensitivity to other solver parameters have all been investigated.

An advanced roughness model has been developed to simulate flow over forest canopies, using a resistive body force within the canopy volume. The model is validated against measured data for simple 2D cases, and for a complex 3D case over real topography. The model is shown to give a more physically realistic profile for the wind speed in and just above forest canopies than the standard roughness length model used in most CFD simulations.

An automated methodology for setting up CFD simulations using the models described has been developed. A custom pre-processing package to implement this has been written, to enable the use of the CFD methodology in a commercial environment.

Keywords: Computational Fluid Dynamics; Complex terrain; Ground roughness; Forest canopy; Wind flow; Atmospheric Boundary Layer.

Contents

1 Introduction

Wind resource assessment is a very important part of the process of developing a commercial wind farm. Generally, this has been done using a combination of field measurement programs and mathematical models. The mathematical model provides a description of the wind flow over the whole of the proposed site, which can be used with the recorded site data to help site wind turbines in the windiest spots. Most of these models have traditionally used simplified descriptions of the wind field, based around linearised equations, as a complete description is too complex to be solved analytically. Simple numerical models have been used to good effect for many years, but are generally only applicable to relatively smooth topography, due to the simplifying assumptions used in their formulation.

As wind farm sites have moved to more complex, upland areas, these models have been found to be increasingly inappropriate. An alternative approach is to use a full CFD (Computational Fluid Dynamics) model of the site. This offers the potential to model any site, but at greatly increased numerical complexity and computational demand. However, the gains in accuracy look to be such that Powergen Plc, among others, have, over the last few years, started to look at this sort of modelling strategy. CFD is a very powerful and general technique, but one which needs careful setting up of the model if it is to produce meaningful answers. The purpose of this research work is to expand upon Powergen's current CFD modelling expertise, and to produce a well validated and tested model, that is more reliable and accurate than Powergen's current model. It would also have to be part of a commercially usable methodology, not something only of use in a research or academic context.

The work is funded by Powergen, and largely undertaken at Powergen's Power Technology Centre at Ratcliffe on Soar.

2 Background information and literature survey

Wind engineering started to be seen as important in the 1940's, following events such as the collapse of the Tacoma Narrows bridge. Other fields besides civil engineering, such as air pollution prediction, aviation, and of course meteorology, all began to put more effort into producing more accurate models of the atmospheric boundary layer. This research was mostly concentrated on field measurements, wind tunnel studies and simple analytical models. During the 70's and 80's, the increase in cheaply available computing power made numerical models a viable alternative, leading to what would become known as computational wind engineering (as distinct from meteorology). The complexity and scale of such models have been increasing in line with computing power ever since. Relatively simple models have been developed to describe the atmospheric boundary layer, based on work on small scale boundary layers.

2.1 Atmospheric Boundary Layer models

The atmospheric boundary layer is remarkably complex, with a wide variety of physical processes occurring simultaneously, and influencing each other. This makes a definitive analytical model almost impossible, so simplified models have been developed for specific aspects.

This work mainly concentrates on the fluid dynamics of the atmosphere, with the simplifying assumption that other physical processes (such as heat and moisture transfer) can be neglected.

2.1.1 The ABL

The most basic description of the localised movement of the atmosphere (i.e. the variation of wind speed with height at a particular location) is based on the huge body of work done on small scale flow over flat plates.

Viscous flow over a surface (generally termed a 'flat plate') will develop a boundary layer. This is a region of flow slowed down by the extraction of momentum from the flow through the boundary (wall), due to the no-slip boundary condition (the fluid immediately adjacent to the wall is stationary). Viscosity in a fluid has the effect of diffusing momentum, so as momentum from the bulk of the flow diffuses towards the wall, the layer effected by the wall (the boundary layer) grows in thickness.

Very close to the wall, molecular viscosity forces dominate, and eddy motion is damped out. Flow is therefore laminar in a region very close to the wall, and is termed the laminar sub-layer. Further away from the wall, the physical scale is such that eddies can form, and high Reynolds number, turbulent flow occurs.

The turbulent mixing in the flow also acts to diffuse momentum, and so can in some ways be thought of as similar to viscosity. This eddy-viscosity hypothesis forms the basis for many turbulence models. Turbulence is much more effective at transporting momentum than molecular viscosity, so the velocity gradient in the turbulent mixing layer is lower (as adjacent 'layers' of fluid are maintained at more similar velocities).

The ABL can be separated in to 2 regions

1. a surface layer (the SBL), 50-100m deep of approximately constant shear stress. The flow is insensitive to Earth's rotation, and determined by surface friction and vertical temperature gradient.
2. A second layer extending 100-1000m, with variable shear stress, and structure influenced by surface friction, temperature gradient and Earth's rotation.

2.1.2 Thermal structure of the ABL

The complex thermal structure of the ABL is one of the main things that results in it behaving differently from a large-scale version of laboratory shear flows. A simple flat plate boundary layer would keep growing in thickness indefinitely, and would reach a steady state, with no variation in time other than turbulence. This can be simulated relatively simply. However, the ABL does not ever reach a single steady state, as the thermal structure (and hence the flow structure) is constantly changing

over daily and yearly cycles. A full numerical simulation of the ABL would require a transient model, and detailed knowledge of the flow and thermal structure at the boundary conditions.

Two types of ABL behaviour can be distinguished. The Stable BL and the Convective (or unstable) BL. These two states are due to the radiative addition and subtraction of energy from the system (sunlight warming the ground during the day, and radiative cooling to space during the night). As the energy input to the system is continuously changing, so is the boundary layer.

Under cloudless skies, the boundary layer grows during the morning, with a capping inversion moving up as it grows (to about 1.0 – 1.5km). The CBL (convective boundary layer) persists, with much the same height for most of the afternoon. Convective mixing transports heat and momentum, giving a shallow velocity gradient through most of the BL thickness. The thermal structure changes rapidly at sunset, with the capping inversion breaking down, and a new inversion layer starting at ground level due to radiative cooling of the ground. This stable layer grows steadily through the night to about 100-200m at midnight. Gravity driven drainage winds form on even slight slopes.

The stability of the atmosphere depends on the temperature profile (often termed lapse rate) relative to the adiabatic lapse rate. As an air parcel moves up, there is less pressure from the overlying atmosphere, and so expands, cooling as it does so, at about 1°C per km. This is known as the adiabatic lapse rate. As temperature and height are linked in this way, temperature is often given as potential temperature, the temperature an air parcel would attain if brought adiabatically to 1000mbar.

If the potential temperature decreases with height, upward moving air will find itself warmer than its surroundings, and so continue moving up, producing a convective boundary layer. If the potential temperature is lower near the ground, air displaced vertically will experience a restoring force, giving stable stratification.

Cloud cover prevents the radiative heat exchange with the ground, and so thermal driving forces are not dominant, giving neutral stability. Vigorous turbulent mixing, such as occurs in high winds, will also produce a neutral or near-neutral profile. Assuming neutral stability simplifies the description of the ABL enormously, as thermal effects can be ignored. Most of the simplified analytical models used in wind resource prediction assume that if it is windy enough to be useful for wind turbines, it is windy enough to mix the ABL to near neutral stability. In north-western Europe, were cloudy skies and high winds prevail for much of the time, this is probably a reasonable assumption. It would be less good in sunnier climates with strong day/night temperature differences. Mountainous regions would also cause problems. as even relatively small differences in stability can cause significant changes in the wind flow due to the vertical flow disturbances caused by the topography (Montavon, 1998) .

2.1.3 Coriolis effect

The Coriolis effect is in part responsible for the large scale structure of atmospheric flow, however at small scales, it is almost unnoticeable. Due to the wind flowing in a rotating co-ordinate frame, the Coriolis effect exerts a force on the wind perpendicular to the flow direction. This is balanced by the pressure gradient force, and near the ground, also by the surface drag forces. At high altitudes, above the boundary layer, only the pressure gradient and the Coriolis forces are felt, and so must exactly balance each other. The flow therefore is directed along isobars, and so gives a 'zero pressure gradient' flow, with no dissipative forces.

In the ABL, momentum is removed from the flow by drag forces on the ground, directed in a direction opposite to the flow. The combination of drag and pressure forces must be balanced by the Coriolis force. For this to occur, the flow must be at an angle to the isobars. This gives the large-scale flow pattern of air spiralling into low pressure areas, anti-clockwise in the Northern hemisphere.

In the vertical direction this produces what is known as the Ekman spiral. The wind direction changes with height, being parallel with the isobars at high altitudes, and at a significant cross-isobar at ground level angle (in some cases up to 30°).

2.1.4 Log law

The lower 50-100m of the boundary layer is termed the 'surface layer' (of which only a very thin layer at the bottom is laminar). The surface layer has an approximately constant shear stress profile (Schlichting 1979, Kaimal & Finnigan 1994). Assuming this is similar in structure to small-scale flows allows a simple analytic description of the wind velocity profile in this layer.

By extension from molecular diffusion the momentum flux τ is assumed to be:

$$\tau = K_m \rho \frac{\partial \bar{u}}{\partial z} \tag{2.1}$$

where K_m is the turbulent exchange coefficient for momentum (equivalent to the kinematic viscosity in molecular momentum diffusion), ρ is the density, $\bar{u}$ is the average velocity, and z is the height.

A scaling velocity, u_*, known as the friction velocity, is defined with reference to the shear stress on the ground τ_0:

$$\tau_0 = \rho u_*^2 \tag{2.2}$$

with $\tau=\tau_0$ throughout the surface layer (where τ is in the wind direction).

K_m can be written in terms of the two surface layer scaling parameters (velocity and height):

$$K_m = \kappa u_* z \tag{2.3}$$

where the constant of proportionality κ is the von Karman constant (κ=0.4)

This can be substituted into (2.1) to obtain an expression for the velocity gradient in the surface layer:

$$\frac{\partial \bar{u}}{\partial z} = \frac{u_*}{\kappa z} \tag{2.4}$$

This can be integrated to give the classic 'log law' velocity profile:

$$\bar{u}(z) = \frac{u_*}{\kappa} \ln\left(\frac{z}{z_0}\right) \tag{2.5}$$

where the constant of integration has been included in the log term as z_0, known as the roughness length, and is the height at which the velocity would be zero if the log profile were extrapolated downwards.

In reality, the roughness length is smaller than the physical size of the roughness elements. For 'sand grain roughness' the roughness length is often assumed to be about $1/30^{th}$ of the height of the roughness elements (Kaimal & Finnigan, 1994).

The log law is limited to the surface layer of the ABL, and to neutral conditions. The log law gives no guidance in itself as to the depth of the surface layer where it is valid, so it is easy to misapply it to too high an altitude. Extensions to the log law have been proposed to alleviate these problems.

The log law also becomes inaccurate close to the height of the roughness elements. Within the volume of the roughness elements themselves, and immediately above them, the flow field will actually be a superposition of the wakes of the individual elements. A suitable distance above this, the flow will smooth out to a logarithmic profile that, if extrapolated downwards, would have zero velocity at height z_0. The real flow field will have a complex structure with a varying velocity at height z_0, and zero at z=0 and the surface of each roughness element.

The log law is a very useful simplification if all your points of interest are suitably far above the roughness elements themselves. For a 60m tall turbine standing on short grass, this is certainly the case. However, for a 10m anemometer mast surrounded by trees of a similar height, a log law profile must be used with extreme caution.

2.1.4.1 Turbulence

Flow above a critical Reynolds number becomes turbulent, that is, momentum forces dominate over viscous ones, and eddies form within the flow. These form at all scales, from large, structured eddies, forming in response to structures within the flow domain (wakes etc.), slowly breaking down into smaller eddies. These finally dissipate the energy of the turbulence when they reach the Kolmogorov length scale, and viscous forces dissipate the energy.

Turbulence is an extremely complex phenomenon, but several simple ways of looking at it have been developed. A standard starting point is to think of the instantaneous flow *u(t)* as being a steady mean flow $\overline{u}$, with a fluctuating velocity field u' superimposed on top of it.

$$u(t) = \overline{u} + u' \tag{2.6}$$

and the variance σ_u^2 of the turbulent variations:

$$\sigma_u^2 = \overline{u'^2} \tag{2.7}$$

This then gives two linked concepts: turbulence intensity, and turbulent kinetic energy.

Turbulence intensity I_u is the ratio of the turbulent (fluctuating) velocity to the steady wind:

$$I_u = \frac{\sigma_u}{\overline{u}} \tag{2.8}$$

where σ_u is the R.M.S. of the velocity variations.

The turbulence intensity varies with the same parameters as wind shear: surface roughness, wind speed, elevation, atmospheric stability, and topographic features.

Turbulent kinetic energy *k* is the energy associated with velocity fluctuations, in addition to the mean flow kinetic energy. This is defined as:

$$k = \tfrac{1}{2}\left(\overline{u'^2}\right) \tag{2.9}$$

in one dimension. (this is strictly the energy per unit mass, but is usually referred to simply as the turbulent kinetic energy in CFD applications)

An empirically based method of predicting turbulence intensity is given in Spera (1994):

Lacking models for the influence of terrain and atmospheric stability on σ_x . and σ_y it has been proposed that the ratio of these components to the vertical is a function of height only, for less than 600m.

The model separates the turbulence into *u*, *v* and *w* components along the streamwise. lateral, and vertical axes respectively. It assumes the ratio of the vertical component of turbulence to the friction velocity, $\sigma_z / u_* = 1.3$, for a neutral atmosphere, where the friction velocity u_* is defined in section 2.1.4.2 below.

The turbulence intensities can be expressed as:

$$\frac{\sigma_x}{\bar{u}} = \frac{0.52}{\ln(z/z_0)}\left(0.177 + 0.00139z\right)^{-0.4}$$
$$\frac{\sigma_y}{\bar{u}} = \frac{0.52}{\ln(z/z_0)}\left(0.583 + 0.00070z\right)^{-0.8} \qquad (2.10)$$
$$\frac{\sigma_z}{\bar{u}} = \frac{0.52}{\ln(z/z_0)}$$

(for $z_0 << z < 600$m)

These equations fit well for changes in surface roughness for $10^{-3} < z_0 < 10$ meters, but with some scatter (about 25%), again from Spera (1994).

2.1.4.2 Monin – Obukhov similarity theory

Monin-Obukhov similarity theory is one of the most powerful descriptions of the Surface Boundary Layer (SBL). It takes a seemingly very complex set of relationships, and shows them to depend on just a few key scaling parameters. The following summary is based on that given in Kaimal & Finnigan (1994) and Garratt, (1992).

Evidence points to the structure of turbulence being determined by just a few key parameters: height *z*, buoyancy parameter $g/\bar{\theta}$, the kinematic surface stress τ_0/ρ , and the surface temperature flux $H_0/\rho c_p$, where θ is the potential temperature, τ the shear stress, *H* the heat flux, and c_p the heat capacity, and a '0' subscript indicating the value at the surface.

Then, various atmospheric parameters, such as gradients and variances, when normalised by appropriate powers of the scaling velocity u_* and the scaling temperature T_* become universal functions of z/L, where L is known as the Monin-Obukhov scaling length:

$$u_* = \left[-\left(\overline{u'w'}\right)_0\right]^{0.5} = \left[\tau_0/\rho\right]^{0.5}$$
$$T_* = \frac{-\left(\overline{w'\theta'}\right)_0}{u_*} \tag{2.11}$$

As the shear stress τ is constant throughout the surface layer, and the same as at the surface, u_* it can in practice be evaluated from values anywhere in the surface layer, not just at the surface.

The Monin-Obukhov scaling length is given by:

$$\frac{z}{L} = -\frac{\left(g/\bar{\theta}\right)\left(\overline{w'\theta'}\right)_0}{u_*^{\,3}/kz} \tag{2.12}$$

where $\left(\overline{w'\theta'}\right)_0$ denotes the temperature flux at the surface. This is a measure of atmospheric stability, similar to the Richardson number but with substitutions, and is more useful, as L can be assumed constant throughout the surface layer. It also implies that the effects of stability and height are interchangeable.

The gradient Richardson number Ri is defined as:

$$Ri = \frac{\left(g'\bar{\theta}\right)\left(\partial\bar{\theta}/\partial z\right)}{\left(\partial\bar{u}/\partial z\right)^2} \tag{2.13}$$

Monin-Obukhov similarity theory describes many of the characteristics of the SBL: wind shear; thermal stratification; variability in vertical velocity and potential temperature; and dissipation of turbulent kinetic energy. However, the variability in horizontal velocities does not follow the similarity theory. This implies a more complex relationship between the turbulence intensities than the simple relations given by Spera.

2.1.4.3 Log law plus correction terms

Many variants on the standard log law have been suggested with alterations to extend it applicability. Most notable of these are attempts to extend the height at which it can be applied, and to allow for atmospheric stability.

2.1.4.3.1 Deaves & Harris formulation

The Deaves and Harris model, as it is known, is classed as a 'logarithmic with parabolic defect' law (Deaves & Harris, 1978), and is essentially empirical. It extends the vertical range of the log law by also imposing a top boundary condition, of a geostrophic wind.

The formulation for wind speed is:

$$u = \frac{u_*}{\kappa}\left[\ln\frac{z}{z_0} + 5.75\left(\frac{z}{h}\right) - 1.88\left(\frac{z}{h}\right)^2 - 1.33\left(\frac{z}{h}\right)^3 + 0.25\left(\frac{z}{h}\right)^4\right] \qquad (2.14)$$

where u is the mean wind speed at height z above the ground, κ=0.4, u_* is the friction velocity, z_0 is the aerodynamic roughness length, and h is the equilibrium boundary layer height.

The model also predicts the equilibrium boundary layer height:

$$h = \frac{u_*}{6f} \qquad (2.15)$$

where f is the Coriolis parameter: $f = 2\,\pi\,\Omega\,\sin(\phi)$, where Ω is the Earth's rotation rate, and ϕ is the latitude of the site in question.

The model matches the boundary conditions of similarity theory at the top and bottom:

$$\frac{u}{u_*} \to \frac{1}{\kappa}\ln\left(\frac{z}{z_0}\right) \quad \text{as } z \to 0 \tag{2.16}$$

and

$$u \to u_g \quad \text{and} \quad \frac{du}{dz} \to 0 \quad \text{as } z \to h \tag{2.17}$$

where u_g is the geostrophic wind speed.

This is in contrast to the simple log law, which matches the lower boundary, but has no upper boundary, and is not a good model for medium to large heights (above ~200m).

The power law model, while not matching either boundary condition, is often better than the simple log law at moderate heights (30-300m)

$$u = u_r\left(z/z_r\right)^{\alpha} \tag{2.18}$$

where u_r is the velocity at reference height z_r, and α is an empirically derived 'shear exponent', usually close to the 1/7 observed in small-scale boundary layers.

2.1.4.3.2 Atmospheric stability

An extension has also been proposed to the log law, to account for atmospheric stability, from Spera (1994):

$$u = \frac{u_*}{\kappa}\left[\ln\left(z/z_0\right) + \Psi_s\left(z/L\right)\right] \tag{2.19}$$

for $z >> z_0$

where Ψ_s is an atmospheric stability function dependant on z/L.

Neutral: $\Psi_s = 0$

Stable: $\Psi_s = +4.5\ z/L$, $z \leq L$.

$\Psi_s = +4.5\ (1+\ln(z/L))$, $z > L$.

Unstable: $\Psi_s = -0.5\ z/L$, $z \leq L$.

$\Psi_s = -0.5\ (1+\ln(z/L))$, $z > L$.

where L is the Monin-Obukhov stability length.

The stability length L is a measure of the ratio of mechanical shear forces to buoyancy forces. It is difficult to predict quantitatively, so can be treated as an empirical constant like z_0.

The above equations decouple the wind shear at elevations above L from the surface roughness, and extend the log gradient at L to higher elevations.

2.1.4.4 Flow over changing terrain

There are three characteristic features of flow over a surface after a change from the upwind surface:

- An internal boundary layer develops, growing in thickness downstream
- Profiles of wind, temperature, etc are not in equilibrium with the new surface
- A complicated turbulent response to the change is observed, with the loss of the local-equilibrium character of homogenous surface flow

2.1.4.4.1 Internal boundary layer depth

Kaimal and Finnigan (1994) give a simple formula for the internal boundary layer (IBL) depth δ_i after a change from roughness z_{01} to z_{02} :

$$\frac{\delta_i}{z_{02}} = A_1 \left(\frac{x}{z_{02}} \right)^{0.8} \tag{2.20}$$

where $A_1 = 0.75 + 0.03M$ and M is a measure of the strength of the roughness change:

$$M = \ln\left(\frac{z_{01}}{z_{02}} \right) \tag{2.21}$$

An alternative by Panofsky and Dutton (1984) gives better agreement with the data

$$\frac{\delta_i}{x}\left[\ln\left(\frac{\delta_i}{z_{02}} \right) - 1 \right] = B_1 \kappa \tag{2.22}$$

where B_1 is a empirical constant of approximately 1.25.

However, neither takes direct account of the upstream roughness, only of the relative change in roughness. The rate of growth is only given as a function of the downstream roughness, whereas in reality, some of the turbulence from which will be advected from upstream (determined by the absolute value of the upstream roughness, not just its relative value), affecting the mixing rate, and hence the rate of growth of the boundary layer.

2.1.4.4.2 Velocity profiles over changing roughness

The internal boundary layer has a velocity profile in equilibrium with the new surface inside, and a profile as upwind outside. Some suggest a sharp discontinuity in shear between the two, and while not completely accurate, this simple assumption is quite good.

The behaviour of the log profiles can be described as (with subscript values 1 denoting upstream values, and 2 denoting downstream values):

$$\bar{u}(z) = \frac{u_{*2}}{\kappa} \ln\left(\frac{z}{z_{02}}\right) + f(z/\delta_i) \tag{2.23}$$

where the function $f(z/\delta_i)$ has limiting values

$$f(z/\delta_i) = \frac{u_{*1}}{\kappa} \ln\left(\frac{z}{z_{01}}\right) - \frac{u_{*2}}{\kappa} \ln\left(\frac{z}{z_{02}}\right), \quad z/\delta_i > 1, \tag{2.24}$$
$$f(z/\delta_i) = 0, \quad z/\delta_i << 1$$

Various forms have been suggested for f, but the simplest, has f=0, for $z<\delta_i$.
This is widely used as a first approximation.

A different approach is to describe a 'self-preserving' profile for the velocity and shear stress in the internal boundary layer.
The self-preserving profiles are :

$$\Delta u(z) = \bar{u}_2(z) - \bar{u}_1(z) = \frac{u_0}{\kappa} g(\eta) + \bar{u}_p \tag{2.25}$$

for velocity, and

$$\Delta \tau(z) = \tau_2(z) - \tau_1 = [\tau_2(0) - \tau_1] h(\eta) \tag{2.26}$$

for shear stress, where τ_1 is assumed invariant with height, $\bar{u}_p$ is the pressure perturbation caused by the pressure pulse at the discontinuity (usually ignored), and velocity scale $u_0 = u_{*2} - u_{*1}$. The dimensionless height $\eta = z/\delta_i$.

The functions $g(\eta)$ and $h(\eta)$ can be solved if closure assumptions are made about the relation between $\tau_2(z)$ and $\left(\partial\bar{u}_2/\partial z\right)$, assuming that shear stress and velocity gradients are linked by eddy diffusivity. Two alternative forms (from Kaimal and Finnigan 1994) for the nondimensional wind shear ϕ_m:

$$\phi_m = \left\{\frac{\kappa z}{\left[\tau_2(z)/\rho\right]^{1/2}}\right\}\left(\partial\bar{u}_2/\partial z\right) = 1$$
$$\phi_m = \left(\kappa z/u_{*2}\right)\left(\partial\bar{u}_2/\partial z\right) = 1 \qquad (2.27)$$

Plotting the dimensionless velocity perturbation $g=(\kappa/u_0)\Delta u$ against the dimensionless height η gives good collapse of the data, except very close to the roughness change. Further downwind the closure assumption of $\phi_m=1$ is more accurate. It also performs better for a smooth-rough change than a rough-smooth change.

Surface shear stresses change very quickly downstream of the roughness change, first overshooting, then returning to their new equilibrium values.

A simple formula that works quite well is from Elliot,

$$\frac{\tau_{02}}{\tau_{01}} = \left[1 - \frac{M}{\ln\left(\delta_i/z_{02}\right)}\right]^2 \qquad (2.28)$$

However, it is critically dependant on the calculation of δ_i.

At larger scales, the IBL will eventually fill the whole ABL. At such distances, the surface stress ratio τ_{02}/τ_{01} may have evolved significantly, eventually falling to roughly 60% of its value soon after the change (from an example in Kaimal and Finnigan).

Taylor found that smooth-to-rough and rough-to-smooth changes filled the whole ABL when $x/z_{01} \approx 10^6$.

However, the direction changes associated with Coriolis effects (Ekman spirals) took longer, and did not occur till $x/z_{01} = 10^8$, but took place through the whole ABL depth simultaneously, and could amount to ±5° from the 20° deflection, with an increased deflection for a smooth-to-rough change.

2.1.4.4.3 Turbulence

The definition of δ_i from turbulent fluxes is the same as from the mean flow, i.e. the 'velocity' internal boundary layer is the same thickness as the 'turbulence' internal boundary layer, and grows at the same rate.

Turbulent kinetic energy (k) budgets show that near the surface production and dissipation are almost in balance, but over most of the IBL depth, advection and turbulent transport are significant, being of the same order as shear production, streamwise (acceleration) production, and dissipation. This is in contrast to the upwind situation where production and dissipation are in approximate balance over most of the boundary layer depth.

Rough-to-smooth and smooth-to-rough transitions have approximately opposite behaviours, in terms of the deviation of the k budget from the upstream equilibrium values. From this, it is clear that eddy-diffusivity based models will have difficulty in the IBL. However, they should be alright in the equilibrium layer very close to the surface, (although this is thinner in r-s transitions), and at some distance downstream. Eddy diffusivities should be used with caution for $x<10\delta_i$.

2.1.4.4.4 D&H with roughness changes

The D&H model can be extended (Cook 1997) to include the effects of changes in surface roughness, with the idea of the development of new internal boundary layers, in equilibrium with the local surface.

The internal BL is assumed to be in local equilibrium as described by the local friction velocity:

$$u_{*2} = u_{*1}\left[1 - \frac{\ln\left(\frac{z_{01}}{z_{02}}\right)}{0.42 + \ln m_0}\right] \tag{2.29}$$

where m_0 is given by:

$$m_0 = \frac{0.32X}{z_{02}(\ln m_0 - 1)} \tag{2.30}$$

where X is the distance downwind of the roughness change.

This has to be solved iteratively (for m_0), and starting from the upwind changes first.

This means you have to decide in advance how far upstream you are going to consider.

Cook has developed a re-working of the basic methodology, which the basic mean wind speed is progressively factored by a series of 'S-factors', which allows you to work from the site progressively back upstream, until the effect of further roughness changes is negligible. However the methodology is complex and also includes other (largely empirical) corrections: 'exposure factor', 'height factor', 'fetch factor', and 'direction factor'. While these make the model more accurate in some ways, the model is complex, and relates the profiles to 'standard conditions' at 10m above the surface.

2.2 Roughness models

The roughness of the terrain surface is a very important factor in flow modelling for wind resource assessment, as it significantly affects the shape of the velocity profile. Surface roughness can vary enormously – there can be several orders of magnitude difference between uplands covered in short grass or in thick forest. This has a big effect on the velocity in the lower boundary layer, and hence on the wind resource available. Hence, it is very important to have a good model of how surface roughness affects the ABL.

Quite simplified roughness models have generally been used in CFD models in the past, as they have generally concentrated on CFD's ability to model complex flow geometries and thermal structure. This has increasingly been seen to be a shortcoming of CFD models, particularly at Powergen's Power Technology Centre (PTC). Studies of several heavily forested sites have highlighted the poor roughness modelling in the PTC standard model.

2.2.1 Roughness length

The most basic handling of surface roughness is that built into the standard log law – that of a single roughness length. This is based on experimental work done mostly on pipe flows, with walls roughened with sand grains. This leads to the empirical relation that the roughness length is usually about $1/30^{th}$ of the element height. This figure will vary for surfaces with a roughness element distribution different to that of sand grains (Schlichting 1979).

For surfaces with 'porous' roughness, such as thick vegetation and forests, the roughness length may be as much as $1/5^{th}$ of the element height (Kaimal and Finnigan 1994). This is because such roughness elements are more effective at removing momentum from the flow than 'impermeable' roughness elements. Vegetated surfaces have thickened low velocity regions in the lower boundary layer, and so need more complex modelling to achieve an adequate description.

2.2.2 Forests and canopies

The simplest modification of the log law is to include a displacement height. In this, if the log law is extrapolated downwards, rather than reaching zero at z_0, it reaches u=0 at z_0 plus d , a displacement height.

This allows for a deeper vegetated layer than would be expected purely from its apparent roughness length. The displacement height is typically 70-80% of the height of the trees. It also corresponds with the mean level of momentum absorption.

$$\bar{u}(z) = \frac{u_*}{\kappa} \ln\left(\frac{z-d}{z_0}\right) \tag{2.31}$$

The value of z_0 for plants (and any terrain) expresses the ability of the roughness to absorb momentum, and not necessarily the physical size of the roughness elements. This can be treated simply with the inclusion of a displacement height.

The value of z_0 varies for different plant densities, from the usual estimate for sand-grain-type roughness of 1/30 of the element height, up to a maximum of 1/5 of the canopy height. As the plants crowd closer together, they absorb more momentum, and so z_0 increases for a given plant height. When too close together however, the resistance to flow is so high that the canopy effectively forms a raised 'ground' surface, and the roughness length drops. The maximum aerodynamic roughness occurs at some intermediate value. Physiological factors also prevent the plants being too close together, so dense vertically homogenous vegetation is probably close to the maximum. Forests with a dense canopy and clear trunk space or understory will behave slightly differently, and have a lower roughness length, and more complex internal flow structure. More complex models can be used if the flow structure within the canopy and immediately above it is of interest.

The roughness sublayer is the region where the presence of the canopy directly effects the character of the turbulence, and extends to about $3h_c$ (h_c=the canopy height) above the ground. Within this, there will be departures form the standard log profiles.

There is a good collapse of data for flow within the canopy, when it is normalised by h_c and u_{hc} i.e the average value of u at $z=h_c$, for plots of u/u_{hc} against z/h_c. (See figures 6.1 and 6.2)

Other velocity statistics also display a very good data collapse. If $-\overline{u'w'}/u_*^2$ is plotted as a function of z/h_c then all the profiles display an excellent constant stress layer down to the top of the canopy. This enables a change in the definition of u_* for dense canopies, to be the value of $-\left(\overline{u'w'}\right)^{0.5}$ at h_c, i.e. to be related to the shear stress at the canopy top rather than at the ground surface.

Within the canopy the turbulence is strongly inhomogenous in the vertical. In denser canopies, almost all the momentum is absorbed in the top half of the canopy, with essentially zero transferred to the ground surface. Moving down through the canopy, the turbulence becomes less efficient at transferring momentum.

The turbulence and momentum exchange within the canopy seems to be dominated by intermittent, canopy-scale downwards moving gusts. However, large vertical variations in foliage density may distort this picture. Stability within the canopy airspace can vary strongly with height, primarily due to water transport.

A more complete equation for the turbulent kinetic energy budget may be written, including shear production, turbulent transport, pressure transport, buoyant production, viscous dissipation, dispersive transport, wake production, and waving production. Dispersive transport is the counterpart of the standard turbulent transport term under volume averaging. Wake production is the k produced from plant wakes. The waving production term is associated with the movements of plants, and is a net sink of k due to damping.

Scaled budgets are very similar, despite the wide range of scales the data comes from, when multiplied by h_c/u_*^3, where u_* is determined in the constant stress layer above the canopy.

Turbulent transport is very important in the canopy region, and local equilibrium cannot be assumed. Lots of turbulence is generated around the canopy top (from shear just above, and wakes just inside) and transported to lower levels, where dissipation is very high.

2.2.3 Other ideas

One idea that looks promising is the modelling of the canopy by the inclusion of a porous volume within a CFD model. This would allow for more explicit modelling of the flow within the canopy, and should allow comparison of the model with measured wind data from within or near the canopy. This would not rely on wall functions as part of the wall boundary to remove momentum from the flow, but would do it via body forces within the main flow. Turbulence generation from the roughness would have to be considered carefully. There seems to be no references to this approach in the literature.

An alternative approach to including the effects of trees, albeit on a smaller scale, is given by Rehm, et al. (2000). This models a single tree analytically as strings of spheres, calculates the drag from this, and inserts this into a CFD model. This apparently produces good results for flows around trees and buildings in urban environments.

2.2.4 Validation

Wind tunnel studies have been performed on several occasions to look at the effect of forestation on the wind flow over hills. One study by Neff & Meroney (1998) showed up to a 70% drop in available wind energy for thickly forested hills compared to the unforested hilltop. Felling a region of trees around the hill top could reduce this drop to about 20%. However, the interaction between the forested regions and the shape

and size of the hill was shown to be strongly non-linear. For some hill shapes foresting some regions appeared to increase the wind resource compared to a completely deforested site, possibly by affecting boundary layer separation over the hill crest. This is clearly an area that needs attention and much careful modelling.

2.3 Wind flow models

2.3.1 Background

More complex models have been developed that attempt to describe the detailed flow of the ABL around topographic obstructions. The main problem of wind flow modelling could be seen as the physical scale of the problem, and the number of physical processes operating, and the complexity this leads to. Problems are usually of such a size as to be between conventional aerodynamic modelling and meteorological modelling, containing the complexities of both. Tools from each subject area have been applied with some success, but each with their own limitations in terms of physical modelling.

Small-scale aerodynamics models are designed to accurately portray the fluid flow in a volume (as described by the Navier-Stokes equations), and generally do not have to take other physics into account. Meteorological models, on the other hand, need to take account of other physical processes which affect the overall flow (such as thermal and Coriolis effects, moisture transportation, etc.) more than the detailed fluid dynamics, which can be relatively simplified.

Civil engineering applications have tended to use extensions of traditional aerodynamic approaches, while air pollution studies have generally been based on meteorological models. Wind resource assessment has not had such a historical tie with one subject area, and so a wider variety of approaches have probably been tried out in this area than in others.

Analytical approaches, based on simplified models of boundary layers, have been used, most notably the methodology devised by Jackson and Hunt. Most of the other

models have been some sort of numerical, discretised model, with varying levels of sophistication of flow physics. These range from basic mass-consistent models, to full CFD approaches. Again, a variety of CFD codes have been used: commercial, general-purpose, aerodynamics codes; meteorological codes; and various custom-written software.

2.3.2 The Jackson & Hunt methodology

This is one of the classic works in the field (Jackson and Hunt, 1975), and one of the most standard models for flow over low hills.

It is a linearised, 2D boundary layer model that assumes that the flow over the hill can be described as a small perturbation to the upstream flow. It splits the flow field into an inner and outer layer. The inner one remains parallel with the ground, but speeds up over the hill crest, and responds to changes in surface stress. The outer layer deforms to allow for the upwards flow deflection over the hill, and matches with the velocities of the inner layer and outside-boundary-layer flow.

The model does a good job of describing the flow over relatively low, rounded hills. It is less good if the hill gets too steep or angular, and breaks down severely if flow separation occurs. It is in these sorts of situations that a CFD approach should be a big improvement.

2.3.3 The NOABL model

The NOABL model is what is termed a 'mass consistent' flow model. It solves a flow field based on interpolating between measured data points. The velocity field at each grid point then has a correction applied, based on the topography, with the constraint that the flow field must be non-divergent (i.e. that mass is conserved).

The model is obviously highly simplified, but it has the advantage of relatively computationally cheap. Although the results from it are not considered to be highly accurate these days, it still finds a role in initial feasibility studies, where its quick run

time enables the most promising sites to be selected from a large number of candidates. A 1km resolution database of results for the whole of the UK has been made publicly available, and is used in preliminary studies of wind power potential. Other mass-consistent models have been developed, such as MINERVE (Finardi, et al, 1998) as extensions to NOABL to include other flow physics, but their use does not seem widespread.

2.3.4 MS3DJH and MSFD models

These models are extensions of the Jackson & Hunt commonly just 'J&H model') methodology by Mason and Sykes (1979). The surrounding topography is discretised on to a regular grid, then a 2D spectral method used to model it. In the MS3DJH (Walmsley et al. 1986) model, the equations for the J&H model are then solved analytically at the point of interest. In the MSFD model (Beljaars et al. 1987), a more complex turbulence model is used which does not have an easy analytical solution, so a finite difference method is used in vertical direction to solve the J&H equations. This seems to improve the predictions in the wake region, when several models are compared with the Askervein hill data. These models seem to have become the standard implementations of the original J&H methodology.

2.3.5 WAsP

The Wind Atlas Analysis and Application Program (Mortensen et al. 1987-2003) has become the industry standard for wind flow prediction for wind energy studies. It has been developed at the Risø National Laboratory over the last two decades.
WAsP uses the 'BZ-model' of Troen (1990) to calculate wind flow fields over topography. This is based on the MS3DJH model, but uses a zooming polar grid of topography, (rather than a rectangular one), which is analysed to calculate the flow perturbation at the centre. The ground roughness is also integrated into the model with a spectral model. This calculates the 'inner region' (as in J&H) as a balance between surface stress, advection and pressure gradient. There is also a facility to include local sheltering effects.

This gives a good model of flow over low and relatively gentle topography, and is generally considered to provide accurate predictions in cases with moderate roughness and changes of roughness. However, it is still theoretically invalid for steep hills. Comparisons of WAsP against measured data (Brammer, 1997) show it to get progressively less accurate as the terrain becomes more complex.

2.3.6 RAMS – Regional Atmospheric Modelling System

RAMS (Regional Atmospheric Mesoscale Model) is a 'mesoscale' meteorological code, which can include a wide variety of atmospheric physics (thermal, moisture, radiation, etc.) It was developed initially at Colorado State University, and is now commercial. It is predominantly used for weather forecasting, pollution dispersion studies, and other atmospheric physics work. It has fairly complex flow modelling as well as the ability to model thermal and moisture transport processes. It has been used by some researchers to model flow over terrain, and as a comparison case.

2.4 Other computational work

2.4.1 CFD

Computational fluid dynamics models are based on the solution of the Navier-Stokes equations. For this scale of work, they are usually based on RANS (Reynolds averaged Navier-Stokes equations) methods, generally discretised into finite control volumes. Closure of the equations is provided by turbulence models, of varying degrees of complexity.

Results of studies seem quite mixed, with a fairly wide variety of models. Opinions of authors as the success of such models also seems mixed – some claim that even relatively simple models give excellent results, while others say that even the most complex models are still deficient.

Table 2.1 - A summary of previous CFD models.

Researcher	Maurizi et al	Duranti et al	Aspley & Castro	Utnes & Eidsvik
Date	1998	1998	1998	1996
Model type	3D RANS CFD, steady state†	2D and 3D RANS CFD, transient†	2D and 3D RANS CFD, finite volume, steady	2D and 3D Finite element
Application	Wind energy resource assessment	General ABL modelling	Pollution studies and wind energy	Aviation safety
Software		NASTENV	SWIFT	
Thermal models	None	None (neutral)	Boussinesq approximation with potential temperature	None
Turbulence models	k-ε	TSDIA (Two Scale Direct-Interaction Approximation)	k-ε with alterations (gradient transport model)	Standard k-ε.
Boundary conditions	Inlet: log profile with z0=0.03m, v&w=0m/s. Ground: rough wall with 'wall flux' method. Impermeable lateral boundaries	Ground: special rough wall to correct k overproduction.	Ground: rough wall Top: constant velocity Inlet: 'equilibrium' BL Outlet: zero longitudinal gradients	Ground: rough wall, fully developed Inlet: 'fully developed flow' Sides: 'weak zero flux'
Domain	14km x 15km x ~1km Flat cells added at inlet and sides, and 'ramped' into topography	As wind tunnel study	2D: 80x hill height by 13.7H tall 3D: 13km x 5km x 2km	Not detailed for 2D or simple 3D
Grid	Horz.: 200m spacing. Vert.: 42 nodes, starting at 0.75m, GP ratio of 1.16. Lower and higher resolutions tried.	32x76 cells	2D: 100x80 cells 2D: 70x53x40 cells	Not detailed for 2D or simple 3D 3D real topo, 35 cells vert, 1.2E+5 nodes in total
Accuracy	Not compared against measured data. Lowering grid resolution and domain size both change results drastically (by 2m/s at z=30m).	'Excellent' according to authors. Does seem good, but some local discrepancies.	Most of flow field good, but not recirculation. K-ε mods increase re-attachment length from 4.1H to 5H, but still short of experimental value of 6.5H.	Claims to be 'remarkably accurate' despite using the standard k-ε model. Apparently predicts recirculation length very well, as well as 3d effects.
Comments	Limited sensitivity study on grid and BC's done, but not enough to provide definitive guidance. Model generally similar to PTC standard. Useful work on inlet BC / topography interaction.	Very complex turbulence model, seems to capture turb structure well, although hard to compare with other models.	Reasonable results. Turb. model alterations are an improvement, but very complex. Poor with standard k-ε. Grid independence questionable. Summit speed-up good, but wake poor.	Seems surprisingly good, compared to difficulties others have with the k-ε model.

† indicates the actual setting used was unclear in the reference.

Researcher	Carpenter & Locke	Ying & Canuto	Montavon	Brammer
Date	1999	1997	1998	1997
Model type	2D CFD finite element	2D CFD	3D CFD, transient	3D CFD
Application	Wind energy, flow over multiple hills	General ABL modelling	Wind energy	Wind enegry
Software	'commercial'	RAMS	CFX4	CFX4
Thermal models	None	Non-hydrostatic, uses potential temperature	Uses potential temperature and deep Boussinesq approx.	None
Turbulence models	High Reyneolds number k-ε.	2^{nd} order, Reynolds stress, complex.	k-ε.	k-ε
Boundary conditions	Inlet: D&H type profile Ground surface uses 'special elements'	Lots of detail for turbulence model, little about more general BC's.	Ground: rough wall User defined inlet profiles	Ground: rough wall User defined inlet profiles
Domain	8km long, 10km tall.	As for wind tunnel.	45km by 51.6km, 10km tall.	6km x 6km. 1km tall.
Grid	2D: 41 nodes vertically, x 361 long	High resolution vertically: 0.005m to 0.1m. Horz.: †	20 cells vertically, at G.P. ratio ~1.4 50m to 4.5km variable horizontal resolution	60 cells horz. 21 cells vert. With G.P. ratio 1.15.
Accuracy	Generally not very good predictions.	Good, fits well with wind tunnel data. Better than lower order turbulence models.	Quite good, captures thermal effects well. Wind speed predictions for stratified flow good.	Reasonable prediction of speed up ratios. Slightly better than model in WINDFARM.
Comments	Little detail about CFD model, more about wind tunnel experiments.	Mainly validating turbulence model against wind tunnel data.	Large scale. Concentrates mainly on thermal and large scale effects.	Direct precursor of current work

2.4.2 LES

Large Eddy Simulation is a CFD based technique which aims to capture more of the flow physics than traditional RANS CFD by attempting to predict the larger turbulent eddies, rather than consigning all turbulence to an analytic model. Small scale turbulence is taken care of with a sub-grid-scale model (usually that of Smagorinsky). This places LES between classical CFD and DNS (Direct Numerical Simulation) in terms of grid scale.

LES is sometimes used, but is still much less well validated than classical CFD (for this application), and is generally not as 'mature' a tool. It also has the disadvantage of needing very detailed knowledge of the inflow conditions and/or initial flow conditions. This requires information about the turbulence that is generally unknown in these sort of wind flow studies. The computational demand is also much greater than other CFD turbulence models (e.g. k-ε). While the idea of modelling the effect of large eddies on the flow is attractive, (e.g. in the wake of hills) the lack of initialisation data makes modelling more speculative than would be ideal. The extra effort involved in an LES run (both user effort in setting it up and computational effort), and question marks about validation, currently seem to outweigh the gains in accuracy.

2.4.3 Direct Numerical Simulation (DNS)

DNS attempts to model all turbulence features as explicit fluid flow features, right down to the Kolmogorov length scale (where viscous forces dissipate the smallest scale of eddies – usually sub-millimetre). DNS obviously has a huge computational demand, and is currently not used in Computational Wind Engineering except in very special test cases.

2.4.4 Montavon's work

Christiane Montavon's work (1998a, b and c.) is in a similar area to my work, but with the emphasis on thermally dominated flow over large mountains, rather than flow over very 'rough' surfaces. The same software (CFX4) was used as in my work, with the same underlying physical model. The inlet boundary condition uses a complex formulation of Zilitinkevich, that allows for ABL thickness and Coriolis effects, including the Ekman spiral.

The turbulence model is the k-ε model, but with the altered model constants suggested by Duynkerke (1987). This is supposed to be better for atmospheric flows, but some authorities are not convinced (Prof. McGuirk, personal communication). The ground boundary was a rough surface, using the standard wall multiplier method of CFX. No problems with near-wall turbulence profiles or inaccurate velocity profiles were reported.

Thermal modelling uses the deep Boussinesq approximation, that temperature only affects the buoyancy, and does not otherwise affect the density. This allows thermal buoyancy effects while still keeping 'incompressible' flow. This is quite a common approximation where temperature differences are relatively small, and result in density changes that are small enough not to significantly affect the flow field other than through buoyancy effects.

Thermal modelling was implemented in terms of dry potential temperature, rather than absolute temperature. This gives the temperature at a height relative to the adiabatic lapse rate. This allows for the temperature (and hence buoyancy) effects of the decrease in air density with height, without having to have a fully compressible flow model.

2.4.4.1 Gridding.

An area of the Swiss Jura mountains (Chasseral and Mt. Crosin) was used for the full 3D runs, with a domain much larger than the PTC standard model, and the grid generally coarser. The domain was 51.56km by 45km, split into blocks to allow grid

refinement near the points of interest. Horizontally, the grid size varies between 50x50m at the 2 points of interest, to 4.5x4.5km at the boundaries, with a total of 76 by 46 cells. Vertically, the domain was 10km tall, with 20 cells distributed in two layers. The lower layer (up to 2km) had 10 cells, distributed according to a geometric progression with a factor of between 1.4 and 1.5, depending on the ground height. This gives the lowest cells being ~5m tall, and site data measurement points being in the 3rd or 4th level. The upper layer (2km to 10km) also had 10 cells, but distributed according to a geometric progression with a ratio of 1.2. This seems to me to be a relatively coarse grid, especially in the vertical direction. Having only 20 cells vertically seems to be rather few. Also, having very highly flattened, terrain following cells near the ground could result in inaccuracies associated with the flow not being ground-parallel in areas of flow separation.

The coarseness of the grid means that the site data is compared with predicted values from only the 3rd layers of cells from the ground. The implementation of the wall boundary and wall functions would significantly affect results at this distance. Given possible anomalies in the wall boundary condition found in my studies, this could affect the accuracy of the results.

2.4.4.2 Validation

Initial validation runs were carried out against the Askervein hill data for the flow model, and against data from the Boulder wind storm event for the thermal model. These showed satisfactory agreement of the model with the measured data. Modelling of the Jura site showed a good description of thermal winds, and the model to be a realistic atmospheric model.

2.4.4.3 Conclusions

Very significant changes in flow pattern were observed from a neutral ABL to a stable one. In neutral conditions the wind speed was highest at the mountain tops, and lowest in the lee of the mountains, as expected. Stable stratification showed the highest speeds on the downwind slopes of the mountains, as the cooling air fell downhill in a

'drainage wind'. Unstable, or convective conditions are not looked at significantly in Montavon's thesis.

However, such thermal effects need not only stratification, but significant and steep topography to force the air parcels out of equilibrium (about 1000m of height difference in the Jura site). For most sites in the British Isles, even 'upland' ones, the more gentle topography will result in less severe thermal winds. The generally more cloudy weather will mean that stable conditions occur less frequently.

Overall, the effect of stratification is interesting and worth noting, but probably most important in mountainous areas. It may be of less importance to wind resource assessment than accurate surface roughness models in regions of moderately sized topography but significant forestry, for example.

2.4.5 John Brammer's work

John Brammer's work (1997) is described in some detail here, as my work at PTC follows directly on from it.

John Brammer's work basically took Powergen's existing model, and compared it with predictions from the linear MS3DJH/3R model (Walmsley et al, 1986) in the WINDFARM software package (ReSoft, 1997 onwards), and with measured turbine output data at two sites, one flat and gentle, the other with more complex terrain. Brammer was also able to identify and improve some of the more obvious sources of error in the then-current model (mainly in the boundary conditions). His work included a 2D study, looking at boundary conditions and wind speed profile development, and several 3D runs for each site looking at changes in boundary conditions and domain and grid parameters.

Initial 2D work highlighted the importance of consistent boundary conditions. Care needs to be taken to ensure the flow profile specified at the inlet is in equilibrium with the ground boundary condition, or anomalous flow features will arise. Also

unresolved questions were raised concerning differences in the 'apparent' roughness developed over a surface and the roughness specified as a boundary condition.

2.4.5.1 3D work

Various 3D runs were performed for both of the two real wind farm sites looked at. Improved inlet boundary conditions were implemented, including the new velocity and turbulence profiles from the 2D study. The inflow angle was set to be parallel to the ground in the bottom cell, with a linear ramp to horizontal flow at 500m above the ground. This generally gave much improved results over having the full height of the inflow horizontal or parallel to the ground.

Grid dependence tests were also performed, apparently showing that the vertical grid resolution and domain extent was adequate. However, the results were seen to be dependant on the horizontal gridding. Doubling the grid resolution showed an alteration in the predicted speed-up factors. However, the best results were obtained by increasing the overall size of the domain, and using 10 degree direction cases rather than 30 degree cases.

2.4.5.2 Results

The results from these tests were compared with the results from WINDFARM and the measured output data. For Carland Cross, the improved boundary condition run gives very similar results to WINDFARM, with an RMS error in turbine powers of about 6%, and error in annual energy capture of 0.5%. This good agreement between models and measured data reflects the lack of complex terrain at the site.

For Coal Clough, the RMS error in turbine powers was 31% for WINDFARM and 27% for CFX with the large domain model. The best CFX model had a 6.9% error in total energy capture compared to 13% for WINDFARM. The CFX results are a clear improvement, but are still dependant on the wind direction sectors computed, and the domain and grid parameters. The model performs notably poorly for direction sectors with more complex upwind terrain, including flow parallel to steep valley systems as well as transverse to them. It is noted that in complex terrain larger domains

(especially upwind) and higher grid resolutions are beneficial. Doubling the domain extent (resolution still at 100m) improved results, but with 4 times the run time – 50m resolution would have been better, but with very long run time.
It is also pointed out that as the results depend on the computed wind directions, and direction resolution, most effort should be concentrated in the directions of most wind energy.

2.4.5.3 PTC standard model

The 'PTC Standard Model', as referred to in this text, is basically what John Brammer developed for PTC, and represents a relatively simple 'first order' type model. It is reasonably internally consistent, and the gross physical modelling errors have been removed, but its modelling of an atmosphere is still very basic. It does however provide a benchmark 'default' model on which to base comparisons. The fact that it gives reasonably good results at all says something for the strengths of the CFD technique, and the robustness of the commercial solver.

2.5 Other relevant work

2.5.1 Climatic grouping

A whole resource assessment strategy has been devised by Mengelkamp (1999). It is described as a 'statistical-dynamic downscaling procedure', and is an alternative to the usual MCP methodology.

The methodology has been used in part by Montavon in her work, and in simplified form could provide a decision on which CFD cases to run, so as to focus effort on the most important climatic conditions.

The components of the approach are: time series of sets of parameters representative of area, and other site data; a classification scheme to group climate and other parameters into categories; a numerical model to perform a flow simulation for each category; and post processing to weight and sum all results.

Parameters include: geostrophic wind velocity; thermal structure; topography; surface roughness. The modelling strategy can be summarised as follows:

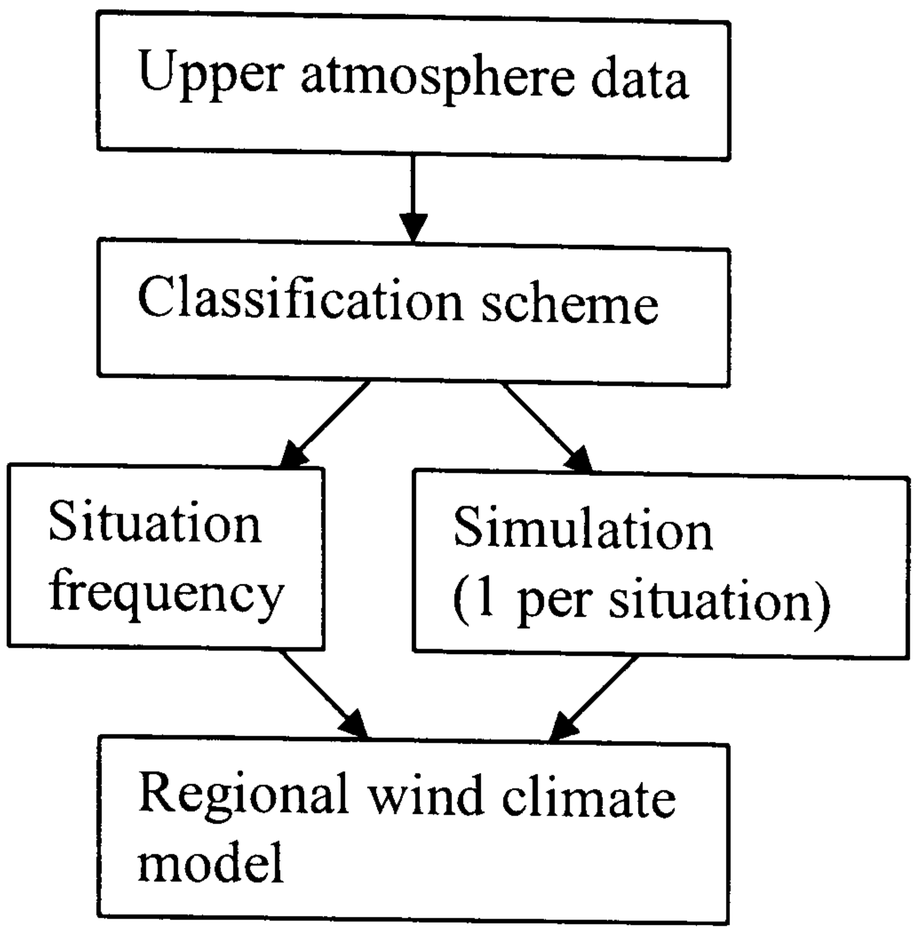

Fig 2.1. - Climatic grouping modelling strategy.

Situations are optimised into 'clusters' to decrease the number of classes, and improve the fit to the frequency distribution. Each cluster (situation) is a set of geostrophic and stability conditions, with the simulation defining the topography and roughness.
The relatively poor prediction of wind turbine power output in Mengelkamp's work is probably not due to deficiencies in the overall methodology, but in the flow model used. The grid resolution of 1km is probably too coarse to model small local flow disturbances that can affect a turbine's power output, although it might provide a general overview of the area.

The general methodology is a potentially very useful approach, and provides a systematic way of distributing computing resources in a way to maximise benefit.

3 Initial work

3.1 Powergen PTC standard model

One of the first areas I looked at was investigating PTC`s standard model, as it then was. This will be discussed here in some detail as it effectively forms the starting point for my own research. The 'PTC Standard Model' is basically the model John Brammer developed for PTC, as described in section 2.4.4.

3.1.1 Basic methodology

The basic flow modelling is of a steady-state, turbulent, viscous, incompressible flow. Atmospheric conditions are assumed to be neutral, and no thermal effects are modelled. This is also true of all the following modelling work.

The turbulence closure used is the k-ε model. Three domains are created, rotated by zero, 30 and 60 degrees, allowing 12 wind directions (1 normal to each side of each domain). A user defined inlet flow is specified, with a log-law profile. The bottom of the domain is set as a rough wall in a user defined function. The simulation is then run to a steady state solution. Data is output from another user subroutine at a constant height above the ground. All 12 directions are combined and wind speeds normalized to give a map of speed-up factors for the site.

3.1.2 Domain

The flow domain is basically a roughly cuboid volume, 6km to a side, and about 1km tall. The bottom surface is body-fitted to the topography (from OS digital topography data). The domain is 61 equal cells per side, and 21 to 28 cells tall, increasing in height upwards with a geometrical progression of 1.15. This gives cells 100m by 100m wide and between about 4 and 8m high for the lowest cells, depending on the number of cells and the topography. This is then repeated with a 30 and 60 degree

rotation of the domain. This enables inlet flow to be set normal to each side to give 12 flow directions.

3.1.3 Boundary conditions

3.1.3.1 General

The model is set so that one face is an inlet, with inflow normal to the face, with a velocity profile specified in a user FORTRAN subroutine (USRBCS). The ground surface is defined as a rough wall, with parameters for each cell being set in another user FORTRAN subroutine (USRWTM).

The top and remaining sides are specified as constant pressure boundaries, with zero relative pressure. The air density is defined across the whole domain, with pressures purely being relative (as the flow is incompressible).

3.1.3.2 Inlet profile -

Velocity

The inlet velocity u is set to a log-law profile, from a supplied roughness length z_0 (usually 0.05m) and velocity u_r at a reference height z_r (usually around 11.5m/s at 32m).

Using:

$$u = u_r \frac{\ln\left(\frac{z}{z_0}\right)}{\ln\left(\frac{z_r}{z_0}\right)} \qquad (3.1)$$

This profile uses the height above ground, so is displaced upwards with topography. It does not however make any kind of allowance for speed up over hills etc.

Although this provides an easy way of dealing with the topography at the inlet, it introduces several errors into the flow field. Firstly the velocity will not be simply displaced upwards, the lower layers will speed up, with the upper layers, in general, staying the same. The degree of distortion of the velocity profile will depend on the steepness of the hill. This vertical displacement will also introduce non-physical, lateral wind shear.

While this approach is a reasonable one for a simple, initial model, it was decided that a more physically accurate one should be developed.

Flow angle

The direction of the flow is set with a 'flow angle ramp'. All inlet cells are set with flow normal to the inlet face in horizontal direction, but angled vertically. The bottom cell of each vertical column of cells is set with flow parallel to the ground surface, with a linear decrease in angle to a cut-off height at 500m, above which all the flow is set normal to the inlet face.

Turbulence

The turbulence intensities at the inlet are set according to the equations (based on those in Spera, page 407). For background, see 2.1.4.1.

$$\frac{\sigma_x}{\bar{u}} = \frac{0.52}{\ln\left(z/z_0\right)}\left(0.177 + 0.00139z\right)^{-0.4}$$

$$\frac{\sigma_y}{\bar{u}} = \frac{0.52}{\ln\left(z/z_0\right)}\left(0.583 + 0.00070z\right)^{-0.8} \qquad (3.2)$$

$$\frac{\sigma_z}{\bar{u}} = \frac{0.52}{\ln\left(z/z_0\right)}$$

These are then converted into turbulent kinetic energy k and energy dissipation ε values according to: (from USRBCS)

$$k = \tfrac{1}{2}\left(\sigma_x^2 + \sigma_y^2 + \sigma_z^2\right) \qquad (3.3)$$

and

$$\varepsilon = \frac{k^{1.5}}{0.78z} \qquad (3.4)$$

3.1.3.3 Bottom wall

CFX allows for the setting of rough walls through a user FORTRAN routine USRWTM to set turbulent wall multipliers. The bottom sheet of cells are set so that the turbulence generated is such that it would match a log-law profile at that height

and roughness length. Higher cells are not set, but worked out from the fluid dynamics as expected.

3.1.4 Numerical schemes

Pressure-velocity coupling is handled with the default SIMPLEC algorithm, and QUICK differencing is used. Any other settings (such as under-relaxation factors) are not specified in the command file in the standard model, so remain on their default settings (see CFX documentation).

3.1.5 Output Data

Data are outputted through another user FORTRAN subroutine, USRPRT, which outputs wind velocities at a specified constant height above ground level, usually the turbine hub height for the site. The data sets are then rotated by a spline interpolation routine onto a common grid so they can be superimposed. The data points are then averaged and weighted according to a wind rose. The resulting data are then normalized to the wind speed at one point (usually the site anemometer mast) and a map of wind speed-up factors produced. This can then be used in other turbine location optimising programs. Only one flow speed case is considered, and from the final speed-up factor map, wind speeds are everywhere assumed to scale linearly, with no alteration in flow pattern.

3.2 Standard Model testing

3.2.1 2D boundary layers

Having seen some of the limitations of PTC's standard model, both in use, and in the theoretical and testing work of John Brammer, it was decided to go back to testing CFX in very simple boundary layer simulations. As there had been questions about CFX's ability to accurately model a rough boundary layer over a flat 2D plate, this was thought to be a key area to resolve before progressing to more complex models.

Fundamental problems with BL modelling might be hidden in a complex 3D case, and cause unexpected errors.

A first round of simplified CFD testing was performed, which provided valuable experience in CFD simulation of boundary layers. The first approach to be tried was using mass flow boundaries as the inlet and outlet, as the CFX manual recommended this as a computationally cheap way of simulating fully developed boundary layers. The domain was a very short 2D domain, with a rough ground surface, and simulated an effectively 1D boundary layer (no lateral or longitudinal variation). This was not intended to be a realistic model of the atmosphere, but as a test of CFX to see how well it simulated boundary layers. In particular, to see if it would produce a 'log law' type velocity profile without one being explicitly given as an inlet profile.

In this respect, the tests were successful. They did show the system was capable of producing a kilometre-scale boundary layer, and it did develop a log law profile.
As this first model was refined to make it more representative of the ABL, it became clear that this approach was not suited to this application. This approach is useful for situations like duct flows, and provides good results where the flow can reasonably be thought of as 'fully developed'. However, it is simulating a fundamentally different situation to that of an Atmospheric Boundary Layer. The height of the domain will be the only limit on the thickness of the boundary layer, with the B.L. 'growing' to fill the entire height of the domain. The depth of the ABL is determined by the thermal structure and the surface roughness, and is virtually always in a continuous state of development, both spatial and temporal. An atmospheric model needs to allow for a variable ABL depth, and not have to have it specified in advance by limiting the domain height. Such a 'shallow' domain would also suffer from blockage problems when hills were introduced. A more sophisticated model would therefore be needed for realistic flow simulation of the ABL.

The initial overall modelling strategy had been to specify as little as possible of the velocity structure of the flow, and let the solver calculate this from the physics of the flow. However, the structure of ABL flow at any given point is a product of both the flow conditions for many tens of kilometres upstream, and the previous time history

of the flow over the preceding day. To simulate this in a sensible period of time some assumptions about flow structure at boundary conditions would have to be taken. This would mean specifying a velocity structure at the inlet that reflected the spatial and temporal history of the flow. This is a far from trivial task. The total number of physical processes going on in the atmosphere is also very large, and so a subset of the most significant ones has to be selected and simulated. This can also require adjustment of boundary conditions to take into account the lack of some physical processes.

3.2.1.1 Particular areas of testing

Two areas that were studied at this stage that did provide useful foundations for later modelling were convergence testing and some issues surrounding inlet boundary conditions.

3.2.1.2 Convergence testing

While performing the initial tests it was realised that the convergence speed varied quite widely between models, depending on the physical domain and on the numerical procedures used. It was therefore clear that some reliable way of monitoring model convergence was necessary, rather than just running the solver for a fixed number of iterations.

CFX provides for convergence checking against 'mass source tolerance', i.e. the total error in the mass conservation equations. The mass source is a dimensional quantity, and a value can be supplied (in kg) so that the solver is stopped when the mass residual drops below this threshold value.

This gives a reasonably good idea of the general state of convergence of the model, but with one major drawback. The mass source tolerance value is dimensional, and what may be an appropriate level of error for a metre scale domain is unrealistically tight for a km scale domain. Therefore, a suitable value has to be calculated for each domain.

The manual suggests non- dimensionalising against the total mass flux through the domain, to provide some domain independence. This system proved quite successful, with good convergence being seen with a ratio of mass flux to mass source of $4x10^6$. However, the system of entering this as a fixed parameter in the command file had two problems. Firstly, a guess of the mass flux had to be made (easy if the velocity profile was fixed for the inlet boundary condition, which was not always the case). Secondly, the required value had to be calculated by hand each time, and entered into an edited command file. This would be a problem in developing an automated run set up system, to cut down on the effort involved in performing such CFD calculations. For this reason it was decided to use the User FORTRAN routine USRCVG, which allows for custom convergence testing. Because this is part of the CFX run-time system, and not a fixed, front-end file, it has access to field variable and domain size information. This allows it to calculate the convergence criteria based on the state of the run at each iteration.

It was also decided that, as the velocity fields are of the most interest, the convergence critieria should be based on the momentum residual, rather than the mass residual. This would tie the stopping criteria more closely to the variables of interest. The stopping criteria finally decided upon was that the largest of the 3 momentum residuals (u,v and w) should be less than one part in ten million of the total momentum of the fluid in the domain. This would provide both domain size and flow speed independent stopping criteria. Over the course of many runs this approach has shown robust and reliable convergence detection behaviour.

3.2.1.3 Gridding

A sensitivity analysis was performed on the effect of changing the gridding parameters. This included the overall size of the domain as well as the grid resolution.

Horizontal grid resolution

The horizontal grid resolution choice is the result of two main factors: processing resources, and topographic data resolution. Theoretically, the grid resolution should be high enough to achieve a truly grid-independent solution. In practice however,

other constrains also apply. If a domain of a given size is necessary to get meaningful results, the resolution might have to be specified according to the computing resources available. One figure that points towards a sensible starting point for grid sizing is the resolution of the topographic data. This is supplied on a 50m grid, so a CFD grid finer than this won't pick up any more physical information, but might be better from a mathematical point of view.

However, after numerous runs at different resolutions, it was found that a 50m horizontal grid gave good results while still having a realistic run time (although still several hours per run).

Vertical gridding.

The selection of vertical grid cell sizing was not trivial. This was mostly due to its entanglement in other issues, especially the implementation of the wall boundary condition.

A general appreciation of the application, and engineering judgement, would suggest something in the region of a few tens of grid cells vertically, with most being concentrated near the ground. This is where the highest gradients are, where most of the flow structure is concentrated, and the region we are most interested in. The standard way of achieving this sort of layout is to distribute the cells according to a geometric progression in height. Each grid cell increases in height by a fixed ratio from the one below. This policy was adopted for the current study in line with most other work in the area.

Much work was done on looking at the main parameters of this gridding strategy; the bottom cell size, the expansion ratio, the number of cells. These of course have to fit in with decisions on the total vertical extent of the domain. . A very wide range of vertical scales has to be allowed for – the wind speed might be required at 10m above ground level, but the domain might have to be several kilometres tall to accommodate significant mountains.

In general, the cells near the wall want to be kept small to improve resolution in this critical area, however, this has to be reconciled with the need to keep the overall number of cells down. If the expansion ratio is bigger, the cells increase in size quicker, and there is a bigger difference in size between the lowest and highest cells. Therefore, a higher ratio gives more resolution near the ground for a given number of grid cells. However, the expansion ratio cannot be too high for numerical reasons. Generally a limit of 20% expansion is considered desirable for good numerical behaviour (McGuirk, personal communication). A value of 1.15 was found to be a good compromise, and was used for most of the later work. In some tests, values up to 1.18 were used, but it was not found to be necessary to go beyond this.

The size of the lowest cell is constrained quite significantly by two opposing drivers. Firstly, the cell's size has to be small enough to allow for the physical scaling of the problem. The wind speed might be required at as little as 10m above ground level, to match small anemometry masts. This obviously requires small enough cells to give adequate resolution of the strong vertical wind gradient at this height. This would imply a bottom cell size of the order of 1 metre. The second constraint on the size of the bottom grid cell is from the rough wall boundary condition. This requires that the cell size be somewhat larger than the roughness length. In normal smooth wall applications, guidance on the cell size is given by the y^+ value where:

$$y^+ = (\rho u_* \, y/\mu) \tag{3.5}$$

where y is the height above the surface, and μ is the molecular viscosity.
This equation is quoted here in the form most often seen in text books. The scaling distance is generally still called y^+, even when the local coordinate system would imply that it should be z^+, for consistency.

However, this parameterisation becomes less clear in the case of a rough wall, where the scaling velocity u_* may be many times higher, and the shape of the boundary layer is controlled by the turbulent viscosity, rather than just the molecular viscosity.
In additions to concerns over the exact accuracy of the 'wall turbulence multiplier' implementation of a rough wall boundary layer, it imposes a hard mathematical lower

limit on the cell size at the roughness length. It is meaningless to try to calculate the velocity from the log law at a height less than the roughness length, as this is the height at which the velocity (of the log profile) goes to zero. Trying to do so gives division-by-zero errors, and generally crashes the CFD solver, or produces empty or meaningless output files.

Given the above problems, and the nature of the log law, the cell size needs to be several times the value of the roughness length. This is not a problem over flat grassland, with z_0 values in the region of 0.03m. However, for towns and forests, with roughness values in the region of 1m, this creates significant grid resolution problems. This limit on grid resolution was one of the main drivers in developing a different method of modelling 'extreme roughness' regions like forests.

In addition to the previous comments on limitations of the rough wall methodology, there appears to be other fundamental anomalies in the wall boundary condition implementation in CFX. A discussion of this forms the next chapter, but its implication for gridding schemes is another drive towards smaller grid cells near the wall, as the results in the lowest few cells are dubious.

The degree of flattening in the bottom few cells is quite considerable (very small height compared to their width and length), and various studies were undertaken to see if this might cause problems. A search of the literature revealed many other authors using similarly flattened cells in this sort of application (e.g. Montavon 1998; Maurizi et al, 1998; Aspley & Castro, 1998) . Indeed, it is very hard to avoid in this kind of work.

The 2D runs used to look at vertical and horizontal resolution were extended to look at the effects of cells flattening. This showed no undue problems arising from such flattened cells. Better results were obtained for a given number of cells, by increasing the vertical resolution near the ground (with highly flattened cells) rather than having squarer cells, but with lower vertical resolution.

Cell flattening probably matters less in this sort of application than in some others due to the nature of the flow. As the simulation is predominantly within a large boundary layer, the flow is relatively ground-parallel (at least in the near-wall region were cell flattening is an issue). This means the streamlines are quite accurately aligned along the longitudinal axis of each cell, with relatively little flow through the top and bottom surfaces of each cell. This reduces the numerical errors that would otherwise be associated with highly flattened cells if the flow were at a significant angle to the cell.

3.2.1.4 Overall strategy

The investigations undertaken in this study come together to give a general gridding scheme with a bottom cell height of about 2m, 35 cells at an expansion ratio of 1.15, and an overall height of about 2000m. These parameters can be altered somewhat to fit specific run conditions. These parameters were incorporated into the custom-written front-end, so that setting up the grid was as easy as possible, and that variations could quickly be produced for testing purposes.

However, these figures were still seen as something of a compromise, and larger numbers of grid cells would probably be used if more computing resources were available. The computational speed is the limiting factor in determining what is going to be a useful model, as 12 runs are normally done, for different wind directions. At a few hours per individual run, this quickly adds up to a long time overall. While longer times might be acceptable in an purely academic environment, the basis of this research was to see if a CFD methodology for this application could be developed for use in an industrial setting. In light of the rapid increase in potentially available computing power, current limitations on grid size/resolution are acceptable in that they can quite feasibly be improved.

3.2.2 Initial conclusions

Many things were learnt about the application of CFD to atmospheric modelling from this early work, and formed the basis for the later studies.

Primarily, that any computational fluid dynamics simulation is not trivial, and that simulation of the atmospheric boundary layer is certainly far from trivial. CFD techniques struggle to some degree with details of boundary layers, as these are not the regions of primary importance for CFD's traditional areas of use. ABL studies have, in the past, often made heavy use of empirical descriptions, and either rather simplified or highly specific analytical descriptions.

These two are not easy to fit together, and some pragmatic decisions have to be made to combine expertise from both areas into a model that can feasibly be implemented. While a CFD model might be inferior in terms of specific details in relation to some specific ABL models, it has definite benefits in terms of the generality of its fluid dynamics. Setting up a coherent and re-usable CFD-based ABL modelling methodology is a significant task.

4 Boundary condition problems

A large portion of the research work has been looking at problems associated with the wall boundary condition in the CFD model.

The situation this model is trying to simulate is a very large scale (atmospheric) boundary layer. However, for initial studies, this was limited to a simplified model - a simple 2D boundary layer over a flat plate, with no 'atmospheric' physics to complicate matters. However, it has not been entirely straightforward to get an accurate result for even this apparently simple case.

Fairly early on in the development process, various peculiarities in the CFD results for the lower boundary layer were noticed. These were discovered to be due to two problems. Firstly, a mis-match between the specified inlet profile and the developed profile. This was eventually rectified by changing the inlet profile, after much work on the exact problems encountered. Second, and ultimately more problematic, was a problem with the wall boundary condition itself.

4.1 Exploring the problem

A problem was first noticed in the velocity profile, which, while conforming to the standard log law, did not have the expected 'apparent' surface roughness. The apparent surface roughness, as inferred from the velocity profile was slightly higher than had been specified in the boundary condition. The profile of the turbulent kinetic energy was also somewhat strange. It was discovered that there was consistently a spike in the value of k at the second cell from the wall, regardless of the gridding parameters used.

Although opinions seem to differ in the literature about the exact magnitude of k near the wall, and in the boundary layer above it, it is agreed that the turbulence is highest closest to the wall (for a fully rough case). It was first thought that this must be due to the implementation of the rough wall boundary condition, using wall multipliers, and much time was spent investigating this. Some areas of potential problems were

identified, but it was eventually realised that the anomaly was still there in the smooth wall case. It could not therefore be due entirely to the rough wall condition, and must be something in the underlying wall boundary condition.

Many simulations were performed with a rough wall, implemented using the USRWTM user FORTRAN routine, as in the example in the CFX4 user manual. This gives results that are close to, but not quite, what was expected.

The velocity profile generated is what would be expected above a rougher surface than had been specified in USRWTM, for example, a profile with an 'apparent' roughness length of around z_0=0.07m, for a specified z_0=0.05m. The apparent roughness length of the developed profile (after 49km) was found by plotting the speed against height on a log axis. If the profile conforms to a log law, this will then give a straight line, the intercept of which (on the z axis) is the roughness length. A least-squares best fit through the CFX profile data for the lowest 200m (which showed only slight deviations from the theoretical straight line) gave an intercept at z=0.07m. This only amounts to a few percent difference in the velocity profiles, but is still significant when translated into available wind energy.

There are more obvious anomalies in the turbulent kinetic energy profile for the same case. Figure 1 shows a graph of the cell centre values against height and shows a definite 'spike' in the value of k in the second cell out from the wall, with the values slowly returning towards a 'straight line' over the next 5 or so cells.

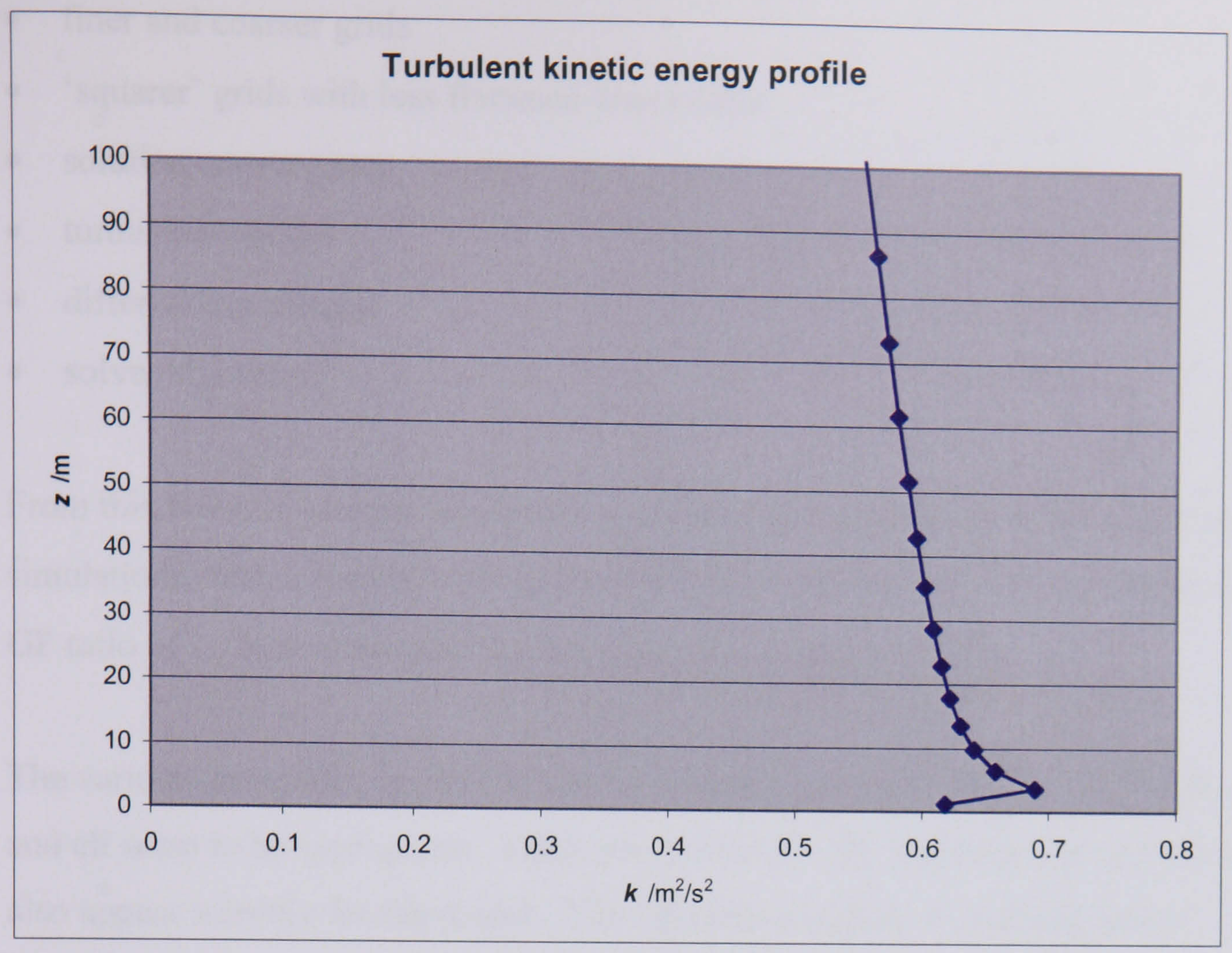

Figure 4.1 - Turbulent kinetic energy k against height z. (bottom 100m of domain only) specified $z_0 = 0.05$m.

This 'spike' was consistently present throughout this research work. Although this phenomenon was not noted in other, published works (e.g. Montavon 1998), either in the text or in the figures. However, other current workers with the same software (Paul Stangroom, personal communication) have noticed the same spike in k values. In consultation, both Prof. J. McGuirk and H. Versteeg (of Loughborough University, personal communication) agreed that the near-wall behaviour looked anomalous, and needed further attention. A summary of a response from CFX is given in section 4.2.

This region of high turbulence levels near the wall could explain the higher than expected apparent surface roughness observed in the velocity profile.

Numerous things have been tried to remove this problem and obtain more accurate results, but with little success. For example, the gridding has been looked at extensively, but with little improvement.

- finer and coarser grids
- 'squarer' grids with less flattened lower cells
- solution convergence
- turbulence model
- differencing method
- solver algorithm

From this work, it seemed reasonable to assume that the grid used in many of these simulations, with a bottom cell height of ≈ 2.3m, increasing in size above this with a GP ratio of 1.15, is reasonable for the roughness length of 0.05m.

The various parameters in USRWTM, have been checked (ELOGR, XYPLUS, etc) , and all seem to be appropriate. Other parameters for the simulation in general would also appear sensible for the model. The simulation appears to be adequately converged. In the above case, the field values have stabilised after about 450 iterations, with the simulation being run on to 600.

Originally it was thought that this must be a problem in the rough wall implementation, but runs with a smooth wall displayed similar behaviour. A simulation run identical to the above rough case, but without the USRWTM user Fortan (and hence a smooth wall) was performed. The turbulent kinetic energy profile was lower, but still displayed exactly the same shape 'spike' in turbulence levels in the second cell from the wall (as can be seen if the smooth-wall value of k is scaled to give the same value at the wall as the rough wall case), as shown in Fig. 4.2.

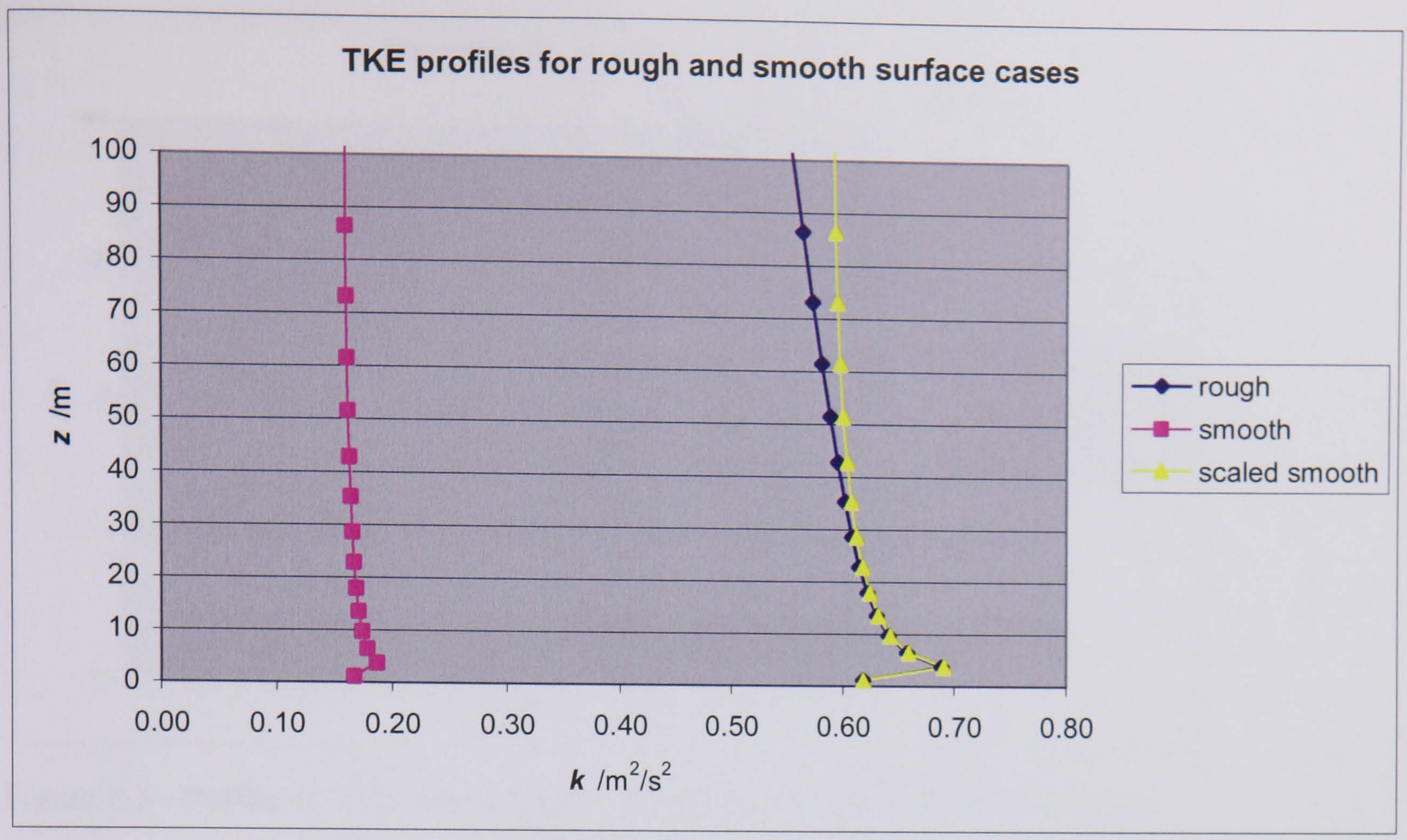

Figure 4.2 - Profiles of k against height, including smooth-wall value scaled by 3.69.

For rough case, z_0=0.05m.

As the gridding was left identical to the rough case for a direct comparison, it was 'officially' too coarse in the neighbourhood of the wall (first cell at too high a value of $y+$) so subsequent runs were performed with finer vertical grids (bottom cell down to 0.02m). These also showed evidence of the same phenomenon. This made the bottom cells highly flattened, so more runs were done with much finer horizontal gridding (down to 0.1m), again with similar results.

To more clearly show the dependence on gridding, Figs 4.3 and 4.4 show results from 5 runs with similar domains, but different heights for the bottom cell. Above this, cell heights then increase in a geometrical progression, with a factor of 1.15. This case has a rough wall (z_0=0.05m), with a domain length of 50km to allow the flow to fully adjust to the lower boundary condition.

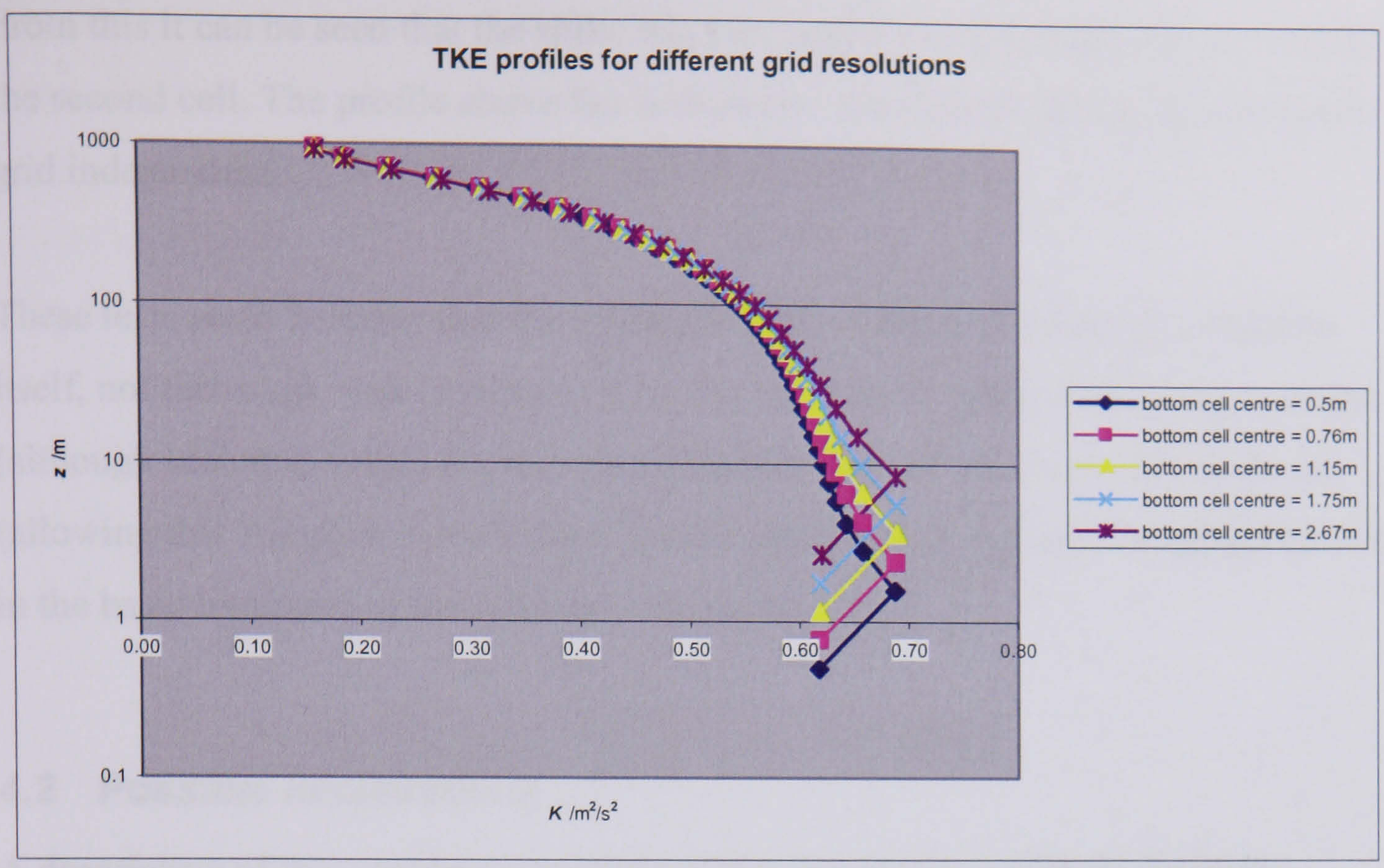

Figure 4.3 - Profile of k for whole domain height (log axis), at outlet of domain.

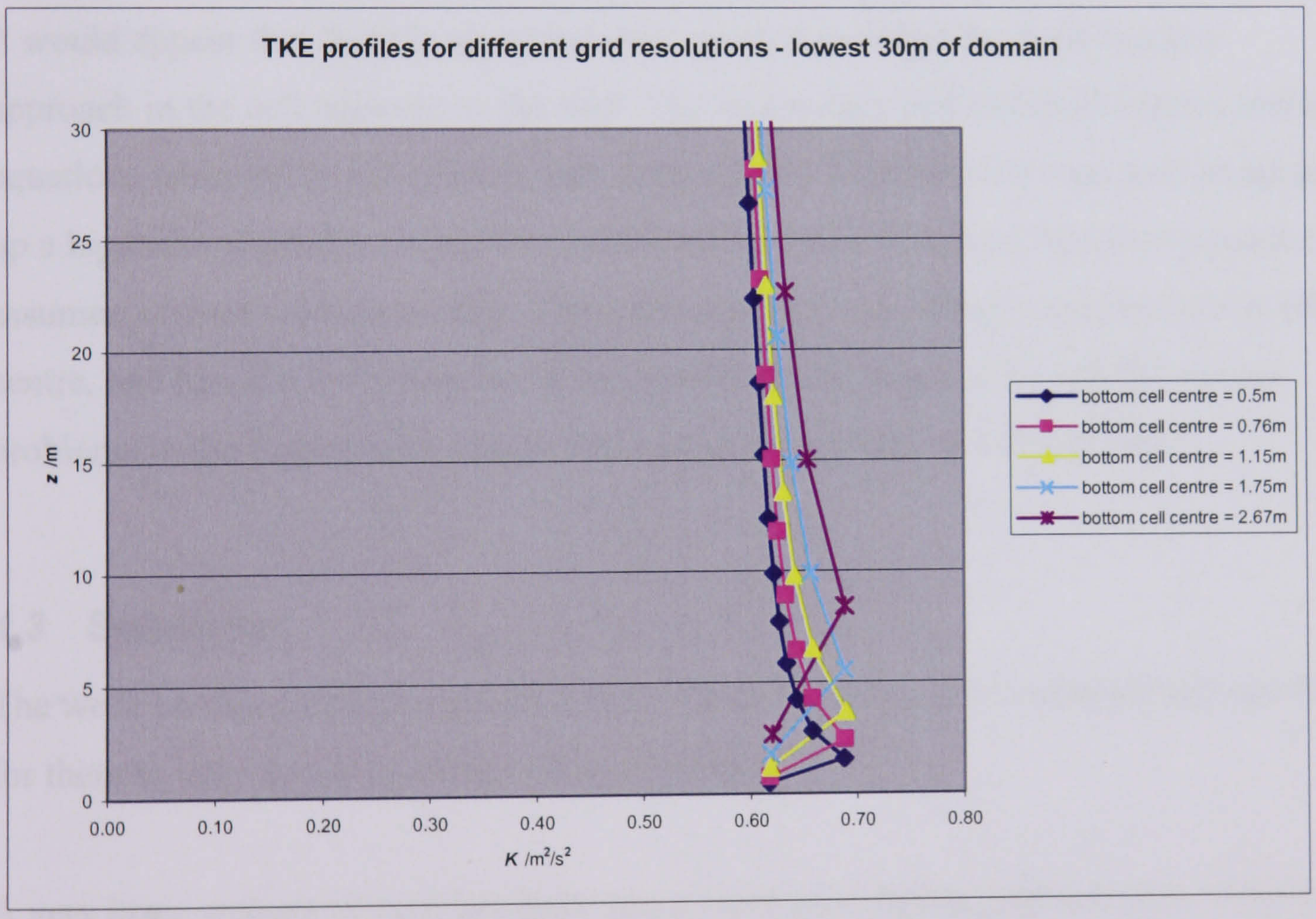

Figure 4.4 - Profile of k for bottom 30m, showing the variation near the wall.

From this it can be seen that the spike stays the same size and shape, but is 'locked' to the second cell. The profile above the bottom few cells can be seen to be essentially grid independent.

These tests seem to imply that the anomaly is due to the wall boundary condition itself, not the rough wall extension of it. The fact that the spike is identical in shape (although scaled in value) for smooth and rough walls in otherwise identical runs (allowing that the grids in both cases are not ideal) would suggest that the problem is in the basic treatment of the boundary condition.

4.2 Possible explanations

A description of this problem was sent to CFX, along with a request for more information on the equations used in the cells near the wall. The material they sent back was reviewed with the help of Prof. McGuirk, and a possible anomaly found. It would appear that there is an error in the equations used in the wall function approach in the cell adjacent to the wall. The momentum and turbulent kinetic energy equations seem to be inconsistent with each other. The momentum equation integrates up a logarithmic profile to find the velocity at the first cell centre, but the k equation assumes a linear velocity profile. This will imply a lower velocity gradient at the cell centre, and hence a low value for shear-generated turbulence. This will then cause problems in the higher cells, due to the mismatched values of velocity and k.

4.3 Solutions

The work on this problem reached a point where it needed to be referred back to CFX for them to help decide the best course of action

A very large amount of time has been spent fruitlessly on this problem area, without really being able to get a grip on the fundamental nature of the problem (as opposed to its symptoms). This problem could not really be solved within the current research programme. It is a very specialised area, and in the internal workings of a piece of very expensive commercial software. As such, it was deemed outside the scope of this

current work, and research proceeded acknowledging that this problem was there, but without trying any further to solve it. Any errors in results arising from it will be highlighted as the fault of the CFD package, and not directly due to the current modelling work.

5 Basic modelling

5.1 Initial testing and ideas

After the initial, background work on the problem had been completed, and the main problem areas defined, work began on putting together the basic model.
It had become clear that the major challenge was not capturing the complex 3D geometry of the flow, as is usually the case in industrial CFD applications, but accurately modelling the subtleties of the atmospheric boundary layer. This meant that a lot of attention had to be paid to the boundary conditions, and much of the research effort was involved in developing strategies to specify appropriate boundary conditions.

Work was not only targeted at the flow conditions at the boundaries, but also the specification of the physical boundaries of the domain itself. Arranging for topography specification, and suitable grid generation was not trivial.
The strategies developed to address these problems will be discussed in the following sections, along with a description of their implementation.

5.1.1 Domain specification and solution strategy

One of the many areas that has to be thought about in this kind of work is the various trade-offs between ease of problem specification, solution speed, and accuracy. The results of the initial work provided a rational basis for the modelling strategy.

The research work would develop - and the final finished package would implement - a specialised but consistent application of CFD. The underlying solver of CFX4 would be used, with various added-on user-defined modules. Although this could be accessed through CFX's own front end, such an approach would be time-consuming and inefficient, as the pre-processor and post-processor are designed to be very general. The pre-processor includes functionality for specifying very complex grids, which makes specifying the topologically simple ones used in this research overly

time-consuming. To speed up the testing and development process a custom front end was developed. This was implemented in Matlab, and designed specifically for defining CFD domains for flow over topography. This produced the script and data files for running CFX4.

User output and post-processing code were also developed to output data at defined locations (e.g. anemometers) rather than loading the data into the general post-processing package and having to then pull out each data point by hand.

5.2 Description of model and Implementation

During this phase of the project, two strands of development proceeded in parallel. The theoretical development of the model continued alongside the development of various custom pre- and post-processing utilities. These implemented the idea outlined in the previous section.

The work was carried out so that the academic research was targeted at producing a useful commercial tool. The model would have to be general, in that it should cope with any site likely to be considered, and not just be limited to certain special cases. It must be feasible in terms of computing resources and input data. It must also not take so many man-hours to set up each new case that it would undo any economic benefit of the system. This is why the system was designed from the start around obtainable input data, and a largely automatic pre-processor to reduce the time taken to initialise each case.

The pre- and post-processor sections were written in the high-level MATLAB language, as this includes efficient built-in support for large numerical arrays and matrices, and a large library of data processing and analysis functions. This allowed the rapid development of the user interface.

The user defined subroutines of CFX all have to be written in FORTRAN 77 to interface with the main CFX solver program. These had a very long write – debug

cycle, as they are not compiled until a CFX run is started, and many aspects cannot be fully tested until convergence and completion of a run (frequently several hours later). This resulted in the user subroutines taking a disproportionately long period of time to develop.

The CFX package defines what subroutines can be included, and a skeleton of code for interfacing with the solver. Although rigidly defined, this structure does provide the potential for adding almost any physics the user can define, as well as grid definition, convergence control, and data output.

The subroutines used in the model include:

USRGRD – grid definition

USRBCS – user defined boundary conditions.

USRCVG – convergence control.

USRWTM – rough wall implementation.

USRPRT – user defined data output.

The details of relevant algorithms are in section 5.4 later in this chapter.

5.2.1 Inlet condition strategy

As the research moved towards more complex models, the main area of focus for the investigation was the boundary conditions.

Two differing approaches seemed to present themselves. The first approach, as had been initially planned, was to include enough physics in the CFD model that it would develop an accurate ABL itself, within the domain, without 'prompting' by boundary and initial conditions. This proved to be difficult. It is hard to provide detailed physical models for all the processes going on, and almost as difficult to work out which could be simplified or deemed insignificant. The other problem was the physical space required to develop an atmospheric boundary layer. Information on the ESDU data sheet 82026 (1982) suggests a 100km fetch is needed for the ABL to reach some sort of equilibrium with a change in terrain (although even then it is still probably evolving thermally). 2D runs in CFX of simple boundary layers matched

with this observed data, in that a domain of at least 60km was necessary for a boundary layer to grow to ~1km in thickness. This also provided some confirmation that the modelled boundary layer was behaving and scaling in a similar manner to the ABL.

These findings gave the inspiration for the next, more pragmatic approach. This relied on the fact that the boundary layer evolved quite slowly, so a profile specified at the inlet would be advected downstream. An empirical ABL profile could be specified at the inlet, without it having to develop over tens of kilometres. Providing the region of interest is smaller than the length over which the boundary layer would develop significantly, the specified ABL profile should persist, with just some deformation of this due to topography.

This seemed to be a potential way of getting a more accurate and realistic wind profile without having to have extremely complex physical models. A test programme was started looking at different analytical and empirical ABL parameterisations, and using these as CFD inlet conditions.

The two profiles looked at first were a 'Deaves and Harris' type profile (Deaves & Harris 1978, Cook 1997), and those given in Spera (1994). These are both based on a log law approach, but adjustments to make them more realistic and allow for wider climatic conditions than strict neutrality. It quickly became clear that there were technical difficulties with this approach, with frequent convergence problems. Upon analysing the results these problems turned out to be due to inconsistencies between boundary conditions. The specified rough ground condition and the flow model would have produced one sort of flow profile – one that is subtly but significantly different from the specified inlet profile. While this different inlet profile should be more representative of the ABL, the rest of the model was not simulating an ABL. The flow was therefore adjusting to the 'new' conditions inside the domain. This approach was not tricking the model into looking like an ABL, as had been – somewhat naïvely – hoped.

While it might take tens of kilometres for the whole depth of the ABL to re-equilibrate with new ground conditions, the region close to the ground changes much faster, with a new, inner boundary layer forming. This often created large anomalies near the inlet, and along the top of the inner boundary layer. This reached about 60m thick after a couple of kilometres, i.e about turbine hub height when the region of interest is about the size of an average wind farm. As velocity perturbations could be of the order of 1m/s, this would clearly cause problems for accurate wind predictions.

5.2.1.1 Final plan – spatial development

This led to the next plan, to let a boundary layer develop spatially. However, to do this as part of the main solution domain would require a prohibitively large amount of computer resources. A boundary layer could be developed in a 2D domain first, and then this used as an inlet condition for the 3D domain. This would allow many tens of kilometres of a suitable 'upstream' roughness to be used to develop a BL profile while not needing excessive computer resources. A database of inlet profiles could then be built up to cover a variety of upstream conditions.

The profiles thus developed could be guaranteed to be compatible with the conditions inside the domain, as they used the same basic physics, and solver and BC settings. The ground roughness settings for the 2D run would be an average of the terrain upstream. The exact value to use would depend on the engineering judgement of the operator. Although requiring more user intervention and expertise, this would enable the user to allow for the complete range of possible upstream conditions. Also, it would be possible to specify changes in roughness in the 2D domain, to account for significant roughness changes (e.g. coastlines) that would be outside the 3D domain, but could still have an impact on the wind flow field.

5.2.1.2 Other allowances

One area of Powergen's 'current' model that was perceived to be inadequate was the handling of topography at the inlet. The base of the inlet followed the topography at that point, with the velocity profile displaced up or down to match, and the vertical

direction matched to the ground angle, with a ramp to zero degrees tilt at 500m above ground. This scheme could introduce anomalous lateral wind shear, and also took no account of the topography in terms of speed-up over hill crests, etc.

The allowance of topography at the inlet is difficult, as this would require an empirical or analytic formulation for the flow over hills – exactly the problem that has caused the use of CFD in the first place. So, some way of 'simplifying' the domain at the boundary was necessary, so that an analytic formulation could be realistically applied. This approach was preferred to using a simplified description of a complex situation, as this would again introduce incompatibilities with the flow structure inside the domain.

After looking at various different methods used in the literature, the most promising looked to be some sort of 'topography ramp', that reduced the topographic variation to zero at the inlet. This used a low-resolution inlet section of the domain to 'ramp' the topography towards the average value at the inlet. This allowed for a 'flat terrain' inlet profile to be used. The loss of topographic information could be justified as the BL appears to adjust to topography relatively quickly. Carpenter and Locke (1999) show after only a few crest-valley cycles a BL shows no further changes for corresponding positions near the ground. (In the very large scale, of course, hills will look like very large roughness elements, and so cause changes in the boundary layer well above the hills themselves, and over many tens of kilometres.)

Having the inlet of the order of 10km upstream of the area of interest would therefore allow the ABL to adjust to conditions within the domain, with a relatively weak dependence on the small scale structure of the inlet conditions. The inlet however, would still have to be a good 'average' representation of the large scale conditions prevailing upstream of the inlet. As well as 'traditional' roughness, this could also include high roughness value to allow for topography, if this was felt to be appropriate. An alternative way of including specific upwind topography (e.g. a pronounced ridge just outside the 3D domain) would be to include a representation of

it in the 2D domain. Although this would be allowed for in the code, this has not been investigated in any of the validation cases, and is left as an area for further research.

5.2.2 2D runs for inlet generation

A collection of runs at different surface roughnesses were performed, and used to create a catalogue of different inlet profiles. Runs could also be performed with other parameters varied. For example, if it were felt that the flow field might be velocity dependent (e.g. flow separation in a critical area of the model) then inlet flow speeds could be chosen to study conditions of interest.

The outlet profile data from the 2D run is then interpolated to the cell centre heights of the 3D domain inlet (as they will, in general, not be coincident). A data file is then written that can be read by the USRBCS routine of the CFX solver.

In summary:

1. 2D run set up and performed.
2. extract outlet from field variable output file
3. data saved to file
4. pre-processor reads file
5. interpolates to 3D domain cell centres
6. forces positive for k & epsilon (removes occasional interpolation erors)
7. writes profile file readable by USRBCS

5.3 3D work - Overview

The ideas for the 3D domains were conceived so that the domains were specified in a standard way, and could be generated automatically by a specialist pre-processor. This removed one of the main obstacles to the use of CFD in this sort of field – the large amount of time and specialist CFD knowledge that would otherwise be required

to set up an appropriate domain and boundary conditions in the standard (and very general) pre-processor.

Although the pre-processor code was written along with the development and refinement of the CFD model, it proved its worth in enabling the rapid development of the test and validation cases.

The basic 3D domain used in the later testing can be summarised as follows:

- Domain – ~1km and 35 cells tall with variable spacing, ~5km wide by 10km long at 50 to 200m resolution (details in section 5.4.2.)
- Inlet boundary – specified velocity, k, and ε profiles, as described in section 5.2.1 and 5.2.2.
- Side boundaries – pressure boundaries (constant pressure, zero normal gradients of velocity, k and ε).
- Top boundary – pressure boundary (as above)
- Outlet boundary – pressure boundary (as above)
- Ground – rough wall, as described in sections 5.4.4 and 5.5.4.

See CFX4 Flow Solver User Guide section 8 for more details of boundary condition types.

The ground roughness values are read from a data file by the USRWTM routine. This allows for variable ground conditions to be included in the model.

The specification of the top boundary had been the subject of some worry earlier in the study. It is important for the boundary to be permeable, to help reduce blockage effects from the topography. However, earlier work had also attempted to make use of the top boundary condition to define the top of the ABL. This was found to be difficult, and ultimately unnecessary. The strategy finally settled on was to use a pressure boundary, the same as at the sides of the domain. If the domain was suitably tall, blockage effects would be small anyway. No explicit control over the height of the boundary layer was introduced, as it was found to grow quite slowly when of the

order of 1km thick, so no 'capping' was deemed necessary. The overall boundary layer thickness is set by the inlet profile specified, which is one that has been developed in a long 2D domain to match the conditions upstream of the main domain. This provides a simple control over the overall thickness of the ABL, in the absence of thermal modelling, which determines the ABL thickness in reality.

5.4 Pre-processing and domain generation

The pre-processor developed in this work performs a lot of tasks that would be quite time-consuming in the standard pre-processors, and automates a lot of the overall process.

The pre-processor is implemented in Matlab, as a group of script files and functions. When it is run, the user is presented with a menu, from which they can: set project name; change configuration parameters; load and save parameters; set roughness and topography maps; set inlet profiles; and define roughness maps.
The parameters that can be set in the pre-processor are:

Downstream length	Distance from domain 'centre' to outlet
Upstream length	Distance from domain 'centre' to start of lead-in
Lead-in length	Length of low-res lead in area (for topo ramp etc.)
Half-width	Distance from 'centre' to side boundaries
Grid spacing	Grid resolution for main part of grid
Domain height	Overall height of domain
z-cells	Number of cells in vertical direction
r	Spacing ratio (in geometric progression) for vertical cell heights
Rotation centre	Physical location of domain 'centre'
Rotation angles	Angles for which runs are generated - can be single or list
Terrain type	Flat, or topo read from file
Roughness type	Constant Z_0; variable Z_0 read from file; or variable Z_0 and porosity read from file (used in advanced model)

Inlet profile type	Flat; logarithmic; or read from file
z_0, z_r & u_{zr}	Profile spec. if logarithmic inlet profile selected
Topography map	Filename of terrain data file
Roughness map	Filename of ground roughness map file
Inlet profile	Filename of inlet profile data file
Output type	Full field; planes at given heights; vertical profiles at specified locations
Output plane heights	Heights above ground of output planes
Output profile locations	Physical locations of profiles
Max solver iterations	Iteration limit if solver not converging
Differencing scheme	e.g. QUICK
Turbulence model	e.g. k-ε

When the user is satisfied with all the settings, all the files necessary for the runs (e.g. one for each direction sector) will be written out to a directory structure, including a script file to sequentially start the runs.

The lead-in length is a low-resolution area at the inlet of the domain which allows the inlet boundary to be moved further from the area of interest without unduly increasing the number of cells in the grid. The transverse cell spacing stays the same, but the streamwise cell spacing is gradually increased, from its usual 25-100m to a maximum of 500m (with a constant expansion ratio). When this maximum value is reached any remaining distance is filled with cells of the maximum length.
This lead-in area is also the region in which the topography lead-in ramp is used.

5.4.1 Control file generation

The pre-processor creates a 'project' file directory, and under this a subdirectory for each direction case specified, labelled with the direction (e.g case180). A control file is generated for each case and written to the appropriate directory. This contains all the directives to the CFX solver as to how to carry out the run. Most of the

information in this file does not change from one run to another, and is loaded along with the basic structure of the file. The values specific to that run are generated by the pre-processor, and included in the file when it is written out. This includes such things as: the maximum workspace allocated to the solver (as this depends on grid size, the pre-processor calculates this according to a simple formula based on the size of previous runs); boundary condition types; PDE solver type; differencing scheme; under relaxation factors; included user FORTRAN modules.
This file is labelled with the project name e.g. `askervein.fc`.

5.4.2 Grid definition

The pre-processor generates a regular 2D (horizontal) grid of points based on the parameters given, one for each cell vertex. Copies of this are then rotated to each of the directions specified. The base topography data file is loaded and the height data interpolated to each vertex point specified in the horizontal grid info. This interpolated height data is then written out as ASCII data to a file (called `topo.xyz`) in each case directory. These files consist of grid size information and a list of x, y and z values for each cell vertex, and will later be used be USRGRD in creating the grid.

The height if the domain is specified by giving the altitude of the top of the domain. In a flat case (with the ground at height zero) this is the same as the height of the domain. The z co-ordinate uses the physical height of the landscape i.e. metres above sea level. This is the format in which the topography height data is supplied. Physical co-ordinates have been adhered to so as to simplify the pre- and post-processing. If the co-ordinates had been altered, for example having the domain centred at (x, y) = (0,0) , or the lowest , point in the landscape as z=0, then much more processing would have to be done on the data. Also, it might not be apparent to other users of the final data set how the co-ordinate system had been transformed. Keeping x, y, z strictly as Ordnance Survey grid references and heights prevents any confusion.

The height of the domain through which the wind blows is therefore the altitude of the top less that of the topography. It is up to the user to define a suitable top altitude in the pre-processor.

The format of `topo.xyz` is as follows:

Line 1: NCI, NCJ, NC, GEXP, DOMHI
Line 2: UCNP, UCNI
Line 3 onwards: X, Y, Z

Where NCI, NCJ, NCK are the number of grid cells in the *i*, *j*, and *k* directions (see note). GEXP is the expansion ratio for the vertical cell height increase. DOMHI is the altitude of the top of the domain. UCNP is the total number of data points in the following part of the file. UCNI is the number of data points along the *i* direction. X, Y and Z are the physical space co-ordinates of the grid vertices, usually the OS grid co-ordinates in metres.

(Note: *i*, *j*, and *k* are the co-ordinate system of the grid, with *i* (roughly) streamwise, *j* lateral and *k* vertical, whereas *x*, *y*, and *z* are physical space co-ordinates – the two systems may well be rotated with respect to one another, although both verticals, *k* and *z*, are coincident. *k* is used here to refer to the vertical grid coordinate to fit with convention, and is not the turbulent kinetic energy.)

5.4.3 Inlet boundary condition specification

Different versions of USRBCS are called depending on which specification type was chosen in the pre-processor. The same data file is produced by the pre-processor, but different parts of it are read by different versions of USRBCS.

The vertical grid parameters are used to generate a list of heights for the cell centres of the inlet boundary. This is then used to create the inlet boundary velocity profile, interpolated from the profile data file specified by the user (if that option was

selected). The same process is also used for k and ε. This profile information is written out to another data file (`inlet.dat`) for each directory, to be read in by USRBCS.

The format is:

Line 1: NCK, Z0

Line 2 onwards: Z, U, V, W, K, EPSILON

Where NCK is the number of cells vertically, and Z0 is a roughness length used in the `log-law` inlet specification setting.

Z, the cell centre height, and the field variables are read by the "user profile" version of USRBCS.

The height of the inlet is constant across the width of any one run (due to the 'topography ramp' at the inlet), so just one set of heights at which the profile is specified is needed for each run. However, these heights will generally change between direction cases, as the average ground height will, in general, be different. One profile specification is therefore needed for each direction case. The basic profile is the same for each, just the heights at which it is specified change to match the cell centre heights. The interpolation from the original profile is done in the pre-processor as Matlab has powerful built-in facilities for interpolation that would have to be hand-coded in FORTRAN if this were to be performed in the user routine itself.

It is up to the user to choose an inlet profile he feels is representative of the upstream terrain. Currently, only one profile is used across the whole width of the domain, to simplify run specification. It is felt that this is a reasonable assumption for most runs. Variations in topography and roughness can of course occur inside the domain, and such features will have ~10km to affect the flow profile before getting to the 'region of interest'.

The program could however be extended to allow for a variation in the profile along the j-direction, for example, in a run parallel to a coastline. Variation in the profile

with direction (e.g. off-sea and off-land wind directions) can be achieved by using two 'projects' within the pre-processor. Two sets of runs can be defined, one for the directions with wind blowing off the sea, with one inlet profile, and the other directions with a different inlet profile.

5.4.4 Ground roughness specification

The ground roughness specification type is decided in the pre-processor. A full 'map' of ground roughness values is written to a file whether constant roughness value or a variable one is chosen. This simplifies the coding, as the only difference needs to be in the pre-processor, and the USRWTM routine can be the same, with only the data it reads in being different. If a constant value is set in the pre-processor, the value for each ground surface cell centre are set to this, and the data file written out. If a variable, map-based surface roughness is required, the pre-processor defines the appropriate value for each cell.

The pre-processor contains a link to a geographical map editor, also written by the author in MatLab, to specify areas of ground roughness, in a manner analogous to the WAsP map editor. A digital map, such as a scanned in Ordnance Survey map, is loaded in, and the scale specified by giving the physical locations of 4 points on the map. Polygonal areas can then be defined using the graphical user interface, and corresponding roughness values attached to each.

A data file containing a background roughness value, the co-ordinates of each roughness area, and its associated roughness value is then written out.
The pre-processor reads in the areas, and works out which area each cell of the grid is in. A table of cell centres and associated roughness values is then written out for each direction case as `rough.dat`.

The format for this file is:

Line 1: NCI, NCJ

Line 2 onwards: Z0

Where NCI and NCJ are again the size of the domain, and Z0 is a list of the roughness length for each cell.

5.4.5 User defined output specification

The user output file contains all the field variables, but for user defined areas. For small domains, it is possible to output the variables for the whole of the domain (using one version of USRPRT), however, this file becomes prohibitively large for big 3D domains (often over 50MB for the usual sort of domain sizes). This size is due to it being an uncompressed ASCII file. This is easy to write out and read back from on a wide variety of computers (i.e. there are no issues in moving it from the UNIX workstation where it is generated to the Windows PC where the post processing is done) but this is at the expense of large file size. A binary format could be more compact but would effectively tie the file to one computer architecture. CFX also outputs its own 'dump' file. This is a binary file of the complete state of the solver, so can be used for re-starts, but is in a proprietary format, and not easily accessible.

Therefore, it was realised that a way of just outputing data from a restricted area was necessary. A different version of USRPRT was written that outputs data for a 'plane' a set height above the ground, and vertical 'profiles' at specified positions. The pre-processor writes out a data file `output_spec.dat` that defines the number of planes, their heights, the number of profiles and their positions. This is read in by USRPRT after the run has completed.

One disadvantage of this system is that the output has to be defined in advance of the run. However, if different output is required after a run has completed, it can be restarted for a small number of iterations with an altered `output_spec.dat` and a second set of output files produced.

Output is written to a user directory created by CFX as a subdirectory of the one the run was started from. This will end up containing either a file called `vars.dat`, the full-domain output file, or one file for each plane (called `height00000.dat` –

where the number indicates the height of the output), and one file called `profiles.dat`, which contains all the vertical profiles. The formats of these files are described in the section on USRPRT.

The format of `output_spec.dat` is:

Line 1: number of heights, number of points

Followed by a list of heights (one per line), then a list of x, y pairs, (one pair per line).

The first line tells the user FORTRAN routine how many heights and points to try to read from the file.

5.4.6 Solver parameters

Some of the solver parameters had been refined during the course of the initial work, and during the 3D testing. The settings documented here represent the values at the end of the testing phase.

5.4.6.1 Turbulence models

The basic k-ε turbulence model was used for most of the initial testing, but it was found that the modified RNG k-ε model gave slightly better results in the large scale 3D runs. This is one of the standard models built in to CFX, and is recommended in the manual for large scale and external flow problems, so should be more appropriate for this sort of work This model uses slightly altered model constants, but the basic physics and assumptions are otherwise the same as the basic k-ε model.

It was discovered during the early testing work on the Askervein Hill validation case (see section 5.6.1), that the RNG k-ε model gave results closer to the measured data. . This model was used in all the later testing work.

5.4.6.2 Solver settings

The differencing scheme used in the initial work was the default hybrid scheme. It was found that slightly better results were obtained by using the higher order CCCT scheme for the momentum equations, while keeping the defaults for the rest of the equations. See section 5.6.4.1 for results from the Askervein test case. The actual solver used is the default 'Stone' solver, as this was found to give reliable and fast solutions.

An increase in under-relaxation factors from the default (low) values is possible, while still keeping reliable convergence. This is because the problem has a relatively simple topology and smooth streamlines, and quite low gradients. These values reduce the number of iterations necessary to achieve convergence. A value of 0.75 was used for u, v, w, k and ε. This might need to be reduced again in cases of steep topography and flow separation.

Convergence testing was handled in a user FORTRAN routine (described below) using momentum source values. However, the control file also specified a limit of (usually) 500 iterations. This provides a backup way of stopping the solver if convergence does not happen. If it is required to continue a finished run, this can be done using data in the dump file, and the model run for more iterations. The limit value can also be set from the pre-processor, if it is known in advance that a very high or low value is wanted. A very low value (say, 3 iterations) can be used with a restart if a second set of user output files are required.

5.5 User FORTRAN routines

5.5.1 USRGRD – grid definition.

This routine is run once on starting a CFX run, and defines the geometry of the grid. It is the second half of the custom grid generation, along with the specially written pre-processor, rather than defining the grid in a general pre-processor.

The topography data file created by the pre-processor (`topo.xyz`) is read in. The first two lines contain grid size information, then follows the x, y, and z co-ordinates of the topography height field. The height data is stored in an array.

The routine then loops over the cell vertex indices in the i-j plane. For each vertex, it reads the ground height from the array, and then calculates the vertex positions in that vertical column according to the geometrical progression parameters specified in the pre-processor. The total number of cells, the expansion ratio, and the overall height of the domain are known, and from this, the bottom cell height can be calculated, and then the others in that column of vertices.

The routine loops up the column and sets the vertex positions, then moves on to the next column. The routine then calculates the height of each cell centre (rather than vertices) and stores this in a 'user common block' (the FORTRAN equivalent of a global variable) for use in other routines, particularly USRPRT.

As this user routine is used by all the options, and is executed at the initialisation of each CFX run, it also contains some file I/O elements common to all the routines. The ground roughness information is read into a 'user common block' in this routine, as it is only run once. The USRWTM routine that uses this info is run on every iteration, but it would be poor use of resources to re-read the file in on every iteration, as would happen if the file I/O was located in USRWTM. File caching by the system would probably prevent a physical disk read each time, but it is still unnecessary processing.

5.5.2 USRBCS – user defined boundary conditions.

This user routine basically provides a mechanism for specifying boundary conditions that are too complex to be given a simple numerical setting in the control file. In this application it is used to specify the velocity and turbulence profile at the inlet.

A single inlet profile is read from file, as specified by the pre-processor, and used to set the cell values across the width of the inlet face of the domain.

The parameters set are u, v, w, k and ε.

5.5.3 USRCVG – convergence control.

This user routine allows for more complex convergence criteria than can be specified in the control file, which is essentially limited to an iteration limit or a check on the value of a single residual.

As the momentum residuals are dimensional quantities, plausible stopping values will change with domain size. Therefore, some calculation is necessary to achieve a sensible stopping criterion. The calculations used in this routine have been described in section 3.2.1.2 . This system has been found to give reliable convergence over a range of domain sizes.

5.5.4 USRWTM – rough wall implementation.

The USRWTM routine is used to introduce a turbulence multiplier at a wall boundary. This is used in CFX as the standard way of specifying wall roughness. The standard example routine supplied with the software has been expanded from allowing one hard-coded roughness length per wall boundary, to allow for spatially varying wall roughness, with values read in from a data file based on a roughness map of the area. The specification of the roughness areas is performed in the pre-processor, as discussed in section 5.4.4.

The routine reads in the data from a 'user common block' on every iteration, the data having already been read in from file in the USRGRD routine at run initialisation time, to reduce disk accesses. The routine then loops over every cell on the 'ground' boundary, sets the appropriate roughness value, and calculates the turbulence multiplier parameter for each.

Currently the ground roughness value is fixed by the pre-processor, but as the routine is run every iteration, there is the possibility that it could be extended to vary the roughness, depending on the flow field. This could be used to implement sea surface roughness, with the roughness (from waves) dependant on the wind speed. Currently.

water surfaces have to be specified as a constant, unchanging roughness, specified in advance, with the user having responsibility for picking a suitable value.

5.5.5 USRPRT – user defined data output.

This user routine provides opportunity for the user to produce his own output files in addition to the standard output summary and dump file. In this application, one of the goals was to reduce the amount of specialist user knowledge necessary, and to automate the process as much as possible. Reducing the need for the user to learn how to use CFX's post-processing software would therefore be an advantage. A USRPRT routine was written to produce output files that would be useful for the rest of the wind resource estimation process automatically, without the user having to extract the data manually with the post-processor from each run case.

Two main versions of the output routine exist; which one is called depends on the choice given in the pre-processor.

The first, used mainly in testing, outputs all field variables at every cell centre. This data set can then be analysed in other programs, for example, Matlab. (Although Matlab is slightly less good at producing complex 3D plots of flow fields than Analyse, the CFX post-processor, it does enable you to compare the outputs of several runs, something that is difficult and time-consuming in Analyse.) This facility was used extensively in the development phase of the work, but will probably be less used in the final application due to the very large size of the data sets.

The second version will output 2D 'sheets' of data at a constant height above the ground surface, and vertical profiles at specified locations. The locations of these are given in a specification file produced by the pre-processor. These files enable rapid production of, for example, wind speed maps at turbine hub height, and shear profiles at turbine locations. Extracting data at a constant distance from the ground is something that cannot easily be done in Analyse.

For the near-horizontal sheets, the routine looks at each column of cells, and interpolates the profile (for each variable) to the desired height, and outputs a table of values to a file. The filename includes the height, to distinguish it in cases were more than one height is requested e.g. `height00040.dat`.

For the vertical profiles, the routine performs a 2D horizontal interpolation to the desired location for each height step, and outputs the result to a file. One file (`profiles.dat`) is used for all the profiles, as there might be many specified in a large wind farm.

5.5.6 Comments on the system

Although this collection of user routines and data files looks rather daunting, the process is quite transparent to the user. Settings are chosen in the pre-processor, and the data files generated automatically - the user should not need to read them himself. However, they can be accessed for troubleshooting, hand-optimisation, or other advanced uses.

The system admittedly seems rather unwieldy, and is the result of piece-wise accumulation during the research process. A more streamlined approach to the data transfer between pre-processor, solver, and post-processor could be implemented, but there was not time to implement this as part of the research project.
While some of the internal details of the system are a little clumsy and difficult to maintain, it is however, perfectly usable, and reasonable to the end user.

5.6 Validation

Validating a model of a complex system like the ABL is not trivial, and validation data is difficult to obtain. Theoretical or analytical test cases are not always available or appropriate. Wind tunnel tests have scaling problems, and large scale real-life data acquisition is expensive. However, one well-known data set exists for measured flow over topography - the Askervein Hill project.

5.6.1 Askervein Hill

The Askervein Hill project is one of the few full-scale field measurement campaigns of flow over a real hill. The project took place in 1982-83, and is still one of the benchmark cases for validating models of wind flow over terrain. Data and descriptions are taken from the main project report ASK83 (Taylor et al. 1985), and various additional papers (Taylor et al. 1987, Salmon et al. 1988, Raithby et al. 1987).

The measurements took place on the isolated Askervein (or Aisgerbheinn) Hill on the Scottish island of South Uist. For location map see Fig 5.1. The hill is 126m high, rising out of the flat coastal plain, and is as close to a 'mathematical' hill shape as you are likely to find, with an oval plan, and smooth outline. Photos of the hill are reproduced here as Figs 5.2 and 5.3.

The project used (at various times) 40 to 50 anemometer masts, giving an unprecedented degree of spatial resolution of the flow field. Recording runs were carried out under different wind conditions, each with wind from a consistent direction.

The anemometers were located along three lines, two ('A' and 'AA') going up and over the short axis of the hill, and the other 'B' going along the long axis of the hill. Only results from 'AA' and 'B' have been used in this validation work. Four named points are also referred to:

'HT' - Hill Top, the highest point on the hill.
'CP' - Centre Point, near the SE end of the hill, at the intersection of AA and B.
'BS' - Base Station, a point on the A865 near the hill.
'RS' - Reference Station, an anemometer mast about 2km SW of the hill.

The numbering scheme for the anemometers is the distance, in tens of metres, from a selected named point. For the AA line, this is the distance SW or NE from point CP

(e.g. AASW40). For the B line, it is the distance NW or SE from HT, (e.g. BSE90). The same scheme has been used here.

All these points are plotted on a map of the area in Fig 5.4.

Figure 5.1 - Location map of Askervein Hill

Figure 5.2 - Photos of Askervein Hill. Taken from near the small crossroads on the A865 about 750m SW of the summit of the hill, looking NE.

Fig 5.3 - Askervein Hill from the NW, looking roughly SE along the hill.

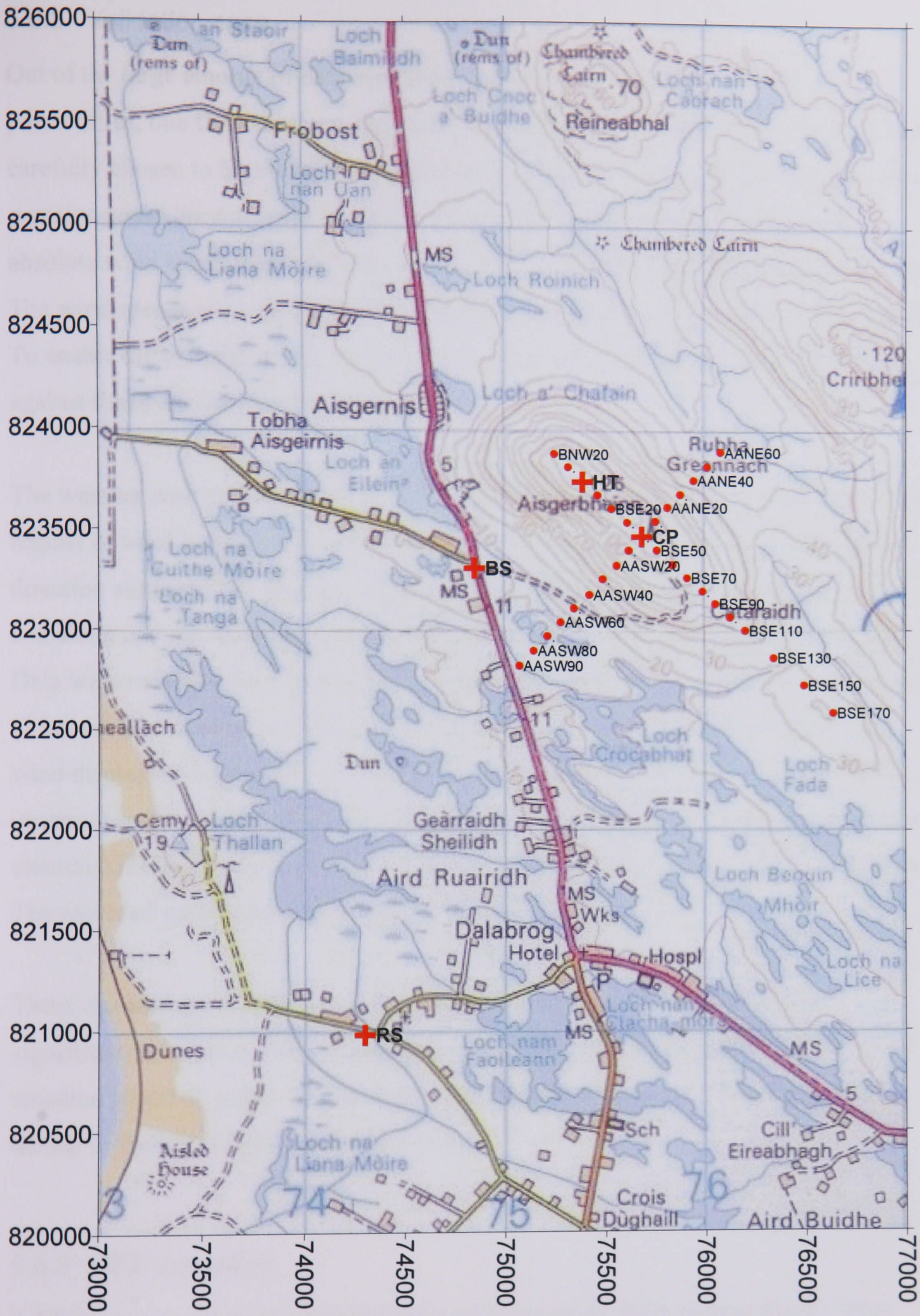

Figure 5.4 - Askervein Hill, and the 1983 anemometer positions.

5.6.2 Validation case

Out of the large amount of data available, and the huge number of modelling possibilities, one flow case was chosen to act as a validation case, MF26-D. This was carefully chosen to highlight flow conditions that should prove interesting. The report contains normalised average wind speeds, to remove the effect of variations in absolute wind speed from one run to another, and temporal variations during each run. The wind speeds were normalised against that recorded at the 'reference station' mast. To enable direct comparison, all the CFX results presented here are also normalised against the prediction for the RS location.

The weather was generally cloudy, with winds of about 7m/s. This is in the operating regime of wind turbines, and should display reasonably neutral stability. The wind direction averaged 225 degrees, roughly perpendicular to the major axis of the hill, and along one line of anemometers (line AA) and perpendicular to the other (line B). Data were recorded for a reasonably long duration by the standards of the experiment (5 hours). The description of the run in the report (Taylor et al, 1985) says that the wind displays a large speed up on the hill crest, with a large reduction in wind speed upstream and in the lee of the hill. Flow separation was difficult to observe and record unambiguously, but the authors of the report suggest it may have occurred in this run. The recorded speed data would support intermittent separation.

These circumstances provide an interesting test case. The test case provides significant but surmountable challenges to the CFD model, and should be the sort of situation where an improvement over linear models should be visible, especially in the lee of the hill if flow separation occurs.

5.6.3 CFX simulation

A CFX run was set up to resemble the conditions of the field measurements. Runs were performed in a single direction, but varying other domain and solver parameters. Given below is the output from the 'view settings' option in the pre-processor for the final version of the Askervein model:

Current settings:

i (streamwise) 2500m upstream of centre, 5000m lead in, 2000m downstream, in 210 cells, spacing 25m

j (transverse) 1500m halfwidth from centre, 120 cells, spacing 25m

k (vertical) domain height=1800m, 35 cells, expansion ratio=1.1700, => max bottom cells size= 1.26m

Total grid cells= 882000

Co-ordinates of domain centre: 75678,823465

Rotation angles 225

Run type: terrain=topo, inlet=profile

Setting topography from file M:\My Documents\cfx\askervein\nf62.xyz

Roughness set from map file M:\My Documents\cfx\askervein\rough_askmap_new.mat

Inlet profile specified from file M:\My Documents\cfx\basic model\roughnesses\prof_0_0005_30ms.mat

Solver preferences: iterations=500, diff scheme=CCCT turb model=RNG K-EPSILON

USRPRT output of plane(s) at heights:

10 60

USRPRT output of profiles at points:

74300 820980

74846 823306

75383 823737

...

A variety of alterations on the basic model were tried out, to investigate the sensitivity of the model to the different parameters. These included both parameters determining the physical situation being modelled, such as domain size and ground roughness, and the mathematical model used, such as differencing schemes and turbulence models. The settings given above gave the best overall results.

5.6.4 Results

Various solver parameters were investigated, to see the effect they had on the final solution, and on the convergence of the run.

5.6.4.1 Solver parameters

CFX has a choice of which underlying numerical solver to use. In the end, it was found that the best was the default setting of the 'Stone' solver for u, v and w, and the 'line solver' for k and ε. Other solver settings did not produce any noticeable change in the final solution, but in general took longer to converge. It was found that the under relaxation factors could be increased from their default values to 0.7 (for all equations). This speeded up the convergence rate in this topologically simply domain, without unduly affecting the final solution.

The differencing scheme used was found to have a significant effect, both on the final solution and the time taken to converge. The default is the Hybrid scheme. This is only first-order accurate, but is very robust and reliable. Some sources (Wright et al 1999) indicate that higher order schemes are necessary in this sort of problem field, especially if flow separation might be present. After testing the schemes available in CFX4.4, it was found that the 'CCCT' scheme gave the best results. This is a variant of the well-known QUICK scheme, which is a 'quadratic upwind' scheme, using two bracketing nodes, and one further upwind node. However, the quadratic formula used can lead to small under- or over-shoots, which can cause problems. Similar schemes have been developed, such as CCCT, but re-formulated from the original to enforce boundedness, and eliminate non-physical overshoots.

The CCCT scheme took much longer to converge, but gave better results, see Figs 5.5 and 5.6. Both schemes did well on the upwind side of the hill, but the higher order scheme did better over the hill crest and predicted a sharper drop off in velocity in the lee of the hill, and was closer to the measured data. It was felt that in cases with higher gradients, such as highly complex terrain, and large changes in roughness, the

extra accuracy of a higher order scheme would be necessary to adequately predict the flow field.

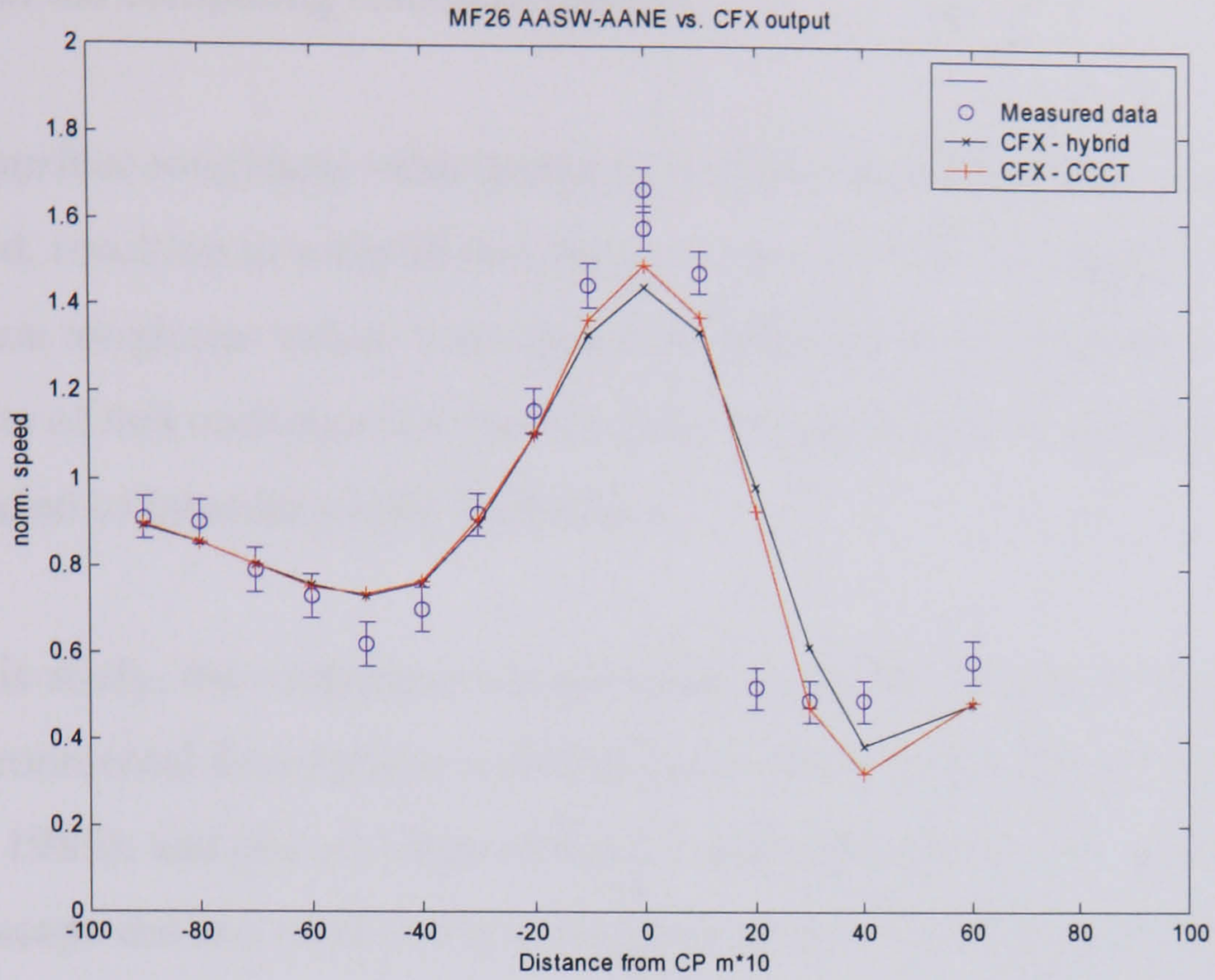

Figure 5.5 - Normalised speed against position. Comparing different numerical schemes for line AA.

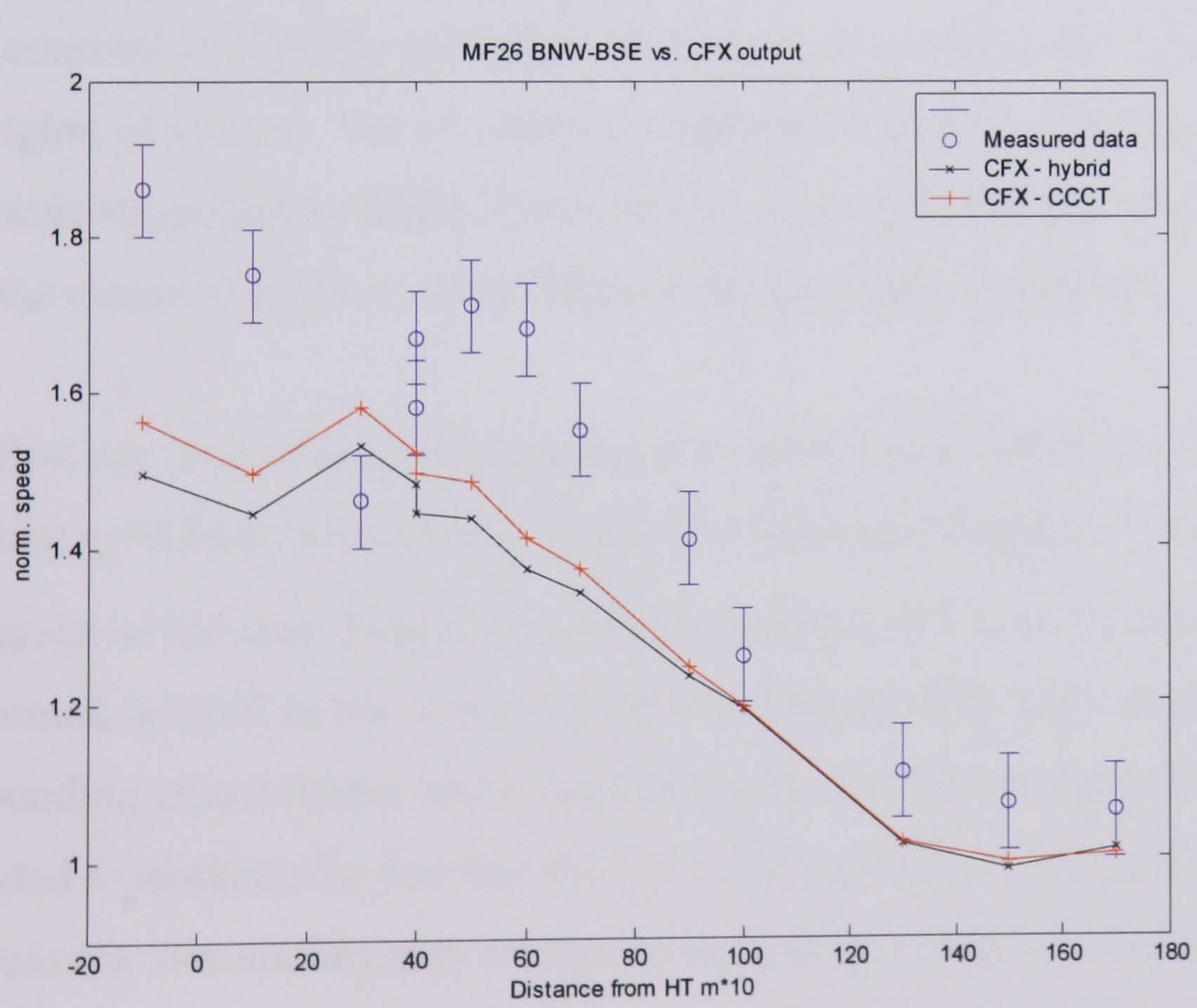

Figure 5.6 - Normalised speed against position. Comparing different numerical schemes for line B.

5.6.4.2 *Physical parameters*

Various physical parameters of the model were altered, to see the effect on the results. and on the computing resources required.

The surface roughness value assigned to different areas of the solution domain was varied, resulting in a significant change in the results, see Figs 5.7 and 5.8. Changes in surface roughness values were therefore included in the sensitivity analysis. The results of this underline the importance of accurate ground roughness descriptions in this kind of boundary layer simulation.

In this study, the roughness was specified using two information sources: environmental descriptions and roughness values given in the original report (Taylor et al 1985); and photos taken of the hill and surrounding area in 2003. Most of the landscape did not seem to have changed much in the intervening 20 years, and the 2003 photographs generally backed up the estimates made in the 1980's.

The roughness value of the sea (i.e. the inlet and the first few km of the domain) was kept constant to highlight the effect of changing the roughness of the land surface near the region of interest. The sea-surface roughness was set to 0.0005m, in the middle of the range suggested by ESDU (Item 82026). The inlet profile was also set to match (i.e. the output of a 2D run over 50km of the specified roughness).

The first run (and other previous tests) were performed with the land surface at a constant z_0=0.03m, which was judged to be reasonably representative of the average roughness of the area. Higher and lower roughness (0.1m and 0.01m) runs were performed, as well as one with a variable roughness. This had a higher value for the surrounding area (0.05m), and a smoother value for the hill itself (0.02m). This was intended to simulate the fact that the hill itself was relatively smooth and open, whereas the surrounding area seemed to have more roughness elements. These include a few scattered buildings, slightly more vegetation, and numerous small lakes. Although the water surface itself would be smoother, the step that there appeared to be down to each pool was judged to increase the overall roughness of the area.

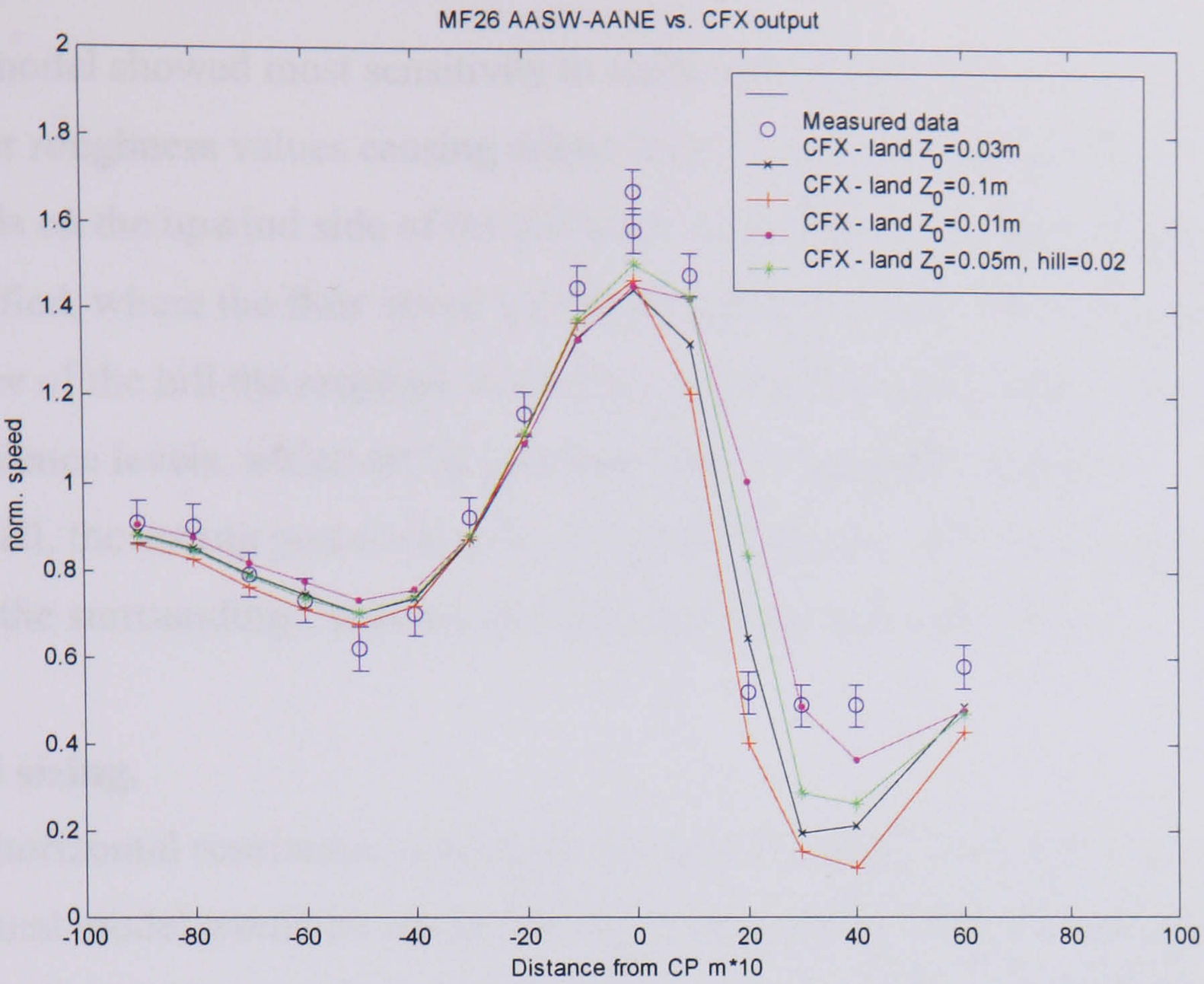

Figure 5.7 - Normalised speed against position. Comparing different ground roughnesses for line AA.

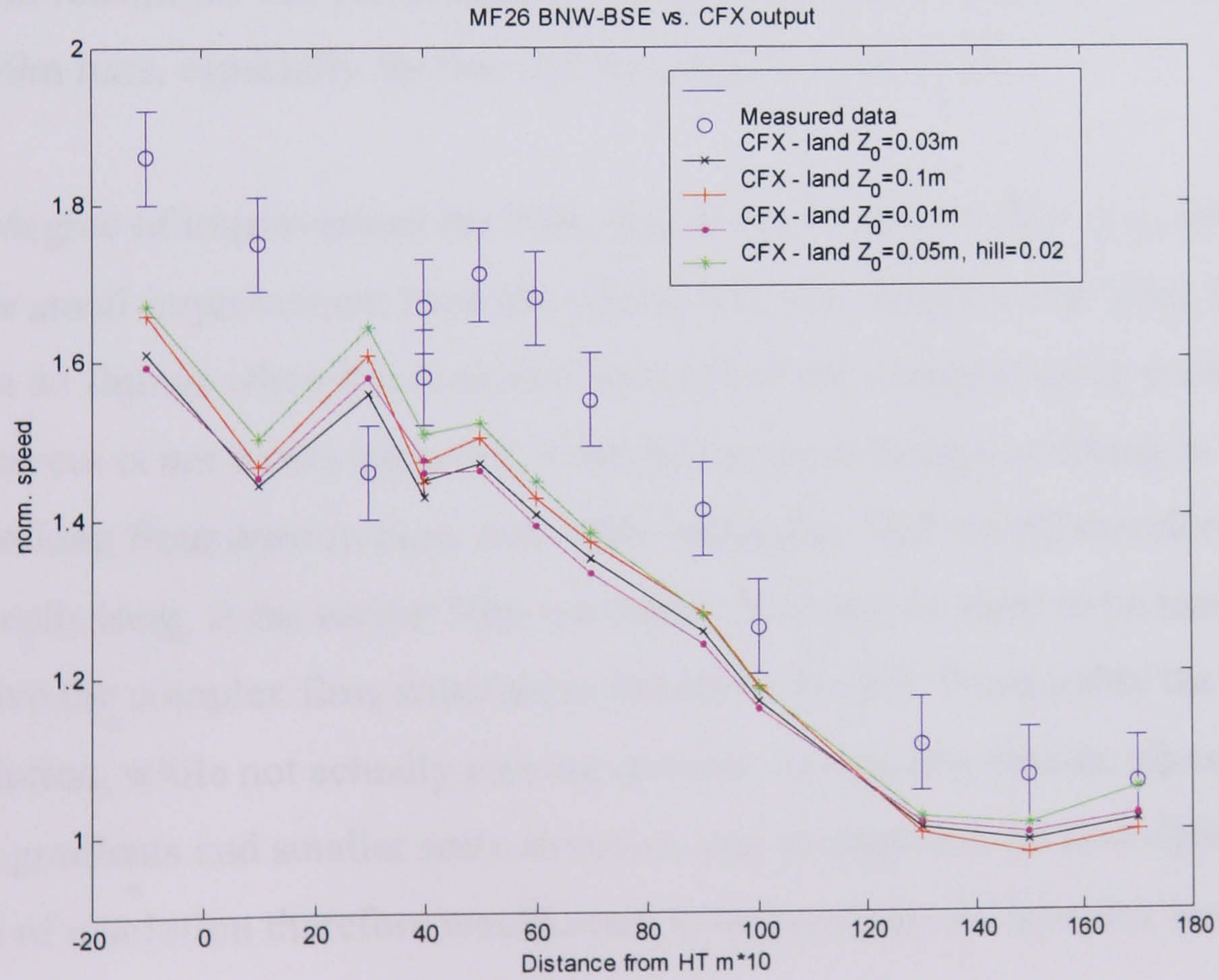

Figure 5.8 - Normalised speed against position. Comparing different ground roughnesses for line B.

The model showed most sensitivity to surface roughness in the lee of the hill, with higher roughness values causing dramatically lower wind speeds (Fig 5.7). The speeds on the upwind side of the hill were little affected by the roughness value specified, where the flow speed is primarily determined by the topographical shape. In the lee of the hill the response of the flow field to the topography is very dependant on turbulence levels, which are in turn dependant on surface roughness.
Overall, the setting perceived to be the most 'realistic', with the hill itself smoother than the surroundings, reassuringly gave the most accurate results.

Grid sizing.

The horizontal resolution of the grid was also investigated. It had been assumed that the final model would be run at 50m resolution, as this seemed from experience to be adequate for this sort of work and similar to the required resolution of the output. The topographic input data is also provided at 50m resolution, so it was perceived that there would be little benefit from going higher. However, as part of the testing, a run at 35m resolution was performed, and found to display markedly better accuracy than the 50m runs, especially for line AA (see Figs 5.9 and 5.10).

The degree of improvement the 35m case showed over the 50m case (when compared to the small improvement from the 100m) case was slightly surprising. However, this is not so strange when it is looked at in terms of the situation being modelled. Askervein is not a very large hill, with the lee slope being something in the region of 300m long from crest to base, and ~80m vertically. This would therefore be about 6 grid cells long, at the earlier 50m resolution. This would seem to be inadequate to resolve the complex flow structure in the lee of the hill. Presumably the 35m resolution, while not actually picking up more topography details, allowed for higher flow gradients and smaller scale structure, and so captured the flow field better. This level of resolution therefore would seem to be necessary in complex terrain of this sort of scale.

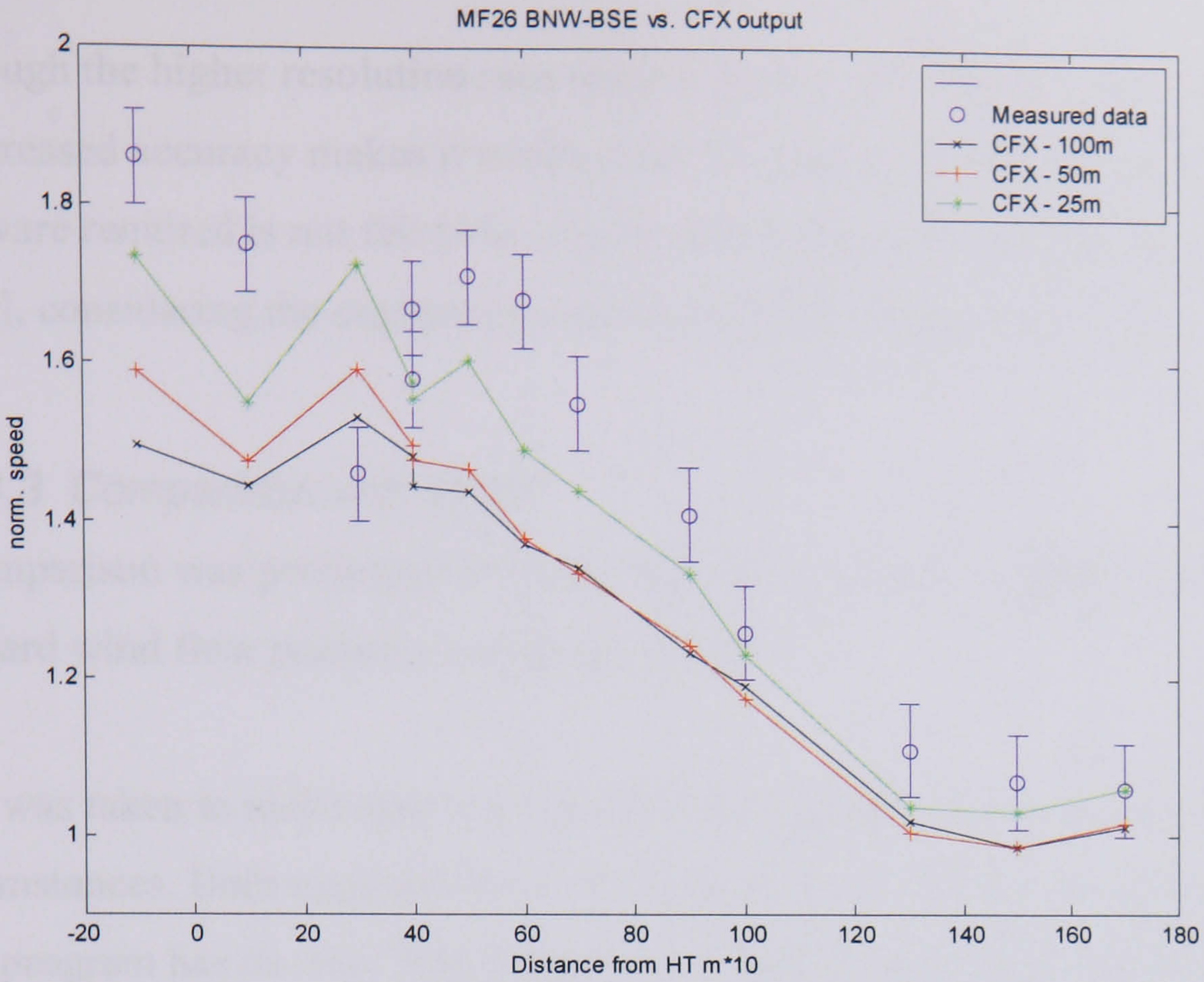

Figure 5.9 - Normalised speed against position. Comparing different grid resolutions for line AA.

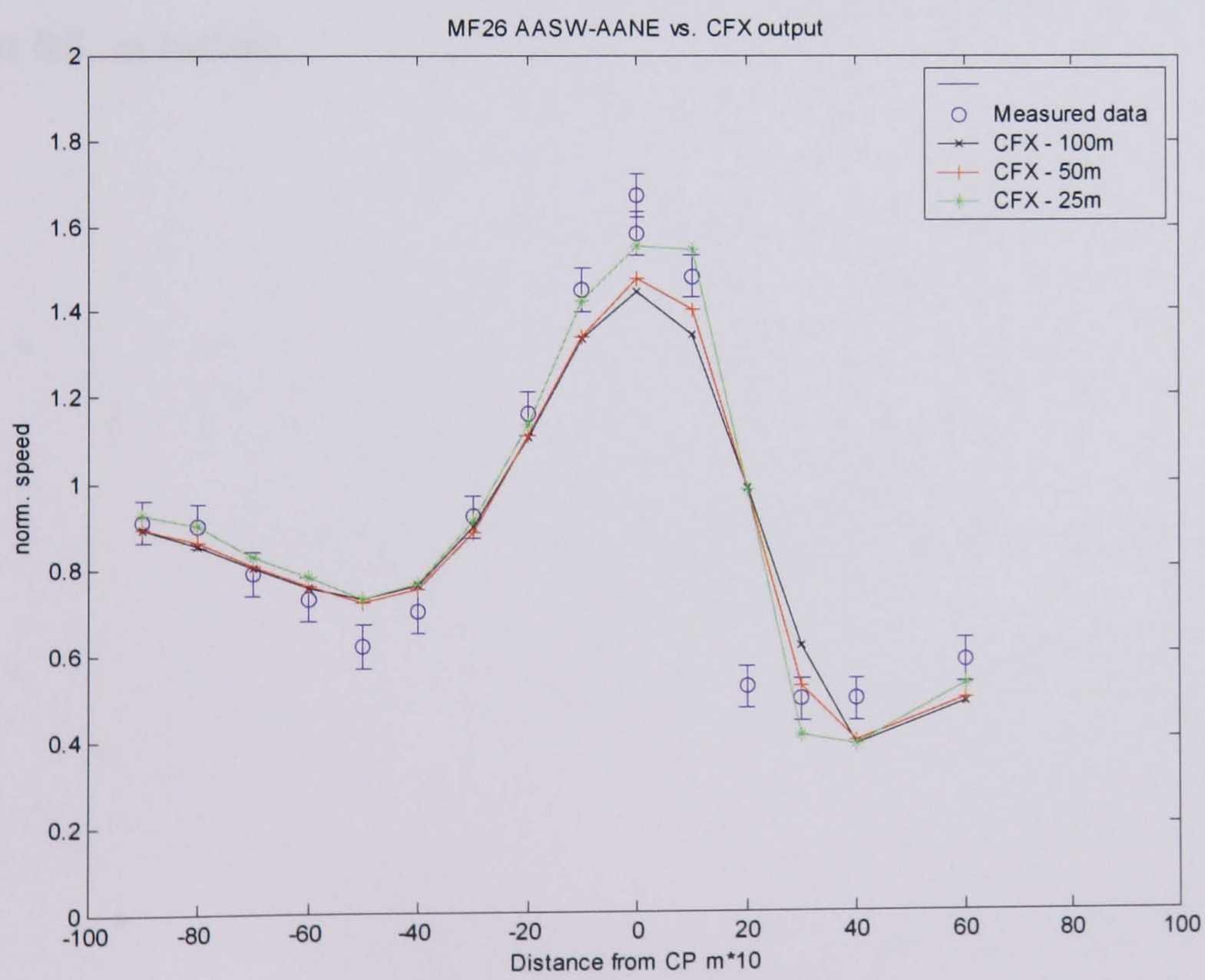

Figure 5.10 - Normalised speed against position. Comparing different grid resolutions for line B.

Although the higher resolution runs require greater computing resources, the benefit in increased accuracy makes it worthwhile. The higher specification of computer hardware required is not felt to be a great problem in the long term utilisation of the model, considering the continuing rapid decrease in computing costs.

5.6.4.3 Comparison with WAsP

A comparison was performed between the best of the CFX models, and the industry standard wind flow prediction program, WAsP.

Care was taken to make sure that CFX and WAsP were simulating the same circumstances. Both used the same Ordnance Survey data for the topography. While each program has its own 'map editor' for defining roughness areas, the definitions were kept as similar as possible. Both were set up to match the 225° wind direction of the MF26 case. WAsP was set up to provide a wind speed estimate at each of the anemometer locations, and point RS. The wind speeds were then normalised against that at RS, as before.

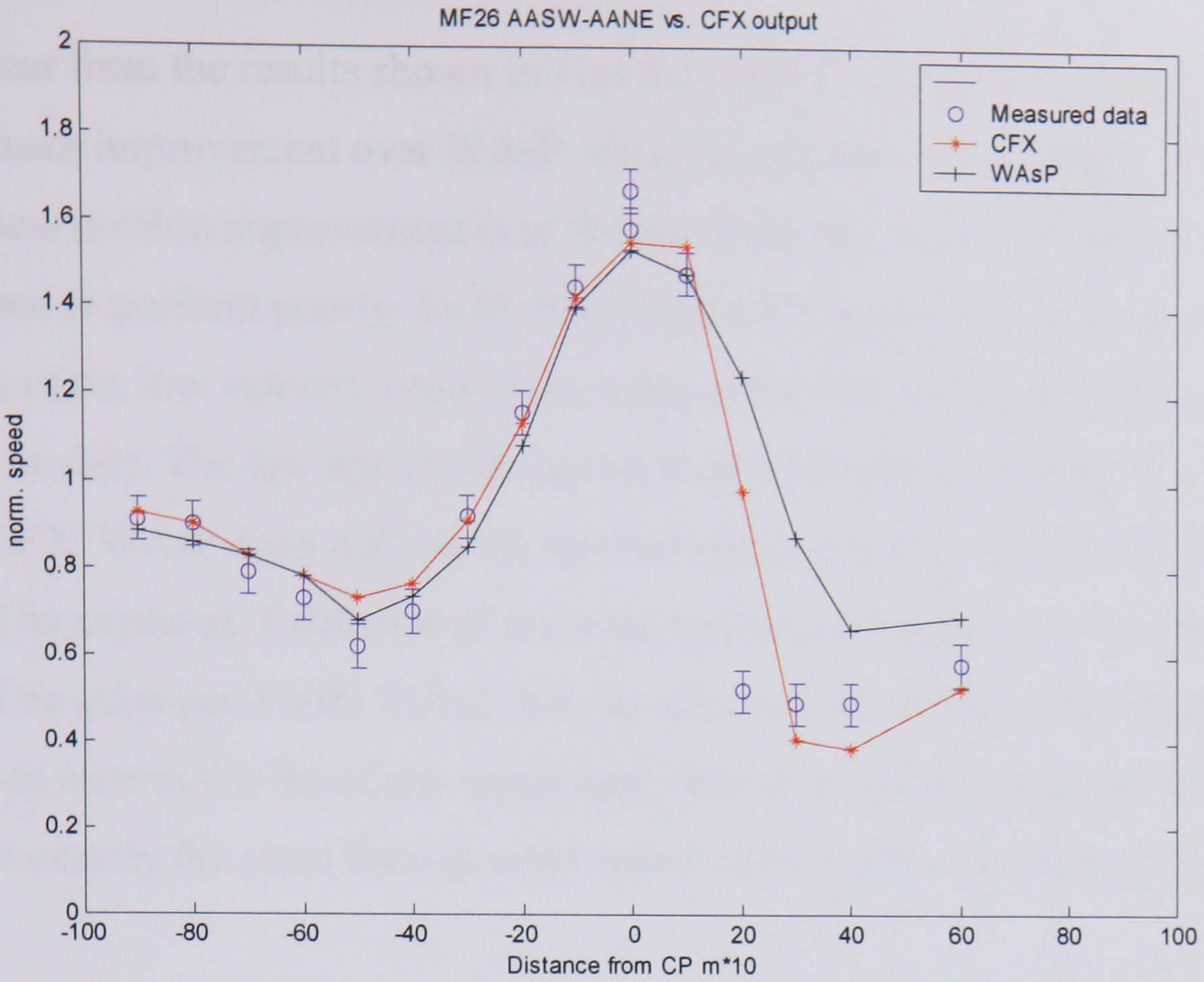

Figure 5.11 - Normalised speed against position. Comparing WAsP and CFX predictions for line AA.

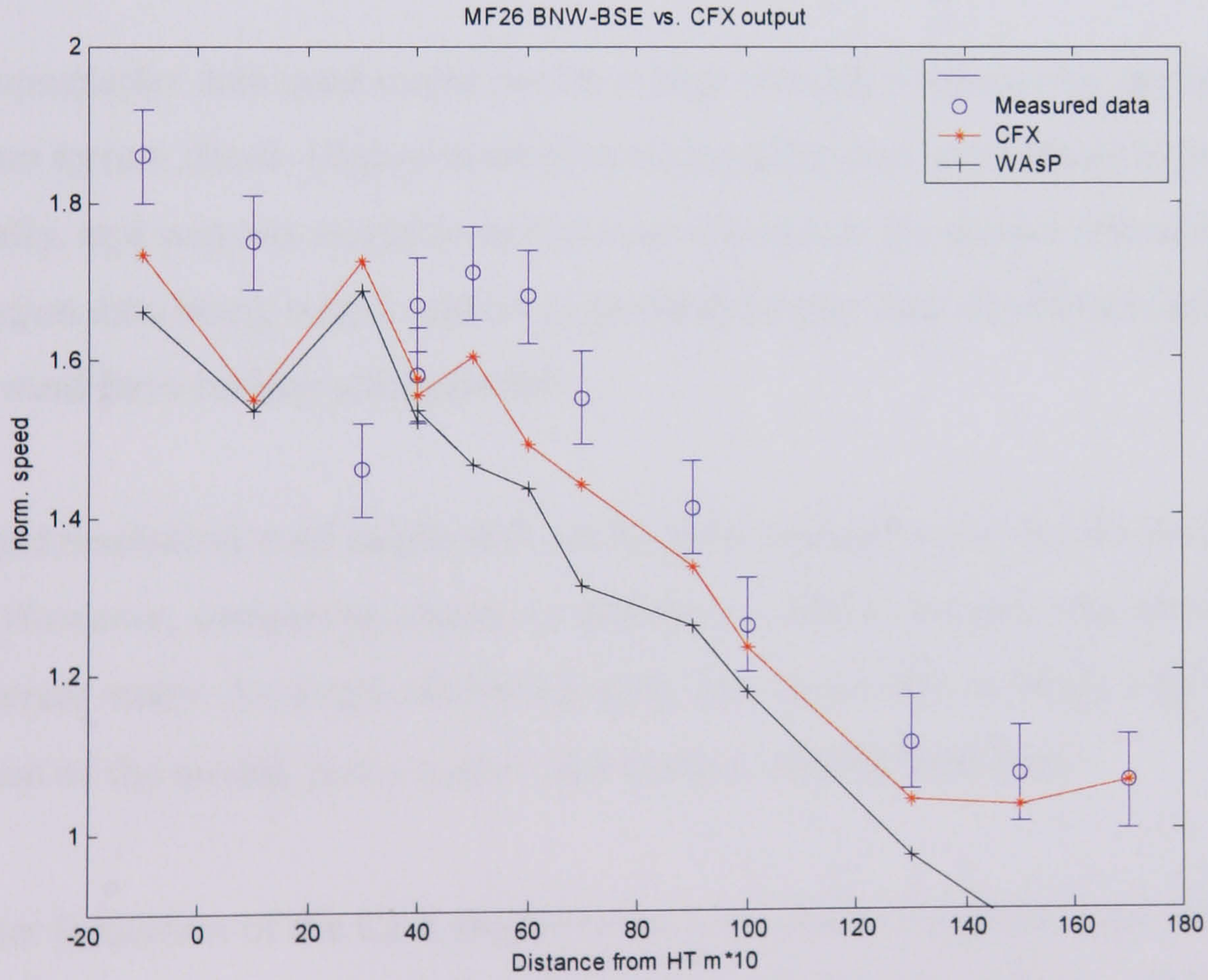

Figure 5.12 - Normalised speed against position. Comparing WAsP and CFX predictions for line AA.

It is clear from the results shown in Figs 5.11 and 5.12, that CFX is capable of a significant improvement over WAsP, even though there are problem areas.
The most notable improvement is in the lee of the hill, where WAsP would be expected to perform poorly. Even though the CFX model does not capture all the details of the low velocity zone in the wake of the hill, it does much better than the linear models. The low speed area just in front of the hill is slightly less well predicted with CFX. WAsP does well on the upwind side of the hill, and on the hill crest, as would be expected. Estimates of the wind resource for turbines on the top of the hill would be quite good with WAsP, but the accuracy would fall of dramatically if turbines were in the lee of any significant hills. It is worth noting that WAsP predicts almost exactly the same drop in wind speed upwind and downwind of the hill.

The non-linear CFX code does much better then WAsP in the lee of the hill, but still struggles to capture the very sharp drop off in wind speed measured in the field experiments. This is probably due to a number of factors.

The topography data used might not be at high enough resolution to capture all the relevant terrain detail. Higher resolution topography data would have to be obtained specially, and was not available in this case. However, the spatial resolution of the validation data being tested against is probably higher than would be required for most wind farm turbine siting studies.

The grid resolution used might still not be good enough to resolve all the details of the flow. However, computing resources and time available limited what could be done in the current study. As mentioned previously, this is not seen as being a fundamental problem of the model, just a matter of awaiting suitable hardware.

Another limitation of the CFX model is the k-ε turbulence model used. While a standard and well-used model, it is known to have difficulty in areas of flow separation and wakes. Inaccuracies in the turbulence model in the wake of the hill could account for some of the problems seen there. Although these runs used the

RNG variant of the k-ε model, as this is generally better for high-Reynolds number flows, it is still the same basic model, with much the same limitations. More complex turbulence models, such as Reynolds stress models have their own limitations. While these should be able to give better results in these difficult conditions, they are less numerically robust, take longer to converge, and require more initialisation data, which may well not be available. All the Reynolds stresses would have to be specified at the inlet, and while this could come from a pre-run (as the inlet profile does in the current set up), such information is not routinely monitored at wind farm sites, so measured validation data would be difficult to obtain. An interpretation of the turbulence values (from the standard deviation of cup anemometer speed) would be the only validation check possible against measured data from the wind farm site.

While a 'basic' model like the k-ε has its limitations, they are reasonably well known, and it has the benefit of being relatively standard. Even though it has problems, it is still theoretically possible for it to predict flow separation, which is completely impossible for the linear models like that in WAsP.

A flow separation bubble was observed in the lee of the hill in some of the CFX runs. A visualisation of such flow separation is shown in Fig 5.13 from the post-processor CFX Analyse, with streamlines plotted through the region.

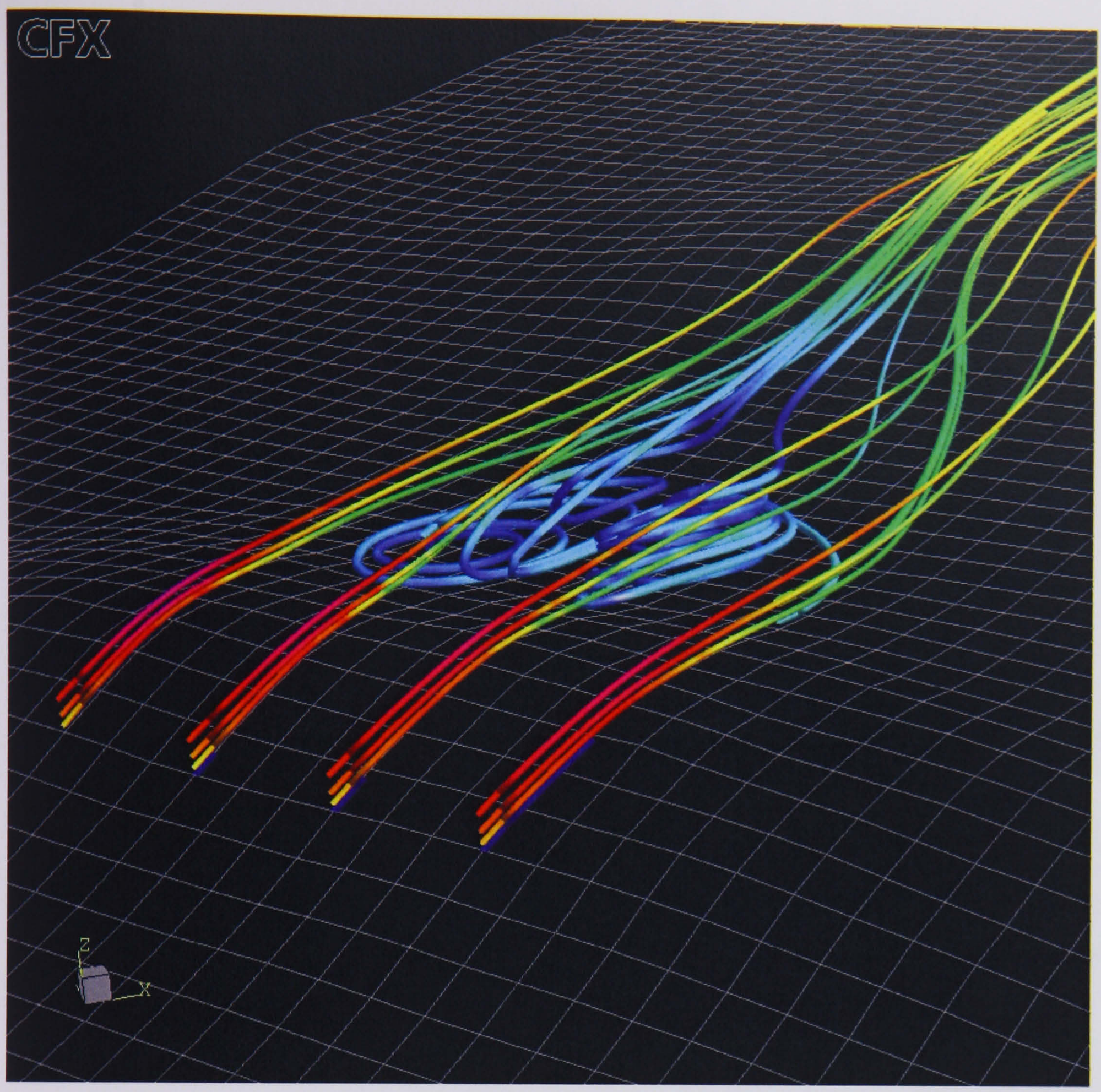

Fig 5.13 - Visualisation of flow separation behind Askervein Hill. View looking North, flow from SW.

The AA line of anemometers would be just on the left hand edge of the separated region, so the accurate prediction of the size of the region would be critical to the predicted vertical speed profile. It should be noted that the cup anemometers used in the field study record flow *speed* of course, not velocity, so would not directly indicate recirculating flow.

The other aspect of such a flow regime that would not be captured by any of the above modelling methods in their current form would be the temporal variation of the flow separation pattern. The separated region would probably not be steady, and may

well move about or oscillate. This would obviously not be captured in the current steady-state CFX calculations. CFX is capable of performing the transient calculations that would be necessary to investigate this area, but due to time constraints it was necessary to limit the scope of this work to steady-state calculations. However, the limitations of this approach is recognised. It may ultimately prove necessary to perform a transient calculation and take a time average from the results to get a true representation of the average flow field in such a region.

5.6.4.4 General comments on results

It is noticeable in all of the above sets of results for the B line that there is a large discrepancy between the predicted and measured values for the BSE30 anemometer site (labelled +30m from HT in graphs). The wind speeds predicted by CFX seem to follow an opposite trend to that measured. In that region of the hill top, CFX generally underestimates the measured wind speed, except for this one point, where it significantly over predicts it. The measured wind speed at BSE30 is much lower than at the neighbouring points, whereas CFX predicts it as being higher. There is clearly a significant anomaly at this location. However, the sudden deviation from the general prediction trend would point to something specific about this location, rather than a general fault in the CFD modelling methodology. The fact that the WAsP results closely follow the CFX ones would also indicate something odd about this data point. Another researcher also using the Askervein data set to validate CFD models has also found similar problems with the data from this location, even with runs from different flow directions [Paul Stangroom, personal communication].

One explanation would be a fault with the anemometer, causing it to read low, but this does not appear to have been documented in the Askervein report. The other explanation is that the flow is influenced by a detail of the topography that does not show up in the OS 50m resolution data. This explanation is lent some weight by maps in the Askervein report. The original Askervein project commissioned a high-resolution survey of the hill, and map of this is included in the ASK83 report. This was only available to the current research project as a poor photocopy. This prevented

its use in the CFX work, but does enable visual inspection of the hill shape. From this it can be seen that the hill crest, or ridge line is not an exact straight line, unlike the lines of anemometers. The BSE30 point is slightly SW of the crest of the hill (upwind in the flow case considered). There is also a small 'bump' in the ridge line at this point, causing the anemometer location to be effectively immediately upstream of a small hillock, rather than on the crest of the ridge. This would not show up on the digital terrain data used in both the CFX and WAsP runs, but could have an effect on the speed recorded at the relatively low (10m) anemometer.

This may well be enough to explain the anomalous result for this location. It does however highlight two points. The spatial resolution of the terrain data is on the limit of being too coarse for accurate simulations on the relatively small scale of Askervein Hill. Most wind farm projects are on a somewhat larger scale however, and the 50m resolution data set should prove sufficient. It also provides a reminder of the disproportionately large effect of small obstacles very close to monitoring points. This is something that should be carefully considered when siting anemometers, and any such concerns recorded.

However, after all of the above shortcomings have been looked at, it is still clear that a steady state approach, even with a fairly basic turbulence model, is capable of providing much superior results to the current linear models. While the linear models provide reasonable predictions for the tops of isolated hills, the CFD approach comes into its own in more complex terrain. Many wind farms are currently being built or considered in hilly upland terrain, where the turbines are often, effectively, in the wake of many hills upstream. This CFX-based methodology has the potential to provide much improved results in this sort of situation.

6 Advanced roughness modelling

During the course of my investigations, it became increasingly clear that surface roughness, particularly forests, were of considerable importance to resource estimation. Vegetation is very efficient at extracting momentum from the wind, and as a result has a remarkably large effect on the available wind resource. The accurate simulation of such situations is far from straightforward, as quickly became apparent. Testing of the current models was carried out, to assess their strengths and limitations. A more sophisticated modelling approach was then developed, which was also tested against measured real-site data.

6.1 Approaches

The standard approach to ground roughness is to describe it as a single 'roughness length', an idea inherited from traditional fluid mechanics. This roughness length is a scaling parameter that describes how much momentum is removed from the flow for that surface. This is fine for predicting the overall response of the flow to the surface, but it contains no information about the structure of the flow close to the rough wall. Two areas need addressing to provide a more complete view of the effect of ground roughness on the flow field. These are the horizontal variability of the roughness, and more detailed modelling of the vertical structure of the flow over roughness elements.

6.2 Variable roughness length

The most obvious increase in complexity in this sort of wind resource model is to introduce a spatial variability in the surface roughness. This is included in the WAsP program, and in various analytical boundary layer formulations, such as the 'Deaves & Harris' formulation. One of the main criticisms of Powergen's current CFX model was that it did not allow for variations in ground roughness length. The CFD methodology itself is theoretically capable of calculating the flow field with an arbitrary surface roughness for each cell of a wall boundary. However, this had never been implemented within Powergen. The resources for writing the user FORTRAN code,

and the roughness data input had not been available due to commercial pressures. Other researchers had implemented variable roughness in their CFD models, (Montavon, 1998; Maruyama, 1999) and these works provided useful insights for developing a strategy that would fit in with the rest of the CFX model.

An integrated system was developed for specifying roughness area information within the custom pre-processor, and supplying this data to the user FORTRAN routines in the solver. This specification system is documented in the 'Basic modelling' chapter, and was included in the Askervein Hill validation cases. However, that test case was mostly aimed at validating the 'topographic' element of the model, rather than the 'roughness' modelling.

The roughness specification system and pre-processor were written so that they could be expanded to include more complex roughness models than the standard 'roughness length' approach.

6.3 Roughness plus displacement

The first increase in complexity in models of ground roughness is to introduce a displacement height. This is a commonly used model in analytical formulations of flow over canopies (i.e. 'deep' roughness elements like vegetation). This assumes that rather than starting from the actual ground surface, the logarithmic profile starts from a 'virtual' surface, some distance above the ground. This makes some allowance for the different spatial distribution of force retarding the flow. In a traditional rough surface formulation all the momentum is extracted at the wall, which is a reasonable assumption for surfaces which look similar to the 'sand-grain' roughness it was developed for. With roughness elements like vegetation, momentum is removed from the flow throughout a volume, giving a deep layer within and just above the canopy which departs from the log law.

In the 'roughness plus displacement' model, the log law profile is displaced upwards to match with the log law profile that develops above the canopy. However, there is

still a region up to about 1.5 times the canopy height that does not obey a log law (Kaimal & Finnigan 1994). This is acceptable if you are interested in the flow field at a significant distance above the canopy. While this condition would be fulfilled for crops and low vegetation (in wind energy studies), it might well not be for tall trees, where heights of interest might be near the tree tops.

Although this roughness model could be implemented in a CFD code, there are several reasons why it was not considered to be appropriate to do so. In addition to the theoretical issues discussed above, the main reason was specific to an implementation in a CFD code, rather than a single BL profile. The analytical formulation says nothing about what happens below the displacement height, as the formula is not valid there. It acknowledges that there is actually still flow in this region, but that it is not described.

A CFD code would have to have a description of the flow everywhere inside the domain. The displacement length would have to be simulated by physically displacing the bottom boundary upwards. For a single location in the x-y plane (a simulation of a 1-dimensional column), and at heights well above the top of the canopy, this would give the same results as the analytical formulation. However, there would be problems in a full 3D version with variable roughness. A change from a small roughness to a large one would cause an increase in the displacement height, and a sudden increase in the height of the bottom boundary. This would be treated by the solver as through it was an actual physical obstacle, rather than an `undefined` region of flow, as the analytical model would. This would effectively introduce a blockage into the flow, including a speed-up over the top of the 'blockage' and associated compression of the streamlines. An additional vertical velocity would also be introduced, with flow going up just in front of an increase in displacement length. None of these effects would occur in the real flow.

The nature of CFD forces you to take a strict, physical interpretation of what is really a mathematical 'trick' or abstract concept. The displacement length addition to the basic roughness length model is therefore not well suited to a CFD-type flow

simulation. A roughness model based in more fundamental physics would have to be found.

6.4 Resistive volume model

The most obvious and appealing way of modelling flow through a vegetation canopy is with some sort of porous volume. This sort of approach is often used in CFD work to allow for the effect of regions of complex geometry, where what is required is the overall effect on the flow, rather than the details of the flow round the obstacles. For example, this approach is used within Powergen to model tube banks in boilers and heat exchangers. This is used in applications where the flow around each individual tube is not of interest, just the overall pressure drop (for example).

This idea is easily extended to trees in wind flow studies, where the flow around each branch is not needed, just the overall flow retardation. There seems to have been relatively little historical work on this approach, although recently a few researchers have used this approach. Lea and Vosper (2002) use a 'drag term' to represent forest canopies, but only looked at flow over 2-dimensional hills. Belcher et al (2003) develop an analytical model for drag forces in a canopy, and evaluate this in a resistive volume. The work is mainly theoretical, and looks at the adjustment of the boundary layer to a canopy, but with less emphasis on CFD modelling.

The idea of treating vegetation as a porous volume, with a resistive body force, is appealing. It uses basic fluid dynamics, of a sort that can be easily included in a CFD model, rather than a boundary layer scaling formula that is difficult to incorporate in a CFD model. Above the level of calculating an appropriate resistance for a given obstacle, the calculations are left entirely to the CFD solver. No assumption is made about the shape of the boundary layer. This gives much more flexibility about the sort of roughness elements modelled. The method of calculating the actual drag force of the trees is described in the next section.

6.4.1 Implementation

There are two aspects to porous volume calculations in CFX. Firstly, the reduction in the fluid volume due to the space taken up by the obstacle, and secondly, the resistive force experienced by the fluid due to flow around/through the obstacle.

Most vegetation that would be considered in wind energy work is relatively 'finely divided' i.e. of small volume and high surface area. This means that the effect on the flow due to the displaced volume of air is small compared to the effect from drag. The shape and large surface area of numerous branches, twigs, leaves etc. makes them very effective at removing momentum from the flow considering their total volume. The blockage due to the reduction in volume would cause a slight speed up in the flow above the volume, and an upward displacement of streamlines.

The calculation of the drag force produced by each obstacle or roughness element is not entirely trivial. However, a simple approach was inspired by Rehm et al, 2000. This work on urban flows modelled trees using an approach it describes as 'strings of spheres'. In this, the shape of the tree (trunk, branches etc.) is outlined as rows of small spheres, approximating the overall shape of the tree. The sphere is a simple shape, and enough work has been done on flow around it, for the drag coefficient to be calculated directly for a given flow regime (Reynolds number, etc.). The drag for each individual sphere can then be inserted into the CFD model as a point sink of momentum.

This methodology was developed for smaller scale work on flow around single buildings or small groups of buildings, where a single large tree can have a noticeable effect on the flow. It would be unnecessary to model every tree in a forest, but some of the ideas could used. The concept of modelling a tree in terms of simple geometry, so that its drag can be calculated theoretically, could be modified and used at larger scales. The term `resistance volume` would be a better description of the model than the original label of a `porous block` model.

It was decided to concentrate the modelling on simulating a commercial conifer plantation. The reasons for this were twofold: conifer plantations are the most common sort of forest that would have to be considered in wind energy studies; the sorts of trees planted (e.g. pines) are, fortunately, of a simple and geometrical form that is amenable to analysis.

From the initial inspiration, the idea changed to using rods rather than spheres to model the trees. Rods of circular cross section still have well defined aerodynamic properties, and also enable easier descriptions of pine trees. These can quite easily be visualised as a collection of cylinders of different sizes, for trunk, branches, and finally needles. Drag coefficients for the rods could then used to calculate the resistive force in the user FORTRAN routine that implements body forces.

6.4.1.1 Multiple rod model

To calculate the required parameters, a short study of representative vegetation was carried out. Individual trees and photos of sections of forest were analysed. It was decided to produce a simplified, single figure that would describe an average cubic metre of conifer forest. It was recognised that the resistance would actually vary spatially along with the variation in forest density, both laterally, and with height. However, it was decided to construct a simple model at first, that would describe 'average' conditions in commercial conifer plantations. Due to the complex nature of the forestry, the averaging process was performed by eye by the author, based on photographs and personal experience of such forests.

The structure of the trees was split into three categories: large branches / trunk; small twigs; and needles. The total length of each category of rod present in one cubic metre was estimated, along with the average width. The categories were judged to be as follows:

- Large items, such as the trunk and large branches: 5cm diameter, 1m total length. This is the equivalent of one good-sized branch going right through each metre

cube. The main trunk of each tree would be wider (for large trees) but would only be present in a small proportion of one-metre cubes.

- Medium/small branches: pine trees seem to have large numbers of long, thin sub-branches, radiating off the main ones. For these, 5m total length, at 1cm diameter was judged to be a reasonable approximation.
- Needles: Very large numbers of pine needles cover the small branches. If needles 2.5cm long and 2mm wide covered all of the 5m of small branches, with a needle on each side, every 4mm, this would give 2500 needles. The total length of these would then be 62.5m.

The drag coefficient for a cylinder perpendicular to the flow was found from Massey (1983) to be remarkably constant throughout the range of scales considered. For cylinder with a length 5 times the diameter, the *Cd* was a nearly constant 0.7, for Reynolds numbers in the range 600 to 60000, which covers pine needles to tree trunks. For infinitely long cylinders, the value was slightly higher and more variable, being between 0.9 and 1.1. As it was calculated that a large proportion of the total drag came from the relatively short needles, the lower figure was chosen.

The drag force generated is:

$$F = \tfrac{1}{2}\rho u_\infty^2 ACd \qquad (6.1)$$

where ρ is the air density, u_∞ is the free wind speed, A is the frontal cross-section area of the obstacle, and Cd is the drag coefficient.

Of this, A and Cd are known in advance, and ρ and u_∞ are (in general) known only in the solver, as the velocity in particular will vary. A combined ACd parameter for all the three item classes per unit volume was calculated:

Resistance parameter = $(1\times0.05\times0.7)+(5\times0.01\times0.7)+(62.5\times0.002\times0.7)=0.1575$

The actual body force could then be calculated in the solver.

While this parameter represented an average volume of tree, not the whole volume of a conifer plantation up to the top of the trees is filled with this - the sort of pines

grown often have a conical shape. From photographs and personal experience, it was judged that less than half the volume up to tree top height was filled with the resistive material (branches and pine needles) the rest being gaps between the tree tops or gaps between trunks. So, a value of 0.07 was judged a reasonable average over the whole volume.

While a reduction in density (and hence resistance) with height could have been modelled, this would have required much more complexity in the pre-processor and initialisation data. Using a single resistance value at a given geographical location could be implemented easily as an extension to the ground roughness specification in the pre-processor and run initialisation code.

The pre-processor was extended to allow for specification of a canopy height and resistance factor, as well as ground roughness. This information was read into the solver at run initialisation time, and passed to the USRBF user routine.
This routine loops though all the cell centres, and checks if they are under the specified canopy height. If they are, a resistive force is calculated using the local wind velocity, and added as a source term to the momentum equations.

While in this work, just one average resistance value was used for all wooded areas, the model could very easily be extended. Lateral variations in the forest density could be accommodated, rather than a simple forest / no forest distinction. The facility for this was written into the pre-processor, as an extension to the z_0 specification code, but in the current study, only one value of forest density was considered.

The height of the forest was modelled by specifying the appropriate number of grid cells as being in the porous volume. Again this could be altered in the pre-processor to account for different stages of forest growth. Vertical variation in the foliage density is not implemented in the current model, but could be added. This could be used to account for the conical shape of pine trees, with less leaf area at the top. Alternatively. thick deciduous forests often show a three-layer pattern, with a dense upper canopy, relatively clear trunk space, and denser understorey of small plants. With suitable

vertical resolution the model would be theoretically capable of simulating such a situation, but this level of complexity was not seen as necessary in the current work.

6.4.2 Validation against analytical models

Validating the model was not easy. Flow within the canopy is very complex and flow measurements are difficult to take accurately, due to the very high gradients and turbulence intensities. Analytical models are difficult to formulate, and none have the power and simplicity of those available in other ABL work, such as Monin – Obukhov similarity theory.

However, Kaimal and Finnigan (1994) present a review of some high-quality field measurement data that have been obtained. This has been used here as a base data set to compare with the results of the CFX models.

As discussed in section 2.2.2 the normal scaling parameters used in boundary layer work have to be altered in the case of boundary layers over deep vegetation canopies. The appropriate scaling height is the canopy height rather than the roughness length. Similar changes have to be made to the scaling velocity u_*. In a simple rough wall boundary layer the shear stress near the wall is constant with height, for the lower part of the boundary layer. The shear stress at the ground (and by extension, just above it) is therefore used in the formulation of u_*. However, if a canopy is present, the constant shear layer goes down to the canopy top, then shear levels decrease towards the ground. The shear stress at the ground surface is essentially zero in a dense canopy, making the usual definition useless. In this case, the value at the bottom of the constant stress layer, i.e. at the canopy top, is used in defining the scaling velocity.

6.4.2.1 Validation cases

A set of 2D models was constructed to test the resistance volume model, and compare it against the standard roughness length model. The domain was 13km long in total, and approximately 1.5km tall. A horizontal resolution of 25m for the main part of the

domain, with a lower resolution lead-in section gave 545 cells in the flow direction. The vertical resolution varied according to the model, from 32 to 45 cells.
All the models had a standard roughness length model for the first 3km, with z_0=0.05m. This allowed for any disturbances associated with the inlet to dissipate before the start of the forest region. The ground roughness of 0.05m was continued on under the resistance volume. The reason for this was twofold. Physically, it was reasoned that the roughness of the forest floor itself would probably be similar to the roughness of the 'grass' region outside, and that this could be included, although its effect would be small compared to the forest. Secondly, and more importantly for the validation cases, there would not be a change in both roughness models. Keeping the ground roughness constant, and adding in the resistance volume, rather than replacing the surface roughness, meant that only one part of the model was changed at a time. Calculated changes in velocity profile would therefore be entirely due to the resistance volume.

The four models can be summarised as follows:

1. 'Baseline' – a constant roughness of 0.05m throughout the whole domain, to serve as a null case, with no roughness change. 45 cells vertically, bottom cell height 16cm.
2. 'z_0 change' – a change to a z_0 of 1m. This represents a forest simulated by the standard roughness model. The specification of roughness lengths for forests is difficult, but this z_0 probably represents dense trees 5 to 10m tall. 32 cells vertically, bottom cell height 2.6m.
3. 'resistance 10m' – a 10m tall volume with a resistance parameter of 0.07 as defined above. 45 cells vertically, bottom cell height 16cm.
4. 'resistance 5m' – a 5m tall volume with a resistance parameter of 0.07. 45 cells vertically, bottom cell height 16cm.

All the models used the same inlet profile. This was one that had been developed in a previous 2D run over flat terrain at a constant z_0=0.05m. The baseline case showed no significant change in the flow profile down the domain, indicating that the boundary

layer was in equilibrium with the specified inlet roughness, and other boundary conditions. Any changes in flow profiles were therefore entirely due to changes in roughness model.

The two different heights of resistance region were to provide possible matches to the z_0 value used in the simpler model. There is not a direct relationship between roughness length and roughness element height, as the roughness length also depends on the element density. For 'sand-grain' type roughness, the z_0 value is classically given as 1/30 of the element height. For 'maximally dense' vegetation, z_0 approaches 1/5 of the element height. (see discussion in 2.2.2) The pine forests the current model is intended to simulate are considered to be somewhere between these two extremes, but nearer the dense end of the range, with a z_0 estimated from experience and field measurements to be at least 1/10 of the tree height.

The vertical resolution of the z_0 change model had to be lowered to accommodate the large surface roughness, as the bottom cell centre has to be higher than the roughness length. The bottom cell centre height was raised to 1.3m, but this is still closer to the roughness length than would be ideal. It is also of lower resolution than would be ideal, with very few calculation points in the region of interest. This serves to highlight a shortcoming of the 'z_0 only' roughness model, in that it can place inconvenient restrictions on the grid resolution. Aside from this, the log law profile is not really applicable until about twice the canopy height.

Vertical profiles were taken at various distances through the domain. The results used in the following analysis were taken from 2km downstream of the change in roughness. This was chosen as indicative of the size of the blocks of forest that often occur in regions considered for wind farms. Lack of time prevented too many runs being performed, so rather than trying to match the CFD results with each of the measured data sets discussed in 6.4.2.2, a single 'indicative' case was used. This would give a qualitative feel for the performance of the model.

6.4.2.2 Results

The CFD results were compared with measured data given in Kaimal and Finnigan (1994) for several natural canopies. The data presented in Kaimal and Finnigan is non-dimensionalised according to the altered 'canopy' scaling parameters detailed in section 2.2.2. This enables a wide variety of canopies, from wheat fields to forests, to be compared on a similar footing. Data from 8 different canopies covering a wide range of scales, see table 6.1, collapse well onto a single curve or band of curves. The velocity profiles (Fig 6.1), while differing in slope, all show the same general trend and overall shape. The shear stress profiles (Fig 6.2) all collapse very well into a narrow band.

Profiles from the CFX runs have been normalised in the same way, and plotted over the top of the curves from Kaimal and Finnigan, to facilitate a direct comparison.

Site	**Type**	**Canopy height**
WT strips	Wind tunnel	60mm
WT Wheat	Wind tunnel	47mm
WT Rods	Wind tunnel	19cm
Shaw Corn	Corn field	260cm
Wilson Corn	Corn field	225cm
Moga	Forest	12m
Uriarra	Forest	20m
Bordeaux	Forest	13.5m

Table 6.1 – Canopies from Kaimal and Finnigan (1994)

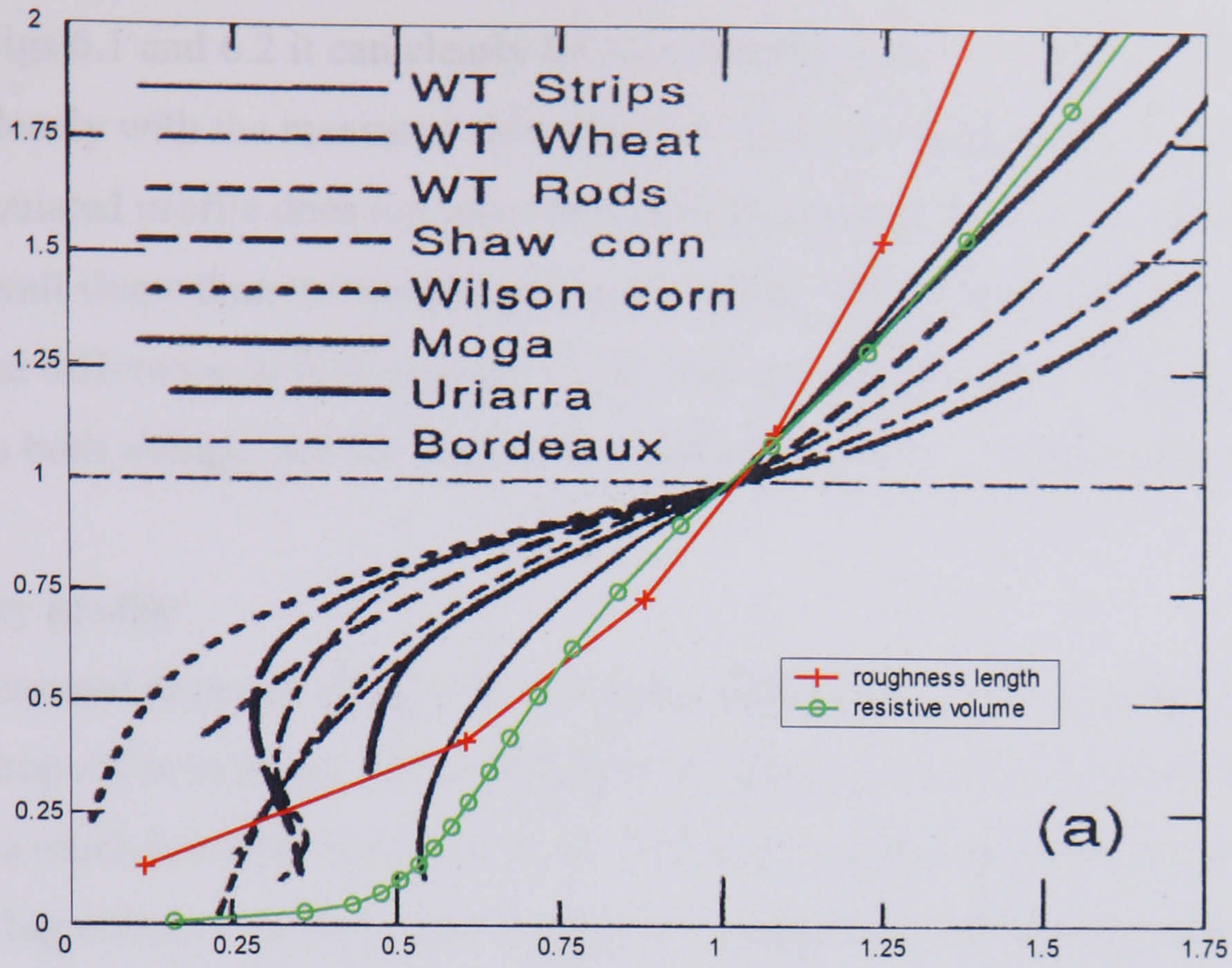

Figure 6.1 - Observed and calculated velocity profiles. Roughness length only model : z_0=1m, Resistive model: volume height =5m.

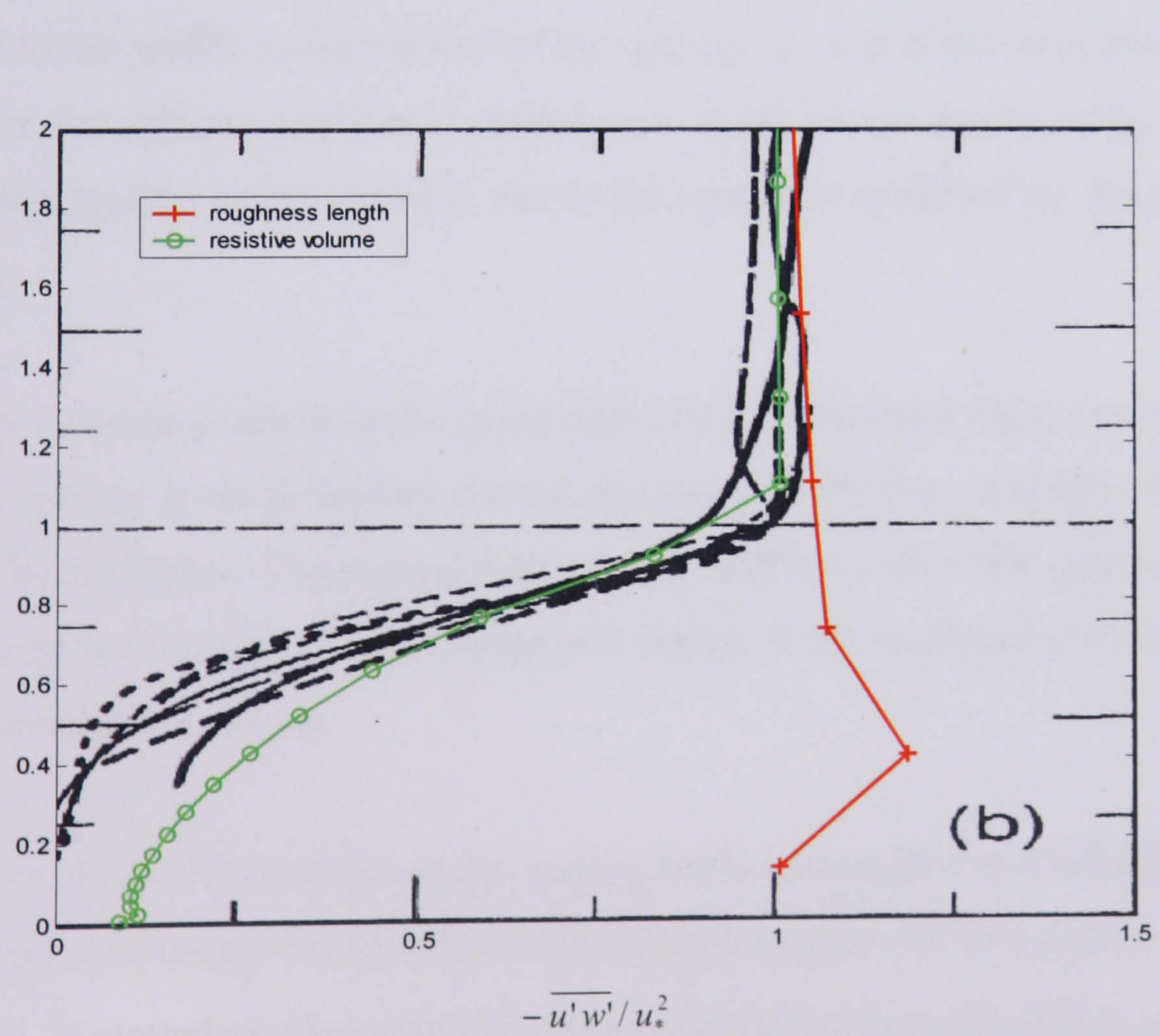

Figure 6.2 - Observed and calculated shear stress profiles. Legend as for Fig 6.1.

From Figs 6.1 and 6.2 it can clearly be seen that the resistive volume model fits much more closely with the measured data than the simple roughness length model. While the calculated profile does not exactly follow the measured data, it is much closer to the overall shape than the roughness length model. The measured profiles highlight the great difference in flow regimes inside and above the canopy. Velocity and shear profiles both change, but the change in shear stress profile is particularly marked.

Velocity profile

The measured data sets show a log law type profile down to the canopy top, with a rapid drop off in velocity in the top half of the canopy. The lower half of the canopy shows a much lower drop off in speed. The density of the canopies can be seen to have a big effect, with the denser canopies showing most of the flow retardation occurring in the top half of the canopy. The resistive volume model results are somewhat outside the band of measured results, but agree much more closely with their general shape than the roughness length model, which displays a single log profile right down to the ground. The resistive model does have a convex-upwards section to the profile in the top half of the canopy, as seen in the measured data, however, the velocity gradient is much lower. In the lowest quarter of the canopy, a secondary log law layer is visible, due to the roughness specified for the ground surface.

The low velocity gradient in the upper part of the canopy (see Fig 6.1) would suggest that the canopy is not providing enough resistance to the flow, and that the resistance should be set higher. The general shape of the profile within a few canopy heights of the ground would support this, being most similar to the measured profiles of the least dense measured canopies.

However, the profile well above the canopy looks as though it is of a higher roughness than the z_0=1m specified in the simple model, and with which it should be matched. If plotted as a log graph (Fig 6.3), and the log-law part of the curve extrapolated to u=0, the intercept is at about z=4m. This would be extremely high for

a roughness length, but reasonable if a displacement length is included. The log part of the resistance model profile could now represent a roughness length of 1m with a displacement of 3m. This is broadly in line with the 5m canopy height specified.

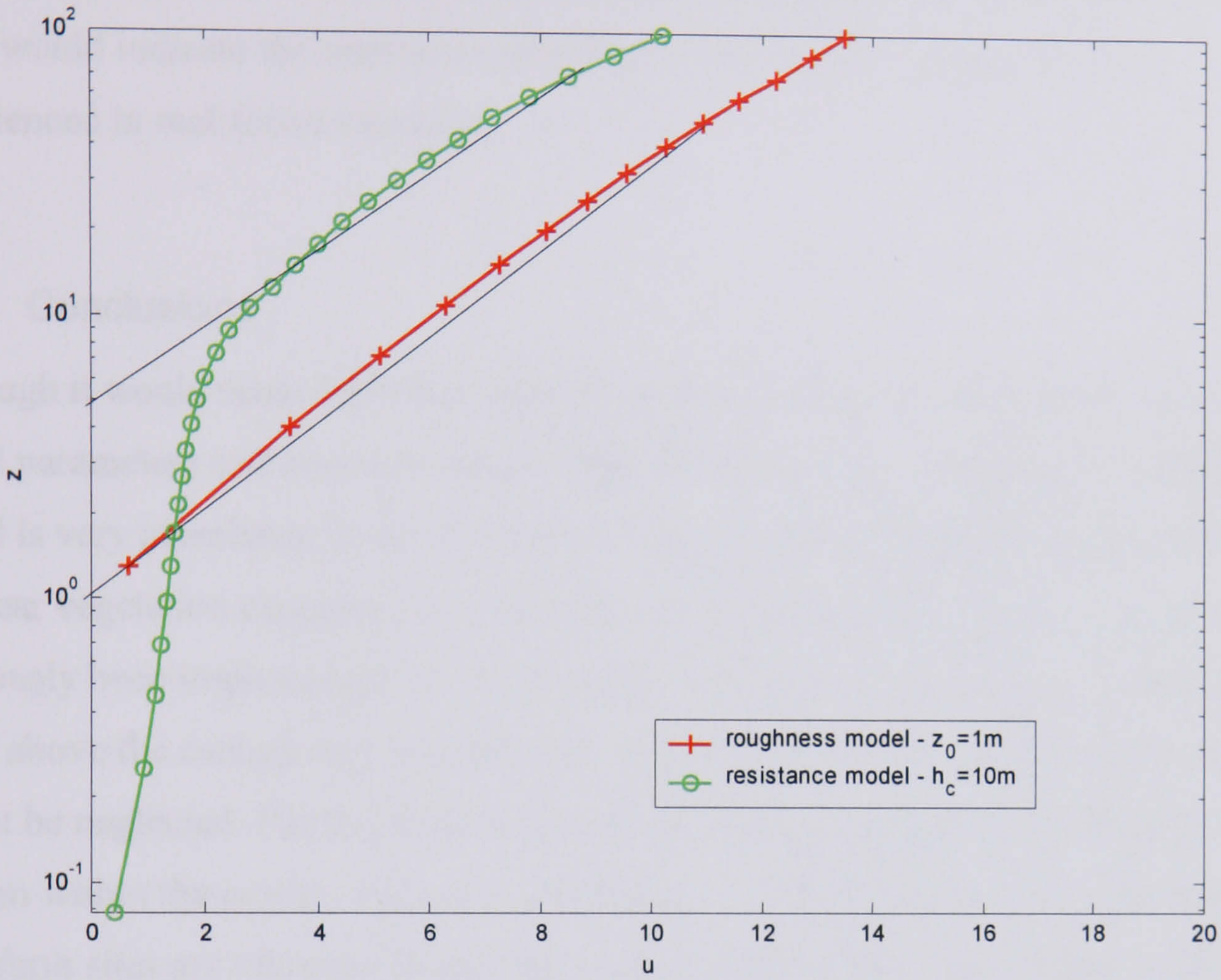

Figure 6.3 - Plot of log *z* against *u*, showing 'log law region' intercepts and inferred roughness lengths.

For dense canopies the displacement height is usually about 75% of the canopy height, as most of the resistance is felt in the top portion of the canopy. A lower displacement height would imply a less dense canopy, fitting in with what was observed earlier about the velocity profile.

Shear stress profile

The shear stress profile (Fig 6.2) shows more clearly the effect of the more complex roughness model. Simple log law boundary layers have a constant shear layer in the lower part of the boundary layer. This is simulated quite well by the roughness length

model in CFX, which has a roughly constant shear up to a few times the canopy height (excepting the anomaly at the second cell centre, as discussed in chapter 4). The measured data for canopies of vegetation shows a drop off in shear with a decrease in height down through the canopy. This behaviour is displayed by the resistive volume model in CFX, although the shear reduces more gradually. This again would indicate the resistance specified in the model is lower than that experienced in real forest canopies.

6.4.3 Conclusions

Although it would seem from this validation exercise that the relationship between the model parameters and characteristics of real forests is still not adequately defined, the model is very promising. It clearly captures more of the detail of the flow structure in and near vegetation canopies than the simple roughness length models that have previously been implemented in CFD models. For wind power studies, it is the wind speed above the canopy that is of interest. However, flow within and near the canopy cannot be neglected. Firstly, the flow profile above the canopy is influenced by what goes on within the canopy. Secondly, the lower levels of anemometry at potential wind farm sites are often not dissimilar to the canopy height. An accurate model of the velocity profile in the proximity of the canopy is therefore vital to accurate adjustment of measured data up to hub height.

The new resistive volume model has the potential to provide much more detailed information about the flow structure in the neighbourhood of forests and other areas of dense vegetation. The modelling of the overall shape of the velocity and shear profiles is quite impressive. However, the figures used in the model for the resistance need some further refinement. It is very difficult to develop a definite analytical formulation for the resistance values for different densities of canopies. The simple method developed here seems to have produced a figure that is somewhat too low. It did however give a figure that was close enough to prove the concept of the model, and display some of its potential. A more in depth study would need to be done, to either refine the current methodology, or develop a new one. This would require much

more data about the distribution of foliage and other biomass in forests. It would also require detailed flow measurements to correlate the vegetation density with the effect on the air flow. Lack of time prevented any such study being undertaken in a meaningful way as part of the current research work, but the foundations for a promising model have been laid.

7 Roughness modelling - Applications

A second round of validation of the resistive model was undertaken, this time using a prospective wind farm site that Powergen was studying. This would show how the model performed under real-world conditions, for a 'commercial' problem.

The main areas of interest in CFD models for wind energy prediction studies are the variation of average wind speed across the site, and in the vertical variation, particularly at specified locations. The first enables the windiest areas of a hillside to be selected, for example. An understanding of the vertical variation, or wind shear profile, is also vital. The anemometers used in the initial monitoring campaign are rarely at the hub height of the turbines that will eventually be built there, and may well be significantly lower. This low-level wind speed data must then be 'sheared up' to the turbine hub height. Detailed knowledge of the vertical profile is most difficult to obtain in the high roughness sites where it is most critical. High roughness gives a large velocity gradient, and errors in extrapolating the wind speed up to hub height can have a large effect on the economics of a wind farm. Modelling the detail of a velocity profile can often be of great commercial importance, and currently relies heavily on empirical adjustments to data and engineer's experience.

7.1 Derrybrien site description

The Derrybrien site is a proposed wind farm site in western Ireland. Overall, the site is a broad, gentle hill, with considerable forestry cover, both on the hill itself, and over the surrounding area.

To get more detailed information on the area than could be obtained from the available Ordnance Survey maps (Ordnance Survey of Ireland, Discovery Series sheet 52) a site visit was made in May 2001 with Dr. Chris Ziesler of Powergen.

7.1.1 The locale

The hill of interest, Cashlaundrumlahan, is on the north-west edge of the Slieve Aughty Mountains, with the flat coastal plain to the north and west. The hill rises to 358m, with a few other similarly sized hills, mainly to the south. The nearest towns are Loughrhea, about 12km north, and Gort, about 12km west. Galway bay is about 30km to the NW. The name Derrybrien comes from a loose grouping of houses on the south side of the hill.

Although quite tall, the slope of the hill is quite gentle, being rather less than found at Askervein. The topography of the area should be easy to simulate; the demanding part of this case is the ground roughness. Much of the surrounding land is forested, some quite extensively. It was this feature that made the site an interesting one to investigate. As an exposed hill top in western Ireland, it would be expected to be consistently windy, however the measured wind resource was surprisingly poor. This was intuitively put down to the large amounts of woodland surrounding the site, but existing prediction methods struggled to accurately predict the resource.

Near the summit of the hill is a 62m tall communications mast. Wind monitoring equipment has been installed on this mast, as well as on a dedicated 40m anemometer mast further west, nearer the hill top.

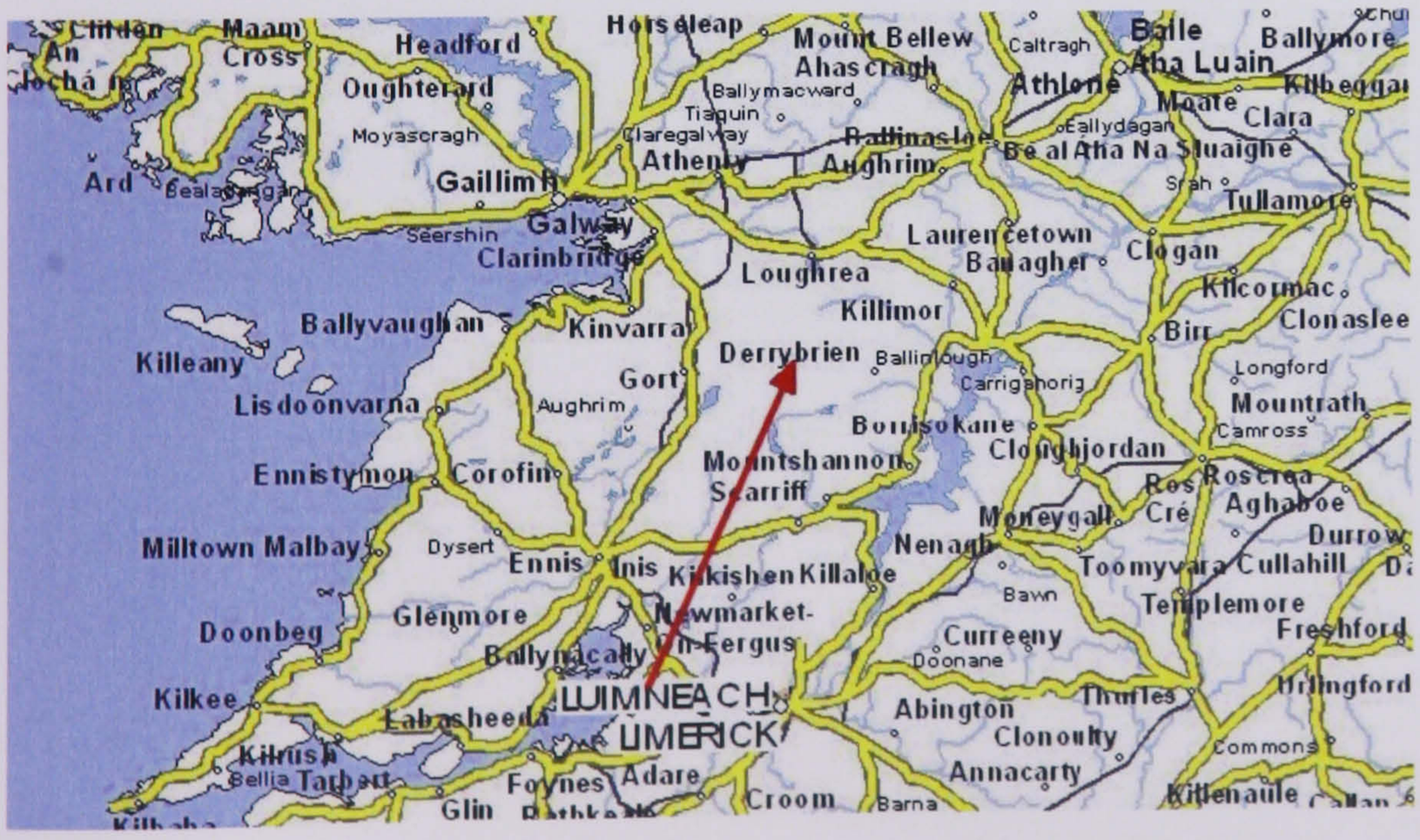

Figure 7.1 - Location of Derrybrien, near the west coast of Ireland.

Figure 7.2 - Overview map of the Derrybrien area.

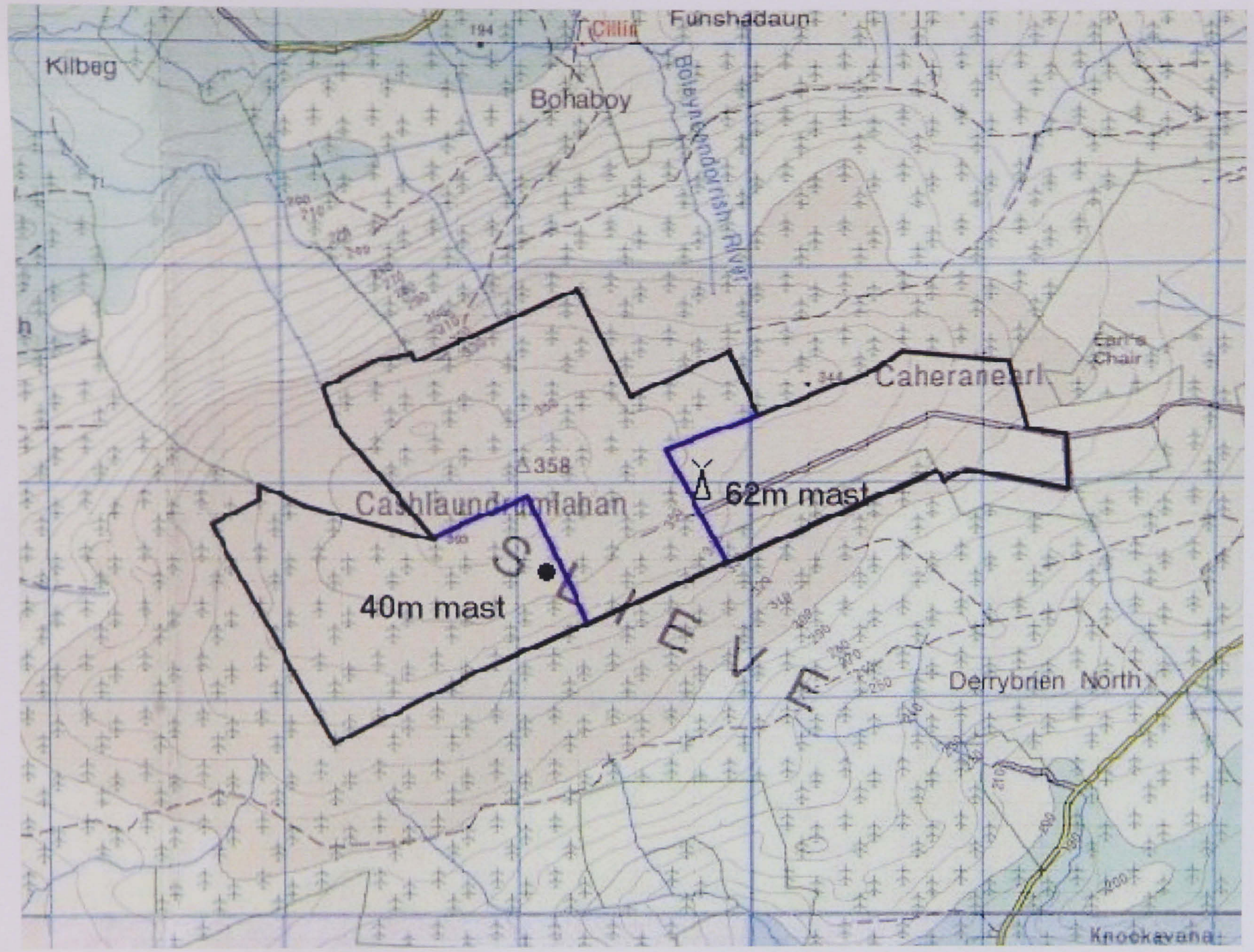

Figure 7.3 - Location of monitoring masts: 62m telecoms mast and 40m anemometer mast.

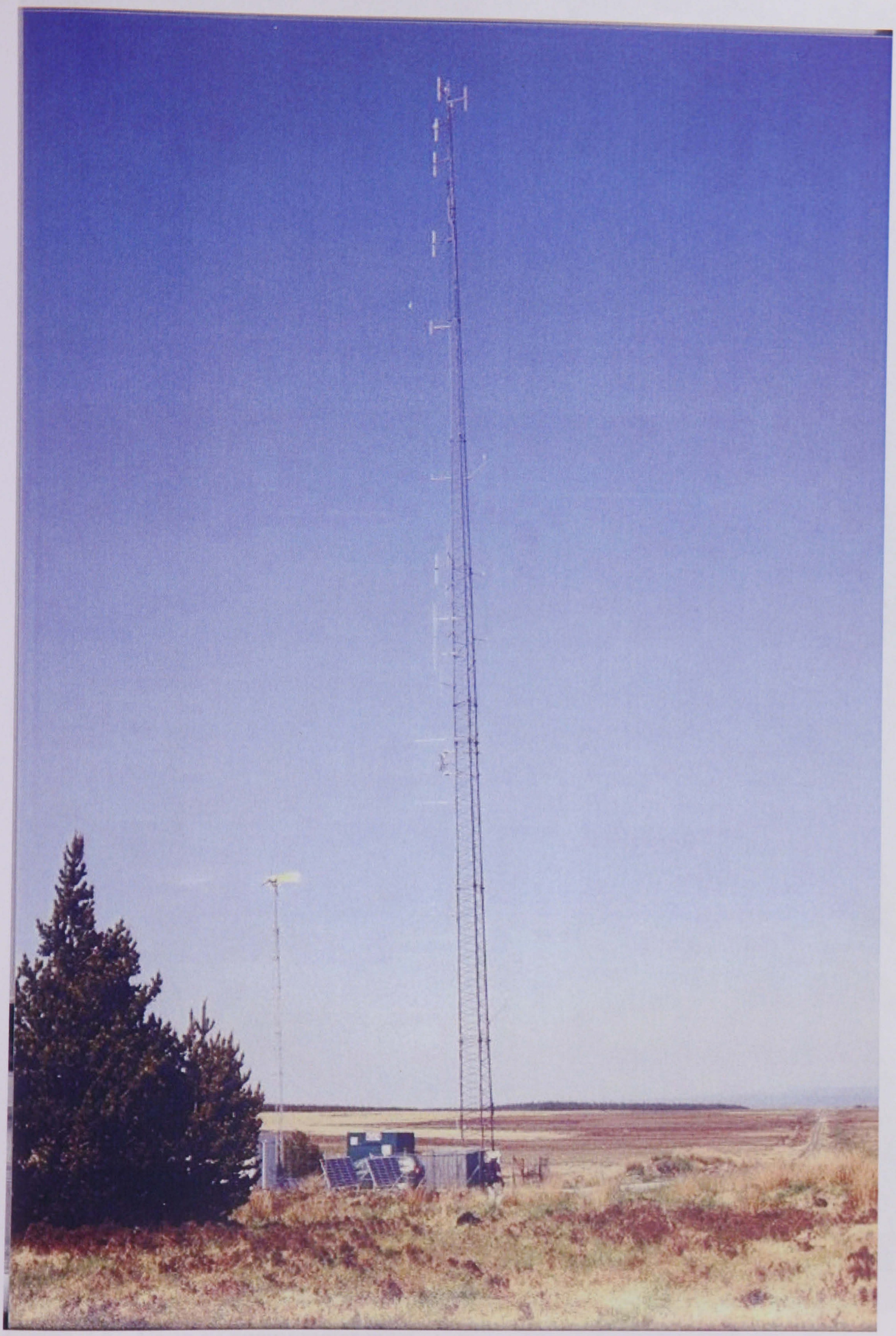

Figure 7.4 - View of telecoms mast, including compound at mast base.

Figure 7.5 - View of anemometer mast

Figure 7.6 - Panorama taken from near telecoms mast, giving an overview of the area. The upper half looks west and north, showing the forest, the trackway through the forest leading to the anemometer mast, and the base of the telecoms tower, and its associated structures. The lower half shows the open area east of the mast, and the site access road.

Figure 7.7 - Panorama taken from near the base of the anemometer mast. The upper half is looking south and west, showing the shorter forestry in those directions. The upper half looks north and east, with the right side showing the taller trees between the two masts, and the cleared access route from the telecoms mast.

7.1.2 Site visit

A site visit was carried out as it was felt that the information available about the site was not adequate. In particular, anemometer locations were to be checked, and a ground roughness survey carried out. This was prompted by previous commercial work at Powergen that had found that interpreting ground roughness information solely from maps could be problematic. This is especially true in heavily forested areas. Firstly, there is no information on the map about the height of the trees - whether they are newly planted saplings or mature trees tens of metres high. This has a great effect on the roughness of such an area. Secondly, the spatial distribution of the woodland changes over time, with new areas planted, and other areas felled. The areas shown as woodland on the map, even the latest edition, are not necessarily what is actually on the ground. It was decided that an up-to-date survey of the extent and height of the forested areas would be necessary to produce an accurate model of the area.

7.2 Validation data

7.2.1 Data monitoring

A field monitoring campaign has been underway at the Derrybrien site for some years. Recently, the monitoring equipment has been upgraded, and now provides a useful data set for validation of flow over forest canopies. Two masts, each with anemometers at 3 heights, and direction vanes, have been recording for over a year (see Table 7.1). The data logger records ten-minute averages of wind speed, standard deviation of speed, maximum gust speed and time, for each anemometer. Each mast also has a direction vane, recording direction and standard deviation of direction in ten-minute averages. Temperature and air pressure are also recorded at the same interval, along with logger internal records, like time and date stamp, and battery voltage.

7.2.2 Data quality

The quality of the data is generally good, with reliable data from calibrated instruments. There are two exceptions to this, however. Firstly, there are some gaps in the data coverage, caused when the data logger memory card became full, and it was some time before it could be changed for a new one, resulting in some data loss. Several long periods of data, spread throughout the year, are available however, so this is not too big a problem for the current work.

Telecoms mast	**40m anemometry mast**
2000 day 295 to 2001 day 92	2000 day 276 to 2001 day 91
2001 day 136 to 2001 day 190	2001 day 124 to 2001 day 190
2001 day 273 to 201 day 344	2001 day 269 to 2001 day 344
Total 287 days of data	Total 315 days of data

Table 7.1 – Available data periods for Derrybrien.

The second, and more inconvenient problem is one that came to light during the course of the data analysis for this study. The top anemometer on the telecoms mast showed a somewhat anomalous variation in wind speed with direction, see Fig 7.8. There is a dramatic drop in the value of wind shear around the 150 degree direction. This implies a dramatic reduction in the wind speed at the top anemometer.

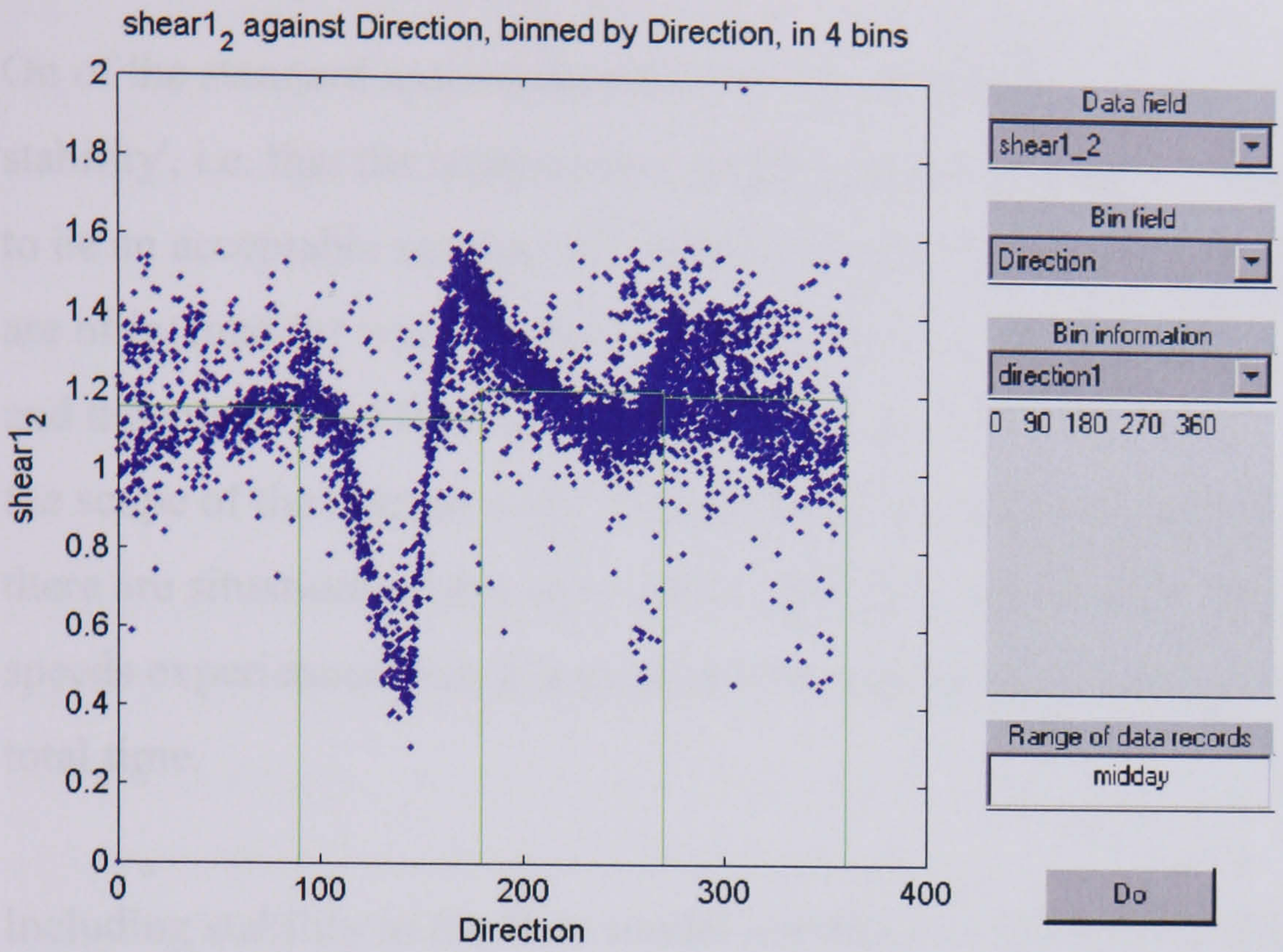

Figure 7.8 - Wind speed variation at top telecoms mast anemometer. Data has been normalised against the middle anemometer (i.e. the wind shear ratio between the top two anemometers). Compare with figure 7.12 - a similar plot for the bottom two anemometers on this mast.

After considerable deliberation, this anomaly was put down to anemometer shielding. This was partly confirmed by a photo of the top of the mast which, upon enlargement, appeared to show the top anemometer very close to (and sometimes in the wake of) a communications antenna. The data from this anemometer was therefore regarded as suspicious. Most of the problem seemed to be in the sector 75-200 degrees. Data from outside this sector have been used in the later analyses, but with caution.

Most of the analysis of the measured data was undertaken in Matlab, which enabled the large quantities of numerical data to be processed easily. The data were processed to give suitable validation cases for the CFX models. The main item to be validated

was the velocity profiles, as no data really existed for the validation of the variation across the site.

7.2.3 Atmospheric stability

On of the standard assumptions in this sort of wind flow modelling is that of 'neutral stability', i.e. that the temperature profile is purely adiabatic. This is generally thought to be an acceptable assumption for this country, and with the high wind speeds that are of interest for wind energy. This assumption was also used in the current work, and the question of thermal modelling was avoided completely, and classed as outside the scope of the current work. This is not to ignore its potential importance however - there are situations where atmospheric stability does make a difference to the wind speeds experienced, but it is generally hoped that these are a small proportion of the total time.

Including stability in the flow model introduces a lot of extra complexity, and demands additional input data, hence the driver for ignoring thermal effects. To get an idea of the validity of this assumption, it was decided to look carefully at the data from Derrybrien, to see if any stability effects could be seen. If few were visible, it would support the lack of thermal modelling in the CFX model described here (at least in the climate of the British Isles). If stability effects were noticeable on some occasions, these could then be identified and treated as special cases. In particular, those periods could be excluded from the data used for the validation of the implicitly neutral CFX model.

Stability measurements are rarely taken as a matter of course at potential wind farm sites, to keep monitoring costs down, and this was true at Derrybrien. So, it was wondered if a suitable proxy could be found for stability measurements, in the absence of multiple temperature measurements. One temperature reading had been taken, but this on its own would not directly give a temperature gradient.

The thermal stability of the atmosphere is usually measured by taking temperature readings at two heights to enable a temperature gradient to be calculated. A gradient

close to the adiabatic indicates neutral stability. If the temperature decreases quicker with height (i.e. hotter air near the ground), an upwardly displaced parcel of air will find itself hotter, and hence less dense, than the surrounding air, and continue to rise. This gives rise to an unstable thermal stratification. Such a condition is caused by solar radiation warming the ground surface, and hence the air near it.
During the night the opposite can occur. The ground surface can lose heat by radiation to space, cooling the air above it, and creating a stable air column. Clear skies, with sun during the day, and radiative cooling at night, lead to non-neutral stability conditions. Cloudy skies, with little radiative heat exchange generally produce neutral conditions.

From this, it was hypothesised that the diurnal temperature cycle might be used to identify times when non-neutral conditions might occur. A large difference between daytime and nighttime temperatures would indicate hot sunny weather during the day and cold clear conditions at night. This would cause a cycle of unstable conditions during the day and stable conditions at night. A small temperature difference between day and night would little radiative heat exchange, and neutral conditions.

Although this method could not be used to get quantitative data on the degree of stability or instability, it would provide some qualitative information on the atmospheric stability. Importantly for this work, it should be possible to identify times when stability was not an issue, with consistent neutral conditions that could be used as validation data.

The single temperature reading does not contain information on the temperature gradient when taken in isolation. However, when it is looked at in the context of a known heating/cooling cycle, the temporal variation can give information on the strength of the thermal cycle. Knowledge of the physics behind the system can be used to predict some information about the temporal variation of temperature. This method could possibly be taken further by using the rate of change of temperature to get quantitative data on the energy input to the system, and hence the temperature gradient.

A data processing routine was written in Matlab to look at the daily temperature profiles of the recorded data. A simple average of the temperature in the early morning, before sunrise, and around midday was used to get a figure for day/night temperature difference for each day.

Some days were found to have a much higher temperature difference than others, with a greater proportion of days in the summer with a large difference. However, the main thing to test was whether this had any effect on the wind shear. The wind shear between the bottom two anemometers on the telecoms mast was calculated, averaged over the same periods as the temperature. (note: the term 'shear' is used here in its common wind energy meaning of a velocity gradient, not in the fluid dynamics sense of shear stress.) The wind shear was plotted against temperature difference, to display any correlation, see Figs 7.9 and 7.10. For the winter period, there was no clear correlation, with no significant trend in shear profiles with temperature difference. However, the summer data showed a definite effect - increased day/night temperature difference correlates with bigger change in shear profile from night to day. This has been shown on Figure 7.10. A best-fit line (calculated using a least-squares method) has been put through each of the morning and daytime data sets.

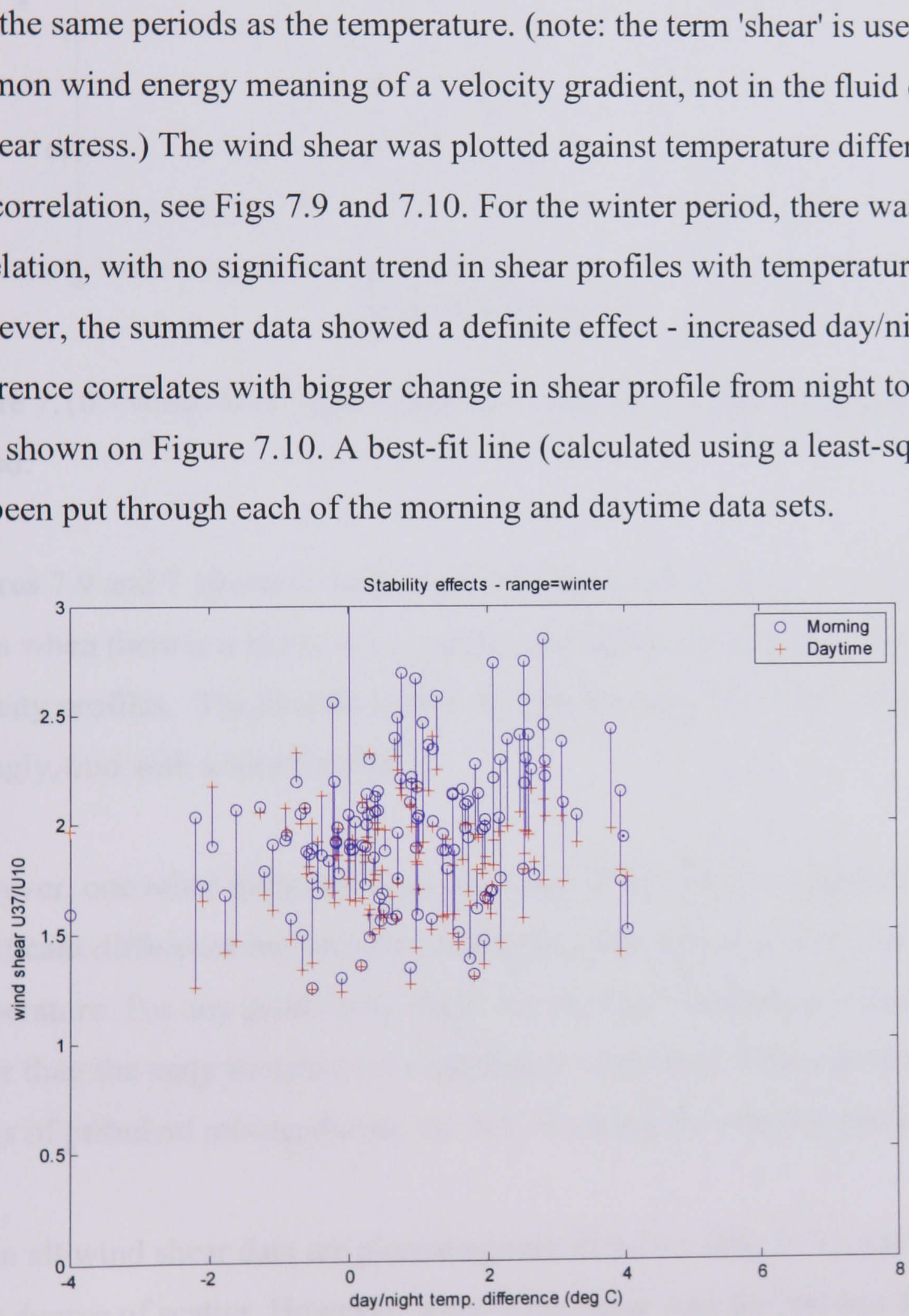

Figure 7.9 - wind shear against variation with temperature difference for winter period.

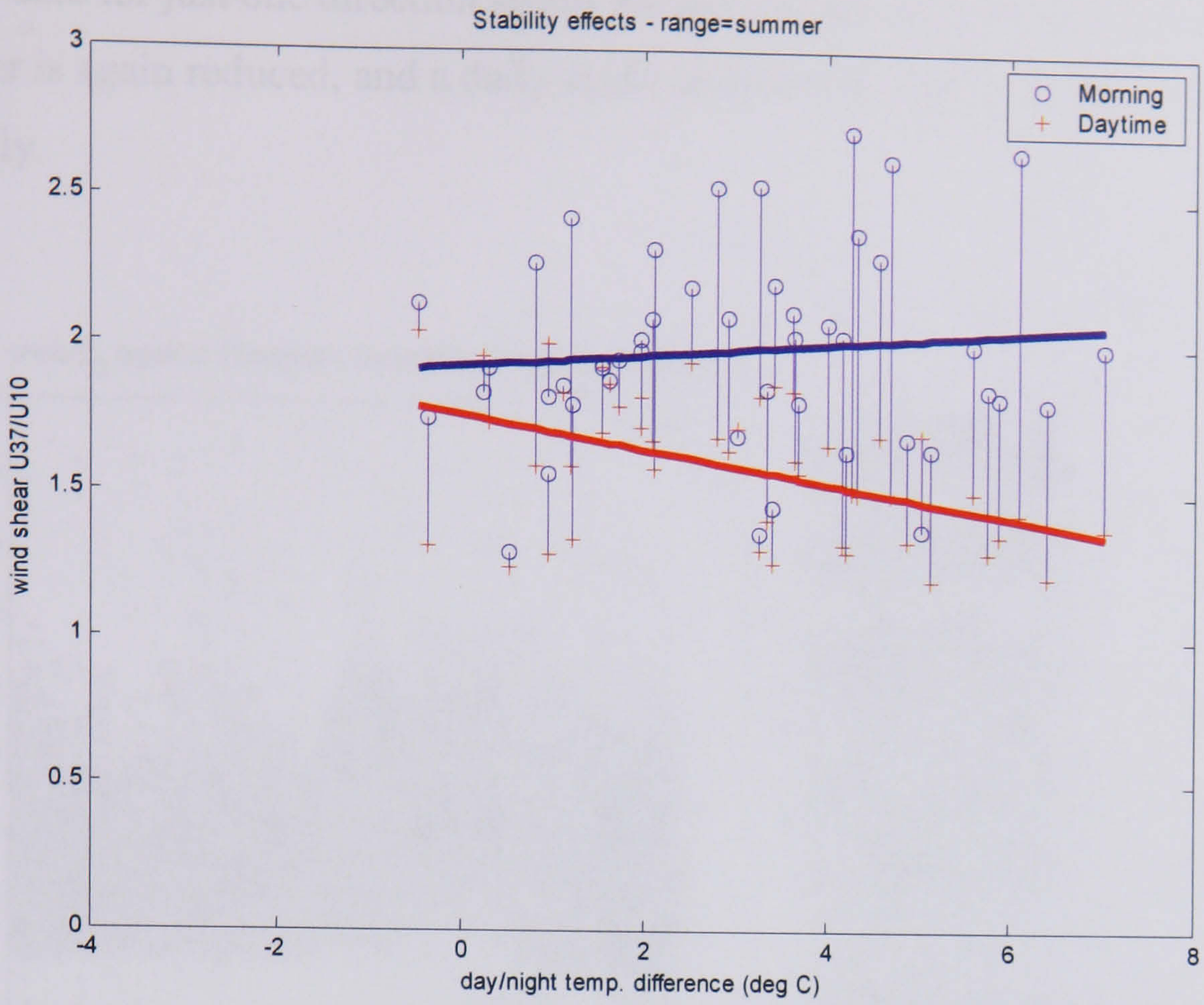

Figure 7.10 - wind shear against variation with temperature difference for summer period.

Figures 7.9 and 7.10 would indicate that this method is capable of identifying some times when there is a likely to be a significant difference between day and night time velocity profiles. The data do follow the trend predicted to some degree, but not very strongly, and with a lot of scatter.

However, one other thing that does come out of this analysis quite strongly, is the significant difference between day and night shear values at all times, regardless of temperature. For any given daily cycle, the daytime wind shear is fairly consistently lower than the early morning (or night time) wind shear. This would imply higher levels of turbulent mixing during the day, lowering the velocity gradient.

When all wind shear data are plotted against direction (Fig 7.11), the data show a large degree of scatter. However, when wind shear data for just one time of day (midday) is plotted against direction (Fig 7.12) this scatter is markedly reduced, with all the data collapsing in to one narrow band. If all shear data are plotted against time

of day (Fig 7.13) the scatter is still very large, and only a weak trend is visible. When shear data for just one direction sector are plotted against time of day (Fig 7.14), the scatter is again reduced, and a daily cycle is observed, although only relatively weakly.

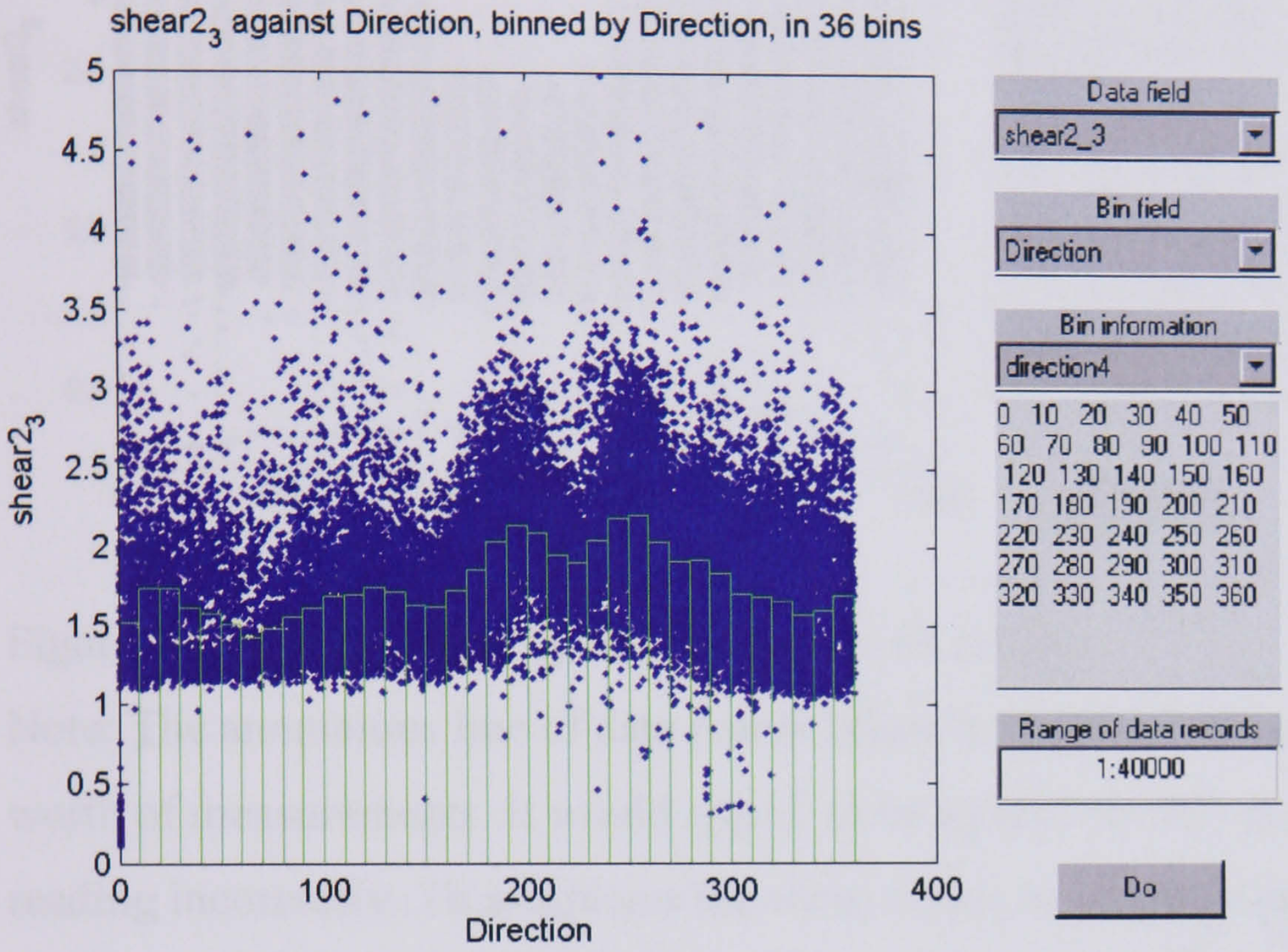

Figure 7.11 - Wind shear by direction for all records

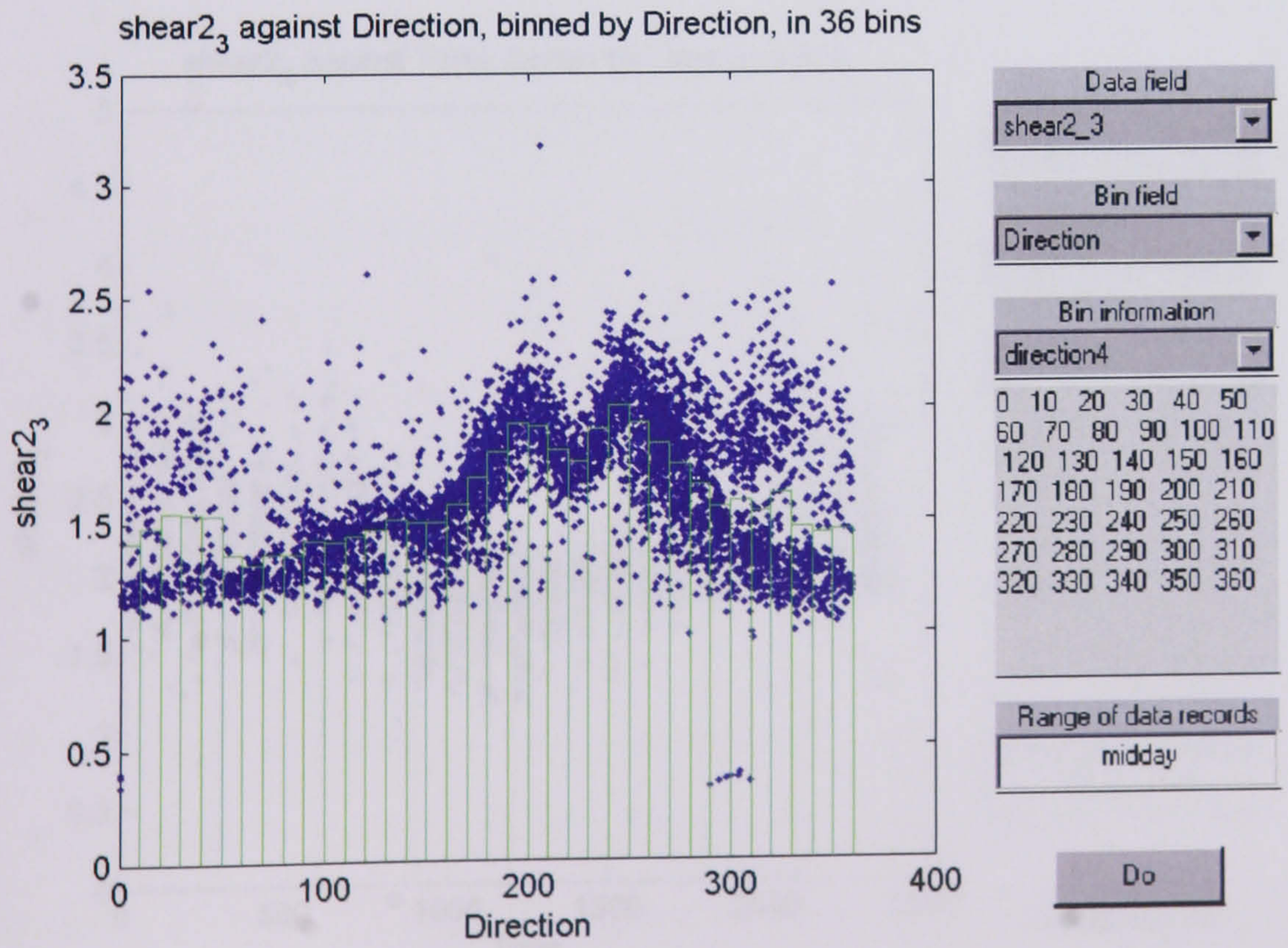

Figure 7.12 - Wind shear by direction for 12:00pm to 15:00pm time period

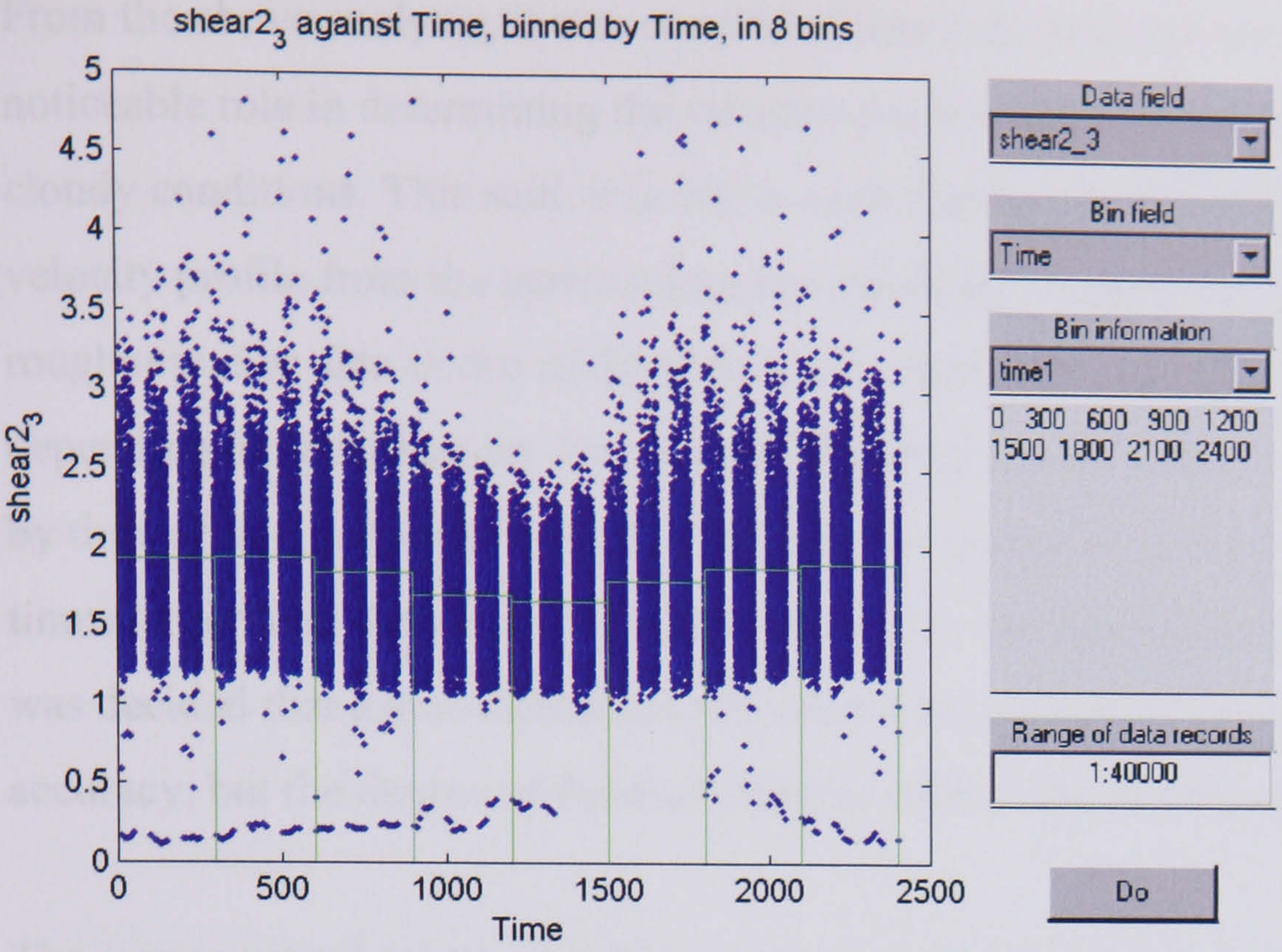

Figure 7.13 - Wind shear by time of day for all records

Note: The anomalous line of data points below 0.5 in Fig 7.13 is due to a single day's worth of measurements. It would appear to be a problem with the 30m anemometer reading incorrectly. This explains the shear values of less than unity, implying that the wind speed at 30m was less than the speed at 10m. The problem does not seem to re-occur, and does not unduly affect the overall analysis.

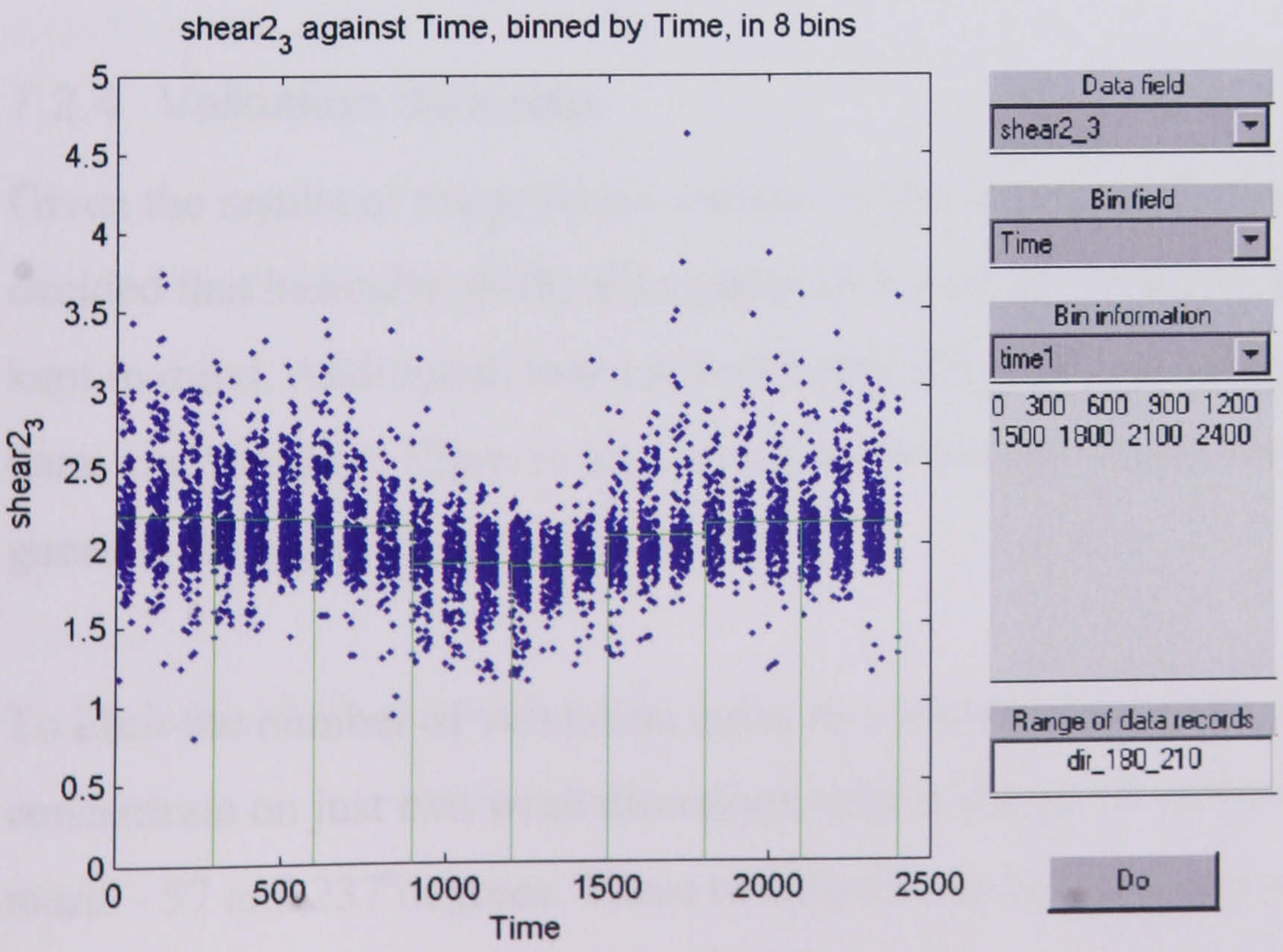

Figure 7.14 - Wind shear by time of day for direction sector 180 to 210 degrees.

From the above analysis, it was concluded that atmospheric stability does play a noticeable role in determining the velocity profile, even in comparatively windy and cloudy conditions. This said, it is still a more minor effect than the effect on the velocity profile from the surrounding environment, such as topography and roughness. For data in the 'midday' time bin, the shear varies between 1.2 and 2.0 depending on the direction. For the 180-210 degree sector, the variation in wind shear by time of day is from 1.9 to 2.2. The variation due to direction is therefore over 2.5 times larger than the variation due to time of day (or stability). This being the case, it was decided that a non-thermal model could be used with a reasonable degree of accuracy, but the degree of thermal stability effects should be borne in mind.

The average wind speed seemed to have a very weak effect on the shear values, so wind speed was not allowed for in the data analysis. At very low wind speeds, anomalously high shear values could be produced. These were removed directly from the data set, rather than by setting a cut-off wind speed that would remove all low wind speed data. All data points with a shear over 5 were removed – this turned out to be very few points in practice. Overall, as wind speed appeared to only have a minor effect on the flow field (over the speed range of interest), only one wind speed case was considered in the CFD model.

7.2.4 Validation data sets

Given the results of the previous section on the effects of atmospheric stability, it was decided that basically all the data gathered would be used, but with stability effects kept in mind. Additional, two cut down data sets, corresponding to 'morning': 3am to 6am, and 'midday': 12pm to 3m , would be produced. These would represent a best guess at the limits of the stability effects.

To limit the number of validation cases to a manageable quantity, it was decided to concentrate on just two wind directions, which would be in the same plane as the two masts - 57 and 237 degrees. These two directions also had the advantage of being outside the sector of 'bad' data for the telecoms mast top anemometer. If other

directions had been considered, the top anemometer would sometimes have to be excluded, making vertical profile assessments unsound.

To remove the effect of scatter due to variations in wind speed etc, all the measurements were normalised. The bottom anemometer on the relevant mast was used for the reference in each case, as no external reference point was available. This also preserves the confidentiality of Powergen's commercially sensitive wind speed data.

7.2.5 Validation model

The CFX model overall set up was basically similar to that used in the Askervein Hill study described earlier. The domain size and resolution were altered to suit the physical size of the problem area. The scale of the topography around the Derrybrien wind farm site is much larger than at Askervein. Also, the full geographical extent of the forests needed to be taken into account. For these reasons, the physical size of the domain was increased. However, the resolution of the model was reduced to 50m, as the topography was perceived to be much 'smoother'. There were no high gradients or sharp hill crests that would necessitate the same high resolution as at Askervein.

The simulation also made use of the forestry information from the site visit in the resistive volume roughness model. Two runs were set up, to match the wind directions of the two validation data sets.

A full listing of the settings used is given here, as defined in the pre-processor.

Current settings:

i (streamwise) 3000m upstream of centre, 5000m lead in, 3000m downstream, in 150 cells, spacing 50m

j (transverse) 2500m halfwidth from centre, 100 cells, spacing 50m

k (vertical) domain height=1800m, 35 cells, expansion ratio=1.1800, => max bottom cells size= 0.99m

Total grid cells= 525000

Co-ordinates of domain centre: 159790,204925

Rotation angles 57Rotation angles 237

Run type: terrain=topo, inlet=profile

Setting topography from file M:\My Documents\cfx\derrybrien\Dbfull.xyz

Roughness set from map file M:\My Documents\cfx\derrybrien\rough_db_new1.mat

Inlet profile specified from file M:\My Documents\cfx\basic

model\roughnesses\prof_0_05_20ms.mat

Solver preferences: iterations=1000, diff scheme=CCCT turb model=RNG K-EPSILON

USRPRT output of plane(s) at heights:

10 25 40 60

USRPRT output of profiles at points:

159104 204579

159790 204925

As well as the textual listing of the domain the pre-processor also produces a graphical output of the domains generated. A copy of this output is reproduced in Fig 7.15..

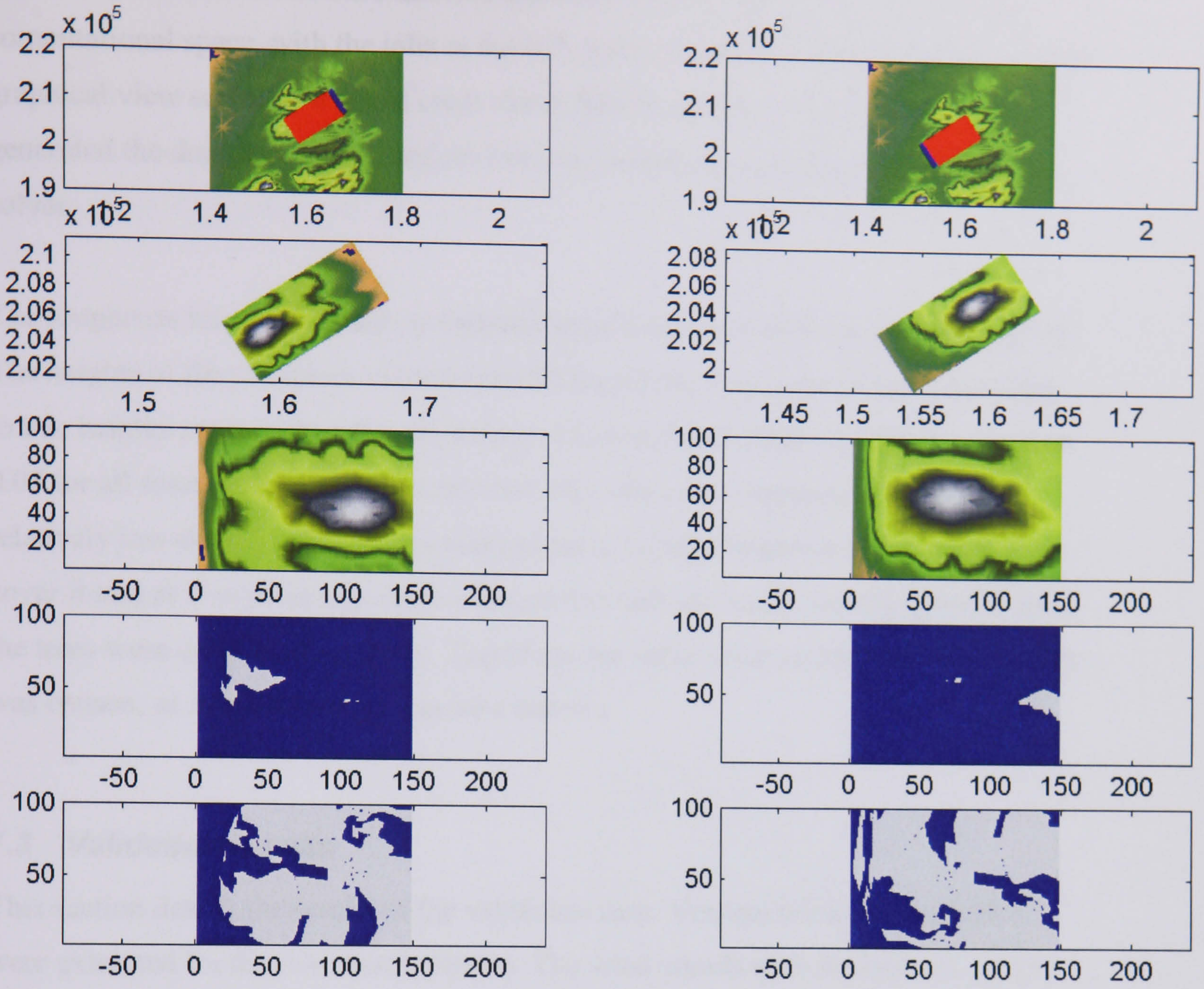

Figure 7.15 - Domains for Derrybrien simulations - display output from pre-processor.

A column of plots is produced for each direction case generated for a particular 'project'. In this project there are only 2 direction cases, 57° and 237°. The top row shows the topography data tile, coloured according to height, with the domain drawn on top. The co-ordinates are physical space co-ordinates, i.e. *x* and *y* are the OS grid co-ordinate Easting and Northing. A red dot is plotted for each grid node, and a line of blue ones at the inlet (these have merged together in this reproduction).

The second row shows the topography of the bottom of the domain. The third row represents the domain in computational space (co-ordinates are *i* and *j* – grid cell indices). The inlet is to the left, and flow is up the i dimension. The topography near the inlet looks 'squashed', as in this view each cell is plotted an equal size, and the cell length in real space increases in the 'lead in' region. The fourth and fifth rows

show roughness and resistance information respectively. Again, this is plotted in computational space, with the inlet at the left, and is coloured according to value. This graphical view serves as a visual cross check that the pre-processor has actually generated the domains you wanted, before committing the resources of starting the solver.

The roughness lengths for the non-forested areas were estimated from the site survey. The heights of the resistance volumes modelling the forestry were chosen according to tree heights measured on the site survey. The resistance value was set to a constant 0.07 for all forested regions. In section 6.4, this value was surmised to represent a relatively low-density canopy, this was judged to be representative of the actual tree cover found at Derrybrien. In some areas, particularly the more recently planted ones, the trees were quite widely spaced. Therefore, the same value as had been used earlier was chosen, as its performance was now known.

7.3 Validation results

This section details the results of the validation runs. Vertical wind speed profiles were extracted for the two mast locations. The wind speeds were normalised against the speed at 10m (the bottom anemometer height) for each location, in the same way as the measured data. This made the two data sets directly comparable.

Each of the sets of normalised data were then averaged to produce single average profiles for morning, midday, and all time periods. The morning profile was produced by averaging all data for times between 3am and 6am, for each of the three heights. Similarly, the midday profile used data between 12pm and 3pm, and the 'all time' profile used all available data for that direction sector. These three profiles give an idea of the variation in profiles due to stability effects, as discussed in section 7.2.3.

There was a very considerable amount of scatter in the results, and the actual data sets have been plotted in Figs 7.16 to 7.19, to give a visual impression of the variation. Simple statistical descriptions of the scatter are not useful as the distribution is very non-Gaussian, with a cluster of points near one end, and a long tail going towards

higher shear values. The data points are plotted with the same symbol as the average profile given in the legend on each plot. The points for the morning and midday periods have been vertically displaced on the graph, and the 'all times' plot left at the anemometer height, to prevent them overprinting on the graph, and hence keep them distinguishable. The average profiles are plotted at their correct positions.

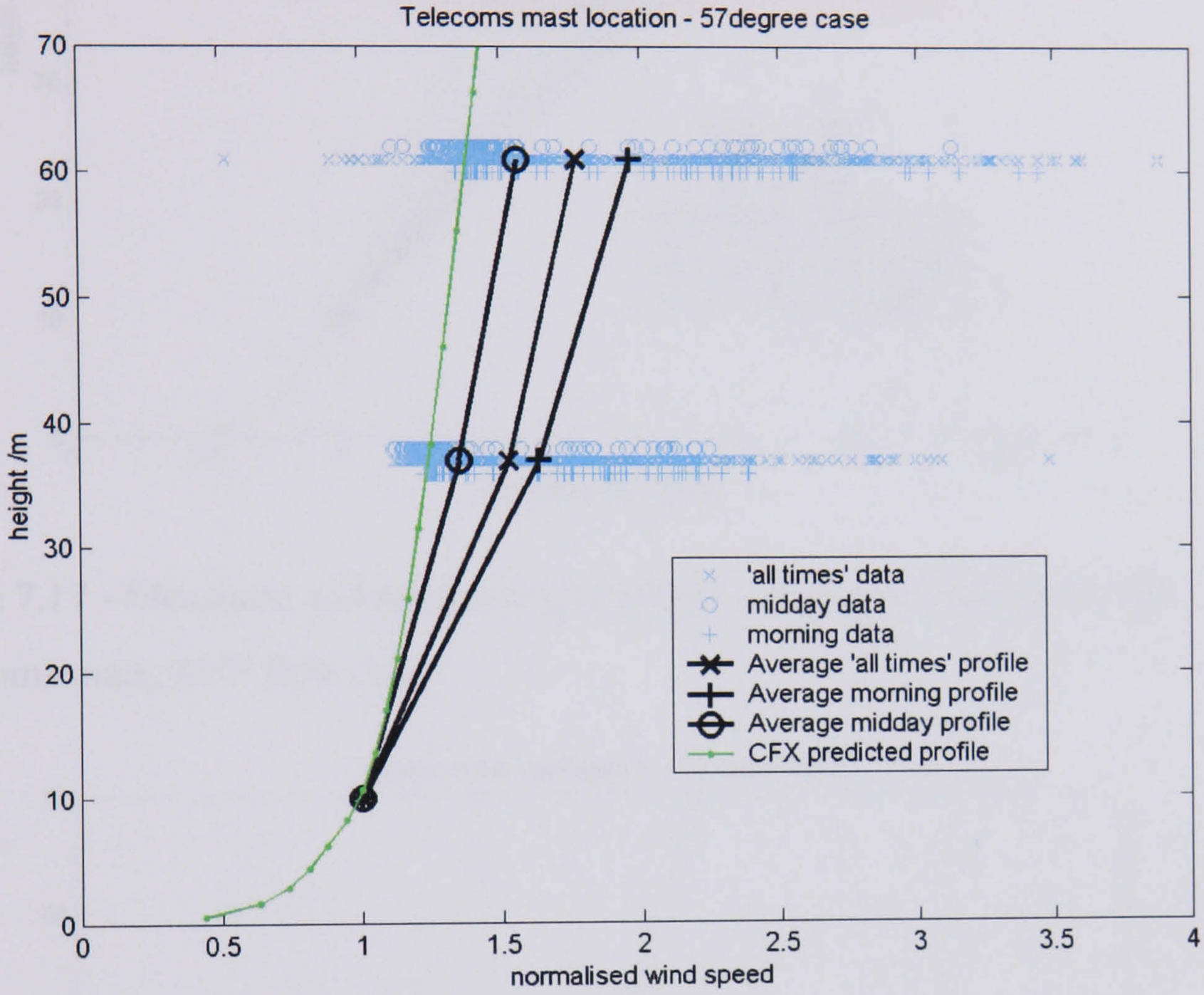

Figure 7.16 - Measured and predicted normalised wind speed profiles for the Telecoms mast, 57° flow case.

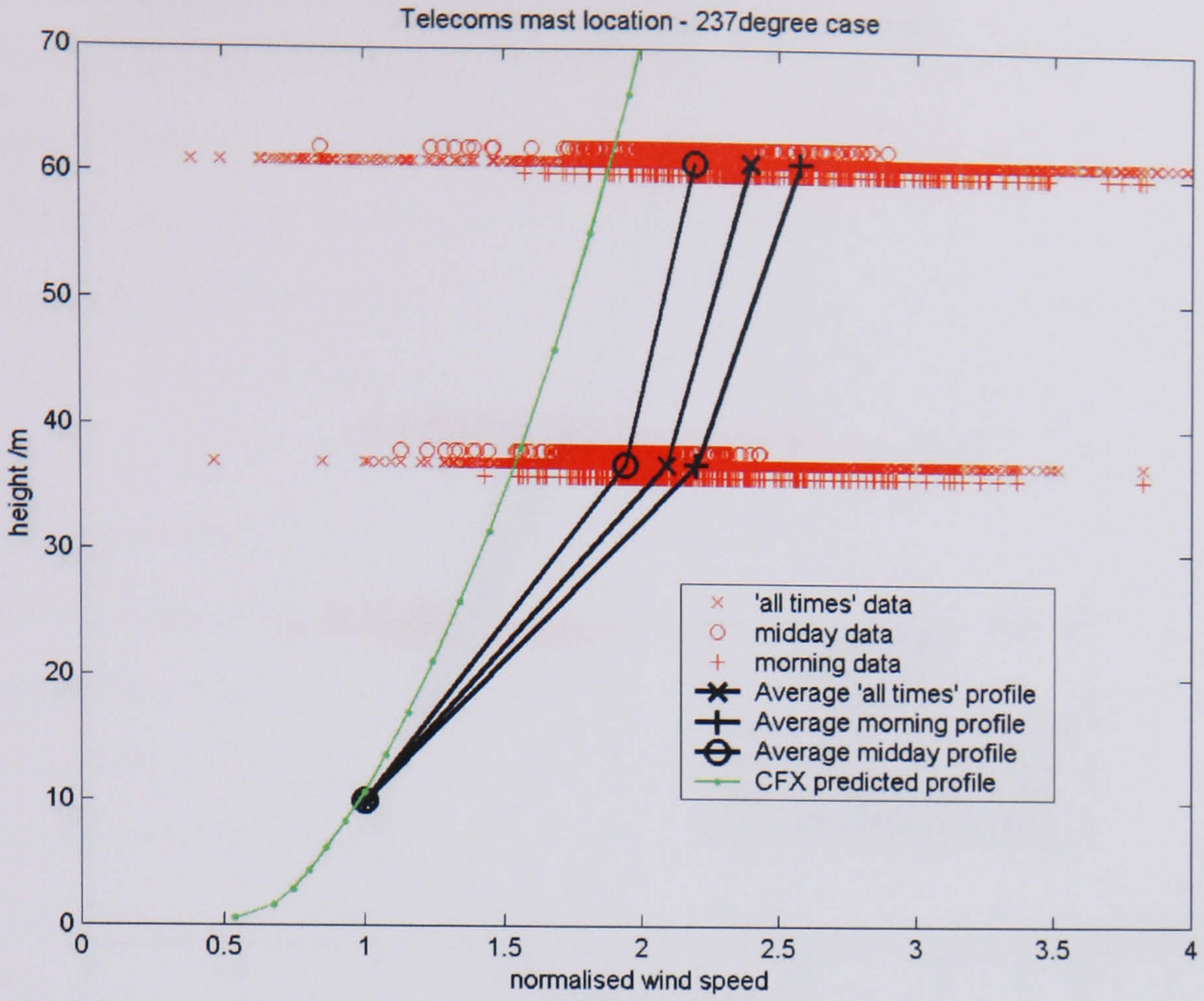

Figure 7.17 - Measured and predicted normalised wind speed profiles for the Telecoms mast, 237° flow case.

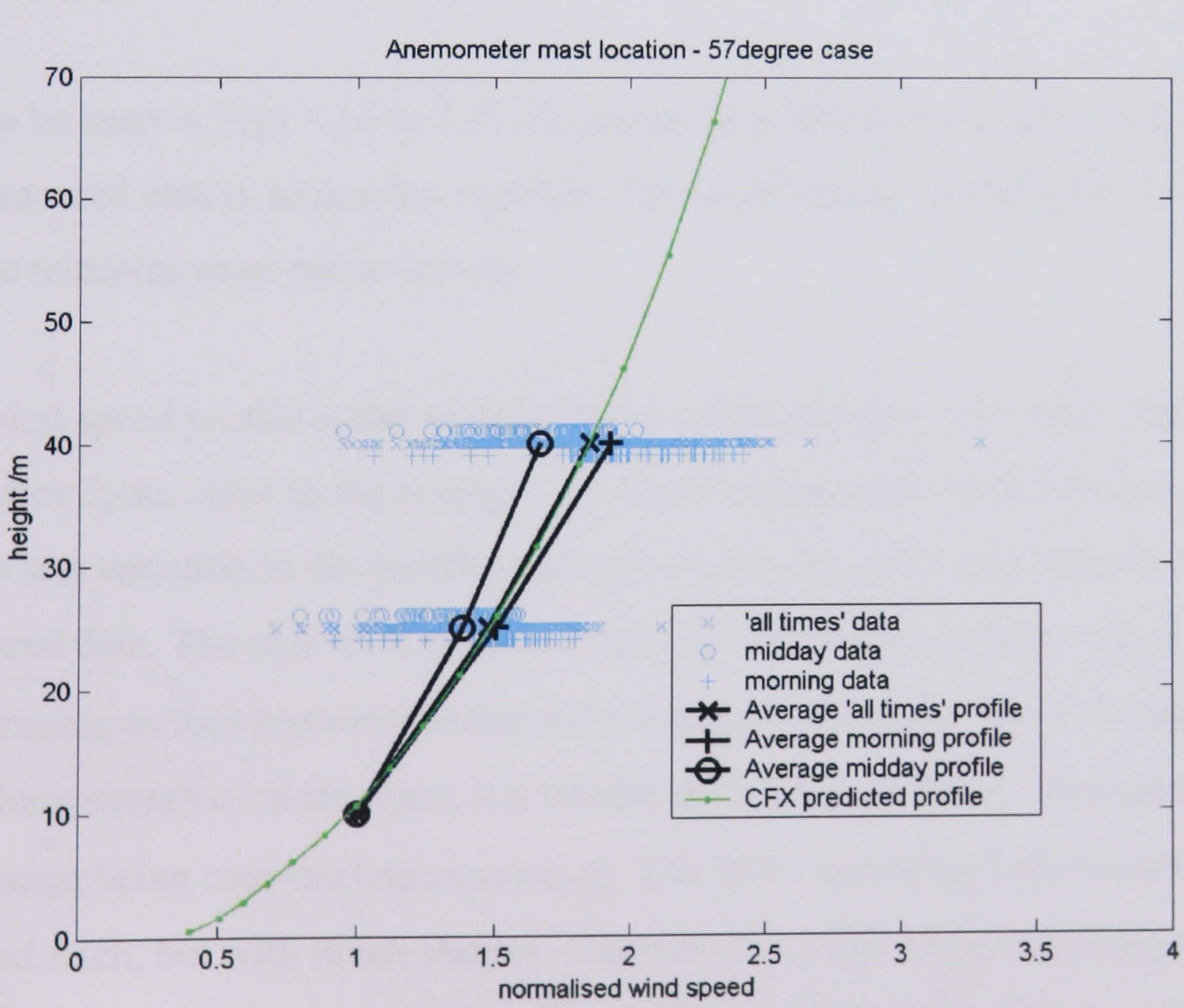

Figure 7.18 - Measured and predicted normalised wind speed profiles for the anemometer mast, 57° flow case.

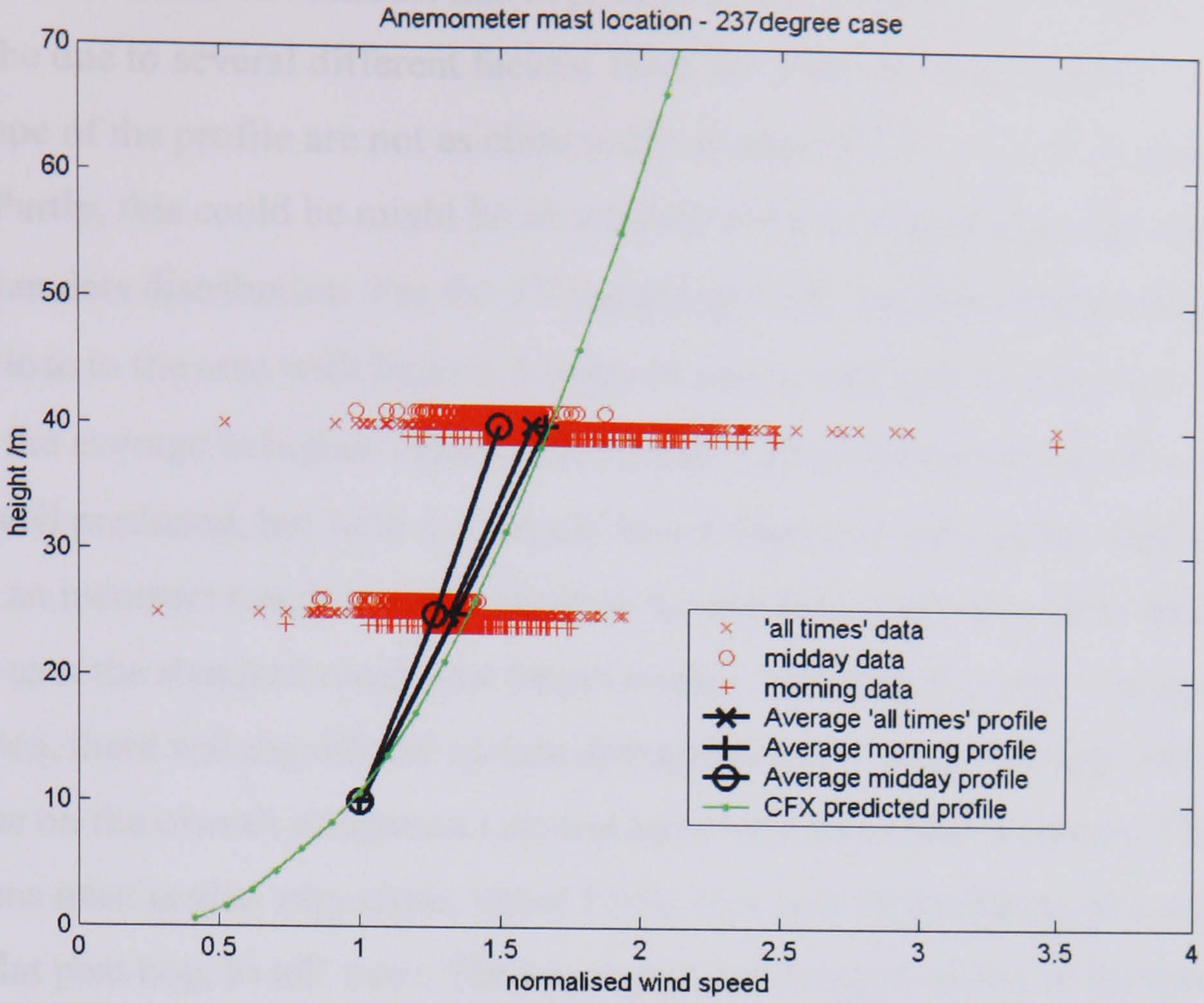

Figure 7.19 - Measured and predicted normalised wind speed profiles for the anemometer mast, 237° flow case.

As can be seen in Figs 7.16 to 7.19, the agreement between the CFX predictions and the measured data is somewhat variable. The anemometer mast is predicted very well, but the telecoms mast rather less so.

The wind speed profile at the anemometer mast is captured very well, with the prediction lying close to the average, 'all times' measured profile. For this mast there is also less variation in the profiles throughout the day, and less scatter in the measured data. The two wind directions are both predicted equally well, which is encouraging as they represent rather different upwind terrain. The 57° case (Fig 7.18) has a long stretch of fairly open, flat terrain, then about 750m of ~8m tall tress (with the change being near the telecoms mast). The 237° case (Fig 7.19) has a very long forested fetch, but with much shorter ~2m trees for ~300m upwind of the mast. The model seems to have simulated the effect of these different roughnesses quite well.

The difficulties the CFX model had in predicting the profile at the telecoms mast might be due to several different factors. Both the predicted degree of wind shear, and the shape of the profile are not as close to the average profiles as for the anemometer mast. Partly, this could be might be an artefact of the averaging process, and the non-Gaussian data distribution. For the 57° case (Fig 7.16), the predicted profile does lie quite close to the area with highest density of data points, but the long 'tail' to the data skews the average to higher values. The overall shape of the profile for the 57° case is quite well predicted, but with a generally lower degree of wind shear. This may be due to an incorrect roughness specification for the unforested area up to the mast, which uses the standard roughness length model. Although this area was generally flat and open, there was significant surface disruption due to peat workings, and the effect of these on the overall roughness may not have been estimated correctly. The telecoms mast is also very close, about 100m, to a very large change in roughness, from flat peat bog, to tall trees. The exact physical location of this in the model, in relation to the output point (the telecoms mast location) could affect the profile obtained. The roughness change, and in this case, roughness model change, will be discretised to the nearest cell. The user-defined profile output function interpolates between cell centres to the desired location. This could mean that the distance between the roughness change in the model and the profile output point could vary considerably, as the physical distance is quite close to the grid resolution of 50m. For the 57° case, the forest starts just downstream of the mast, but such a large increase in roughness would be expected to cause a blockage effect that would be felt a few cells upstream. The relative position of the mast and forest is possibly even more crucial in the 237° case (Fig 7.17), were the mast is just downstream of the change. Here, the shape of the profile is not predicted as well, in addition to the absolute values of wind shear. The model predictions are still within the scatter of the measured data, but only just. Clearly the model is not doing well in these conditions.

It is the author's feeling that this is a grid resolution issue, near to such a large change in roughness. The change in roughness near the anemometer mast is much less severe. Estimates of the roughness lengths for the different areas (used in other work) would put the short trees at about 0.25m, the tall trees at 1m, and the open moor at 0.05m. The change from short to tall tress is a 4-fold increase, but the change from moor to

tall trees is a twenty fold increase. The resistance values assigned to the forest areas are thought to be about right, as the anemometer mast location is predicted so well. Also, the 57° anemometer mast case has wind blowing over the same area of trees as the 237° telecoms mast case (as the runs are in the same orientation as the masts). The fact that the anemometer mast is predicted well for this would imply the anomaly is at the telecoms mast end.

Time and computer resource constraints meant that runs at higher resolution could not be performed as part of this work. However, points less close to such a large change in roughness would suffer less from grid resolution problems. In its perceived end application, this model would be providing a general description of an area, rather than high-resolution results for specific locations. If such results were needed, a smaller-scale, higher resolution run could easily be done. Computing resources are further discussed in the Conclusions section.

A lack of time also prevented comparisons of the resistive model with a ground roughness model for the Derrybrien test case. One of the problems that would have to be addressed before such a case could be easily comparable is that of the large bottom cell size dictated by large ground roughnesses. This would mean the grid resolution might not be adequate for resolving the flow structure at the 10m anemometer locations.

7.4 Comparisons - WAsP

The stated aim of this work is to try to improve on the current industry standard - the WAsP package. As part of the validation work, a direct comparison with WAsP for the Derrybrien area was carried out.

A model was set up in WAsP to match the CFX model as closely as possible, while keeping to the standard set up. The topography was from the same basic data set, and the roughness information from the site survey. The roughness lengths were assigned to the different forest areas according to the guidance given in the WAsP User Guide.

The results of the WAsP prediction are plotted out below, along with the CFX predictions and measured data. For clarity, only the average measured profile for all time periods has been plotted.

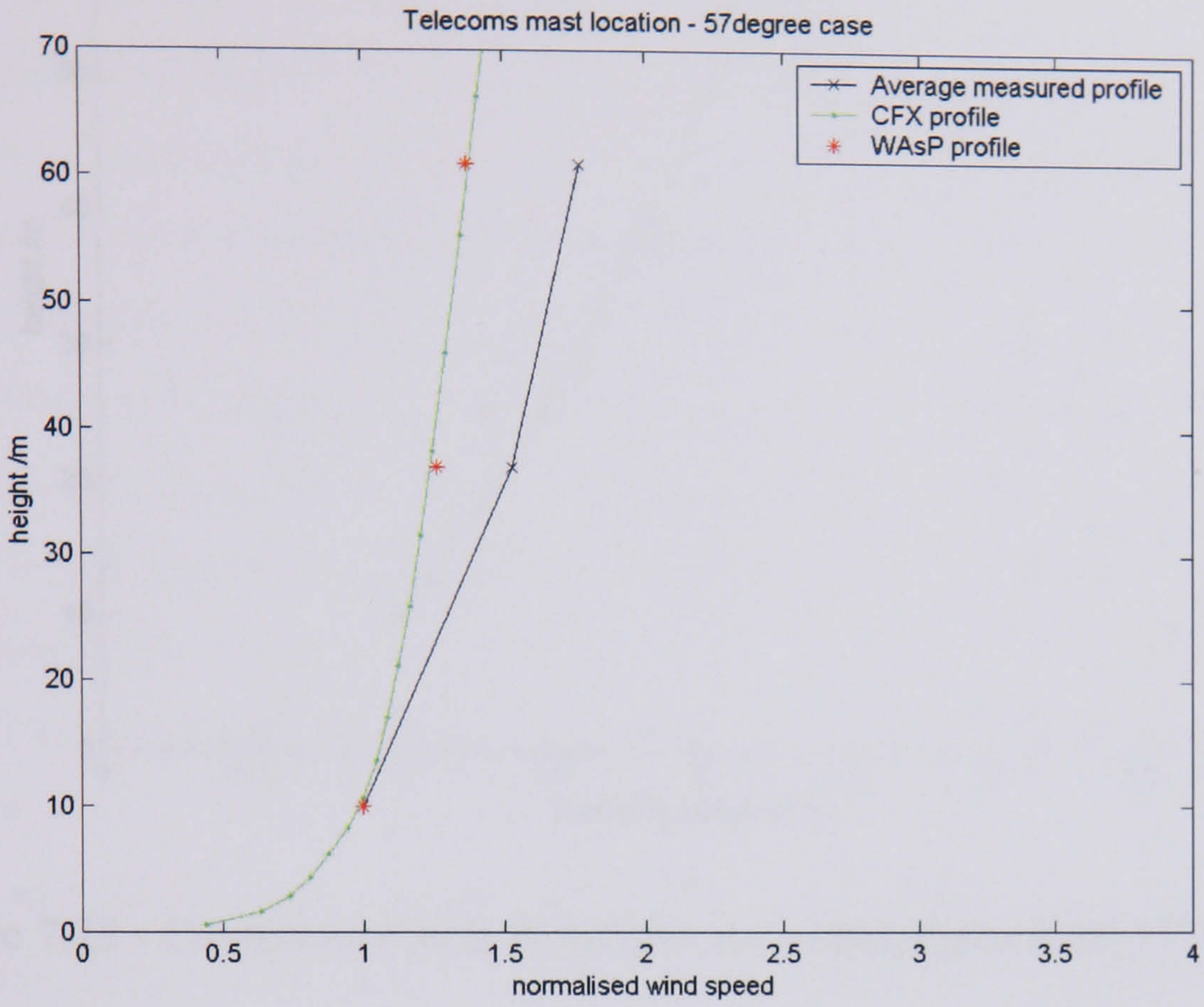

Figure 7.20 - Comparison with WAsP, for the telecoms mast 57° case.

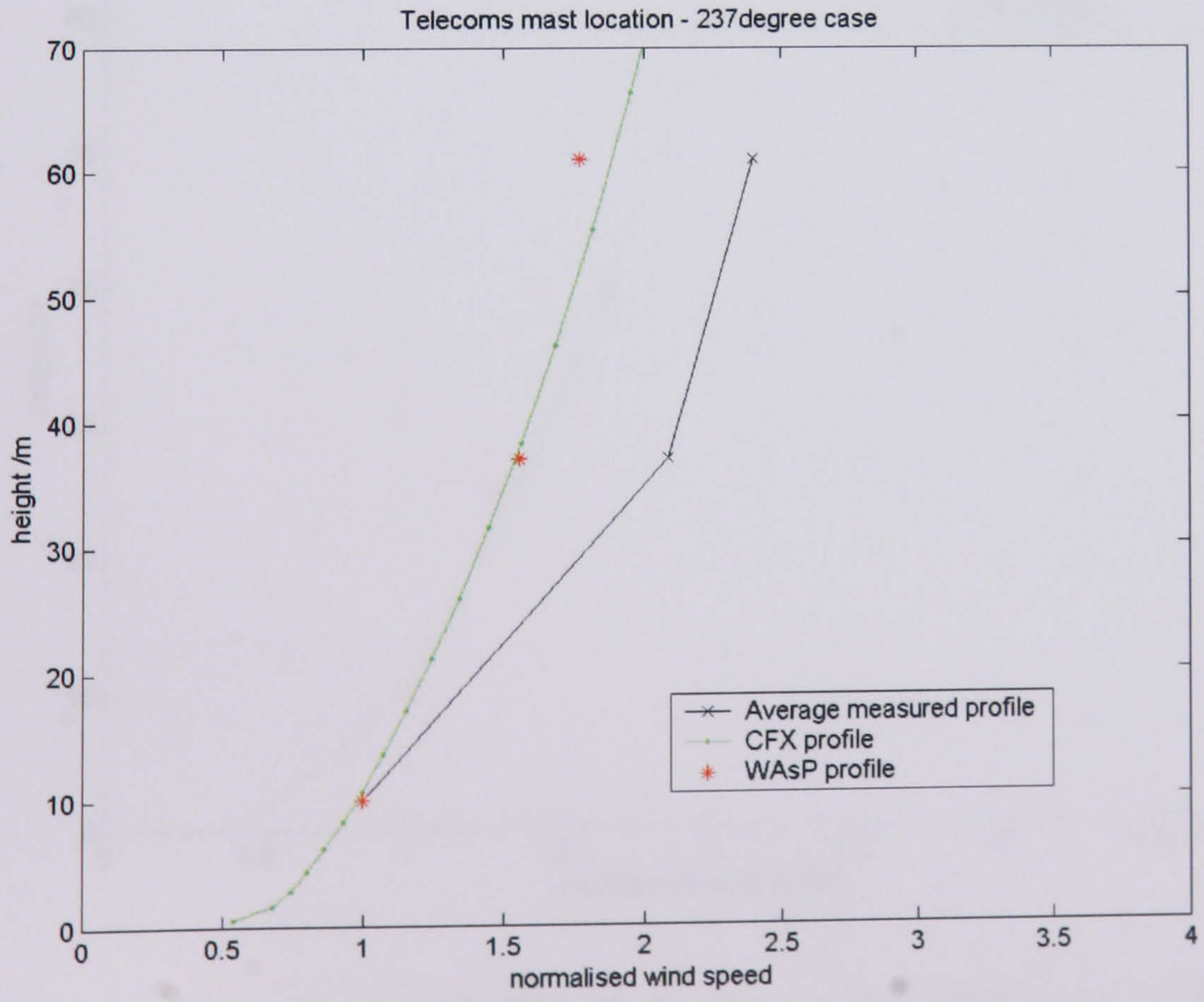

Figure 7.21 - Comparison with WAsP, for the telecoms mast 237° case.

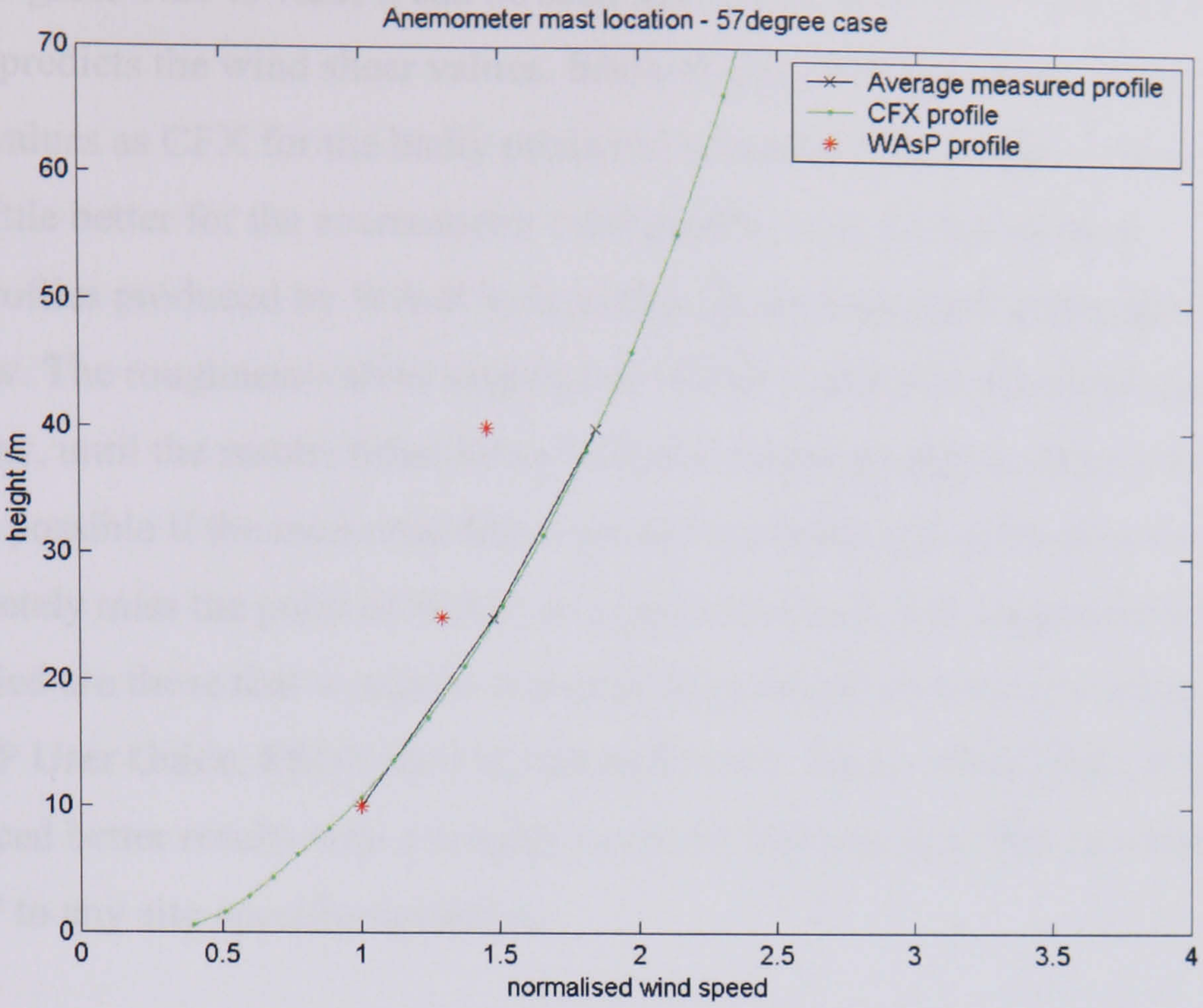

Figure 7.22 - Comparison with WAsP, for the anemometer mast 57° case.

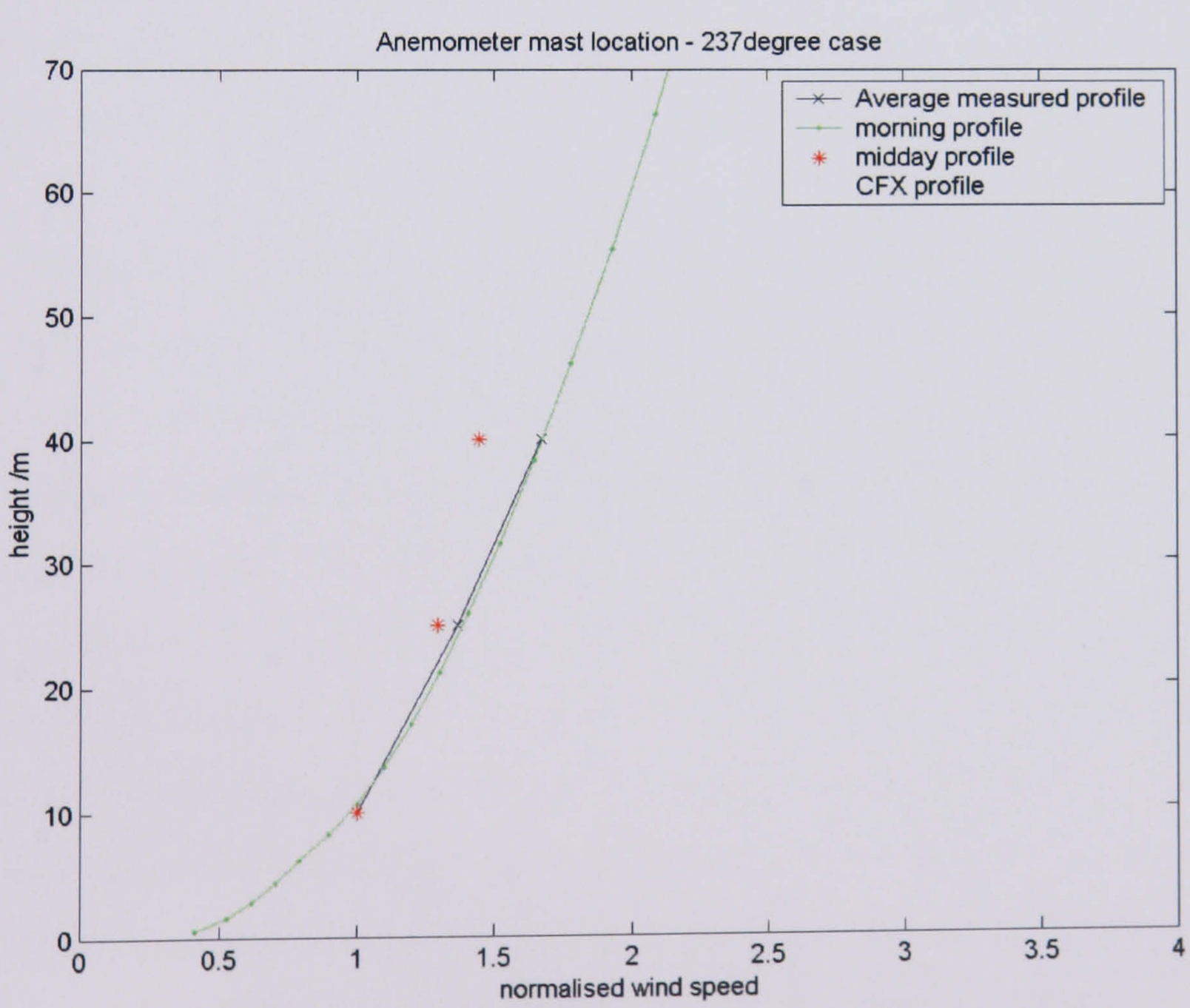

Figure 7.23 - Comparison with WAsP, for the anemometer mast 237° case.

From Figures 7.20 to 7.23, it can be seen that in this situation, WAsP consistently under-predicts the wind shear values. Interestingly, WAsP predicts almost exactly the same values as CFX for the badly predicted telecoms mast location. However, WAsP does little better for the anemometer mast profile, were CFX does well.

The profiles produced by WAsP look as though the roughness values specified were too low. The roughness values supplied to WAsP could indeed be increased in an ad-hoc way, until the results fitted better with the measured profile. However, this would not be possible if the measured data were not available before hand, and would completely miss the point of WAsP as a predictive tool. The roughness lengths specified are those that would be expected from standard tables of surface roughness (WAsP User Guide, ESDU item 82026 and 84011, Spera 1994). The CFX model has produced better results with a roughness model that was specified in advance, and not 'tuned' to any site-specific conditions.

In conclusion, the CFX model seems to perform adequately under most conditions. It is generally an improvement on WAsP, if certain limitations, like grid resolution, are taken into account.

8 Conclusions

In general, the model developed in this study is seen as a success. The aim of this project was to develop a CFD model of wind flow over terrain that could be used in a commercial environment, and that would provide an improvement in accuracy over the currently used models. The system that has been developed has been shown to have succeeded on both theses counts. The CFD model has been validated against one of the best-known test cases in atmospheric boundary layer flow studies, that of Askervein Hill. It has been demonstrated to provide a significant improvement in prediction accuracy over the industry standard WAsP code. The topography of Askervein Hill is not very extreme by the standards of many sites being considered for wind farms currently, and the sort of site where WAsP would routinely be called upon. That the new CFX model can provide an improvement in even this relatively mild case, is a strong argument in favour of its commercial use. The better performance of the new model over complex topography is due to its base in computational fluid dynamics, rather than a linearised model. As such, it has much greater flexibility, and more general applicability. A CFD model can in theory give a solution for arbitrarily complex terrain, limited only by the computational resources available, rather than any inherent limitation of the modelling strategy.

As an extension of the basic model of fluid flow over a surface, a model has been developed to improve the simulation of flow over forested regions. This model has been shown to give quite reasonable results, but needs further work to turn it into a fully reliable prediction tool. In its current state, the model has been shown to work in real world situations, and provide results that are at least comparable, if not slightly better, in accuracy to methods currently used. In more theoretical validation exercises, it was demonstrated to capture more of the structure of flow through canopies of vegetation than simple roughness length models. However, further exploration of the parameter space of the model is needed. This really requires more measured data on the detailed structure of flow through canopies than could be obtained in the course of this project. The model shows great promise, as even in its most basic initial form it displays general performance at least as good as the standard models. It also gives insight into areas within and close to the canopy that roughness length formulations

do not try to model. The detail of flow structure in and near canopies is reproduced in a qualitative sense, even if further testing of model parameters is required to quantify the relationship between real-world forest density and the resistance parameter used in the model. The analytical tree model developed to provide a predictive basis for the resistance parameter (rather than an empirical fit to measured data) gives a plausible and usable figure, but could be refined.

A further refinement to the resistive volume model would be to add a turbulence production term. At the moment, the CFD model makes no extra turbulence due to the forest, beyond what is generated by shear in the standard turbulence model. The resistive body force slows the flow down 'smoothly'. Clearly, a significant quantity of turbulence is generated in the canopy, and an extra source term could be added to the turbulence equations to allow for this. However, this would require considerable study of the nature of turbulence in plant canopies.

Two strong criticism of the use of CFD for this sort of work have been the high degree of user skill and time involved in setting up such a model, and the long run time of the model. The first point is addressed as one of the main areas of this project. A methodology for setting up CFD models of wind farm sites, as a commercial tool rather than an academic exercise needed to be developed. To this end, a custom pre-processor has been developed that makes setting up a CFD run as quick and simple as setting up a WAsP run. The user does not need to have specialist knowledge of CFD to operate the pre-processor, as the details are automatically taken care of in a standard methodology, implemented by the pre-processor. Should more complexity or control be required, the user can still access the fundamentals of the CFD run, but for most runs the process can be quite transparent.

However, running the solver still takes much longer than calculating a wind resource grid in WAsP. This task can be performed 'in the background' though, so the total man hours involved is not too dissimilar. The steady increase in available computing power makes arguments about prohibitive solution times less important than they were.

Concerns about the implementation of the wall laws in CFX4 have been highlighted. As the root of this problem is inside a piece of complex, commercial software, it is not easily rectified, and not in the scope of the current work. The anomaly caused is now known, however, and can be allowed for if necessary. In addition, the new resistive volume model of forests enables low surface roughness and small cell heights to be used in forested areas, thus reducing the impact of errors caused by inaccurate wall functions.

Overall, a coherent package for performing CFD simulations of wind flow over terrain has been developed, and shown to perform well. The overall system is usable in a commercial environment while still delivering higher quality results than current standard systems.

Future Work

- Further theoretical work still needs to be done on the range of values to use for the resistance parameter for different densities of canopy.
- Obtain high quality validation data from a variety of deep canopies, and compare with CFD results, to validate the resistance parameter.
- Investigate the neighbourhood of the smooth-to-resistive transition. What are the horizontal gridding sensitivities, and are there numerical problems associated with the sudden change?
- Resolve issues surrounding the spike in k values at the second cell. This needs to be undertaken in conjunction with CFX.

9 Bibliography

ANTONIA, R. A. and LUXTON, R. E. (1971), *The response of a turbulent boundary layer to a step change in surface roughness. Part 1. Smooth to rough.* J. Fluid Mech. **48 part 4**: 721-761.

APSLEY, D. D. and CASTRO, I. P. (1997), *Flow and dispersion over Hills: Comparison between numerical predictions and experimental data.* J. Wind Eng. Ind. Aerodyn. **67&68:** 375-386.

BELCHER, S.E., JERRAM, N., and HUNT, J.C.R. (2003) *Adjustment of a Turbulent boundary layer to a canopy of roughness elements*. Under consideration for publication in J. Fluid Mech.

BELJAARS, A.C.M., WALMSLEY, J. L., and TAYLOR, P. A. (1987), *A mixed spectral finite-difference model for neutrally stratified boundary-layer flow over roughness changes and topography.* Boundary-layer Meteorology, **38:** 273-303.

BRAMMER, J. (1997), *Modelling of wind speed distribution in complex terrain using Computational Fluid Dynamics.* MSc. Dissertation, CREST, Loughborough University.

CARPENTER, P. and LOCKE, N. (1999) *Investigation of wind speed over multiple two-dimensional hills.* J. Wind Eng. Ind. Aerodyn. **83:** 109-120.

CFX4 Flow Solver User Guide (1995-). AEA Technology, Harwell.

COOK, N.J. (1997) *The Deaves and Harris ABL model applied to heterogenous terrain*, J. Wind Eng. Ind. Aerodyn. **66:** 197-214

DEAVES, D.M. and HARRIS, R.I. (1978), *A mathematical model of the structure of strong winds*. Construction Industry Research and Information Association. London.

DURANTI, S., PEZZUTO, G., and PITTALUGA, F. (1998), *Numerical prediction of neutral atmospheric boundary layers (RUSHIL experiment).* J. Wind Eng. Ind. Aerodyn. **74-76:** 263-272.

DUYNKERKE, P. (1987), *Application of the E - ε turbulence closure model to the neutral and stable atmospheric boundary layer*, J. Atmos. Sci. **45**(5), 865-880.

ENGINEERING SCIENCES DATA UNIT. *Item 82026: Strong winds in the atmospheric boundary layer. Part 1: mean-hourly wind speed*. ESDU, 1982.

FINARDI, S., TINARELLI, G., FAGGIAN, P., and BRUSASCA, G. (1998), *Evaluation of different wind field modelling techniques for wind energy applications over complex topography*. J. Wind Eng. Ind. Aerodyn. **74-76:** 283-294.

GARRATT, J. R. (1992), *The Atmospheric Boundary Layer*. Cambridge University Press.

JACKSON, P. S., and HUNT, J. C. R. (1975), *Turbulent wind flow over a low hill.* Quart. J. R. Met. Soc. **101:** 929-955.

JACOBSON, M. Z. (1999), *Fundamentals of Atmospheric Modeling.* Cambridge University Press.

KAIMAL, J. C., and FINNIGAN, J. J. (1994), *Atmospheric Boundary Layer Flows: Their structure and measurement.* Oxford University Press.

LEA, A[1]. and VOSPER, S[2]. (2002). *Numerical simulations of turbulent boundary-layer flow over forested terrain.* Apparently unpublished article. 1. Institute for Atmospheric Science, School of the Environment, University of Leeds, UK. 2. Met Office, UK.

MARUYAMA, T. (1999). *Surface and inlet boundary conditions for the simulation of turbulent boundary layer over complex rough surfaces*. J. Wind Eng. Ind. Aerodyn. **81:** 311-322.

MASON, P. J., and SYKES, R. I. (1979), *Flow over an Isolated Hill of Moderate Slope*, Quart. J. Roy. Meterol. Soc. **105:** 383-395.

MAURIZI, J. M., PALMA, L. M., and CASTRO, F. A. (1998) *Numerical simulations of the atmospheric flow in a mountainous region of the North of Portugal.* J. Wind Eng. Ind. Aerodyn. **74-76:** 219-228.

MENGLKAMP, H. T. (1999), *Wind climate simulation over complex terrain and wind turbine energy output estimation.* Theor. Appl. Climatol. **63:** 129-139.

MOHAMMADI, B., PIRONNEAU, O., and VALENTIN, F. (1998). *Rough boundaries and wall laws.* Int. J. for Numerical Methods in Fluids, **27:** 169-177.

MONTAVON, C. (1998a), *Simulation of atmospheric flows over complex terrain for wind power potential assessment*, PhD thesis, Ecole Polytechnique Federale De Lausanne.

MONTAVON, C. (1998b), *Validation of a non-hydrostatic numerical model to simulate stratified winds over complex topography.* J. Wind Eng. Ind. Aerodyn. **74-76:** (1998) 273-282

MONTAVON, C. (1998c), *Askervein Hill site: a sensitivity study using the numerical model CFX4 testing the effect of the flow parameters on the resulting flow field.* Report No. 548.104, Departement de Génie Civil, Institut d'Hydraulique et d'Energie, Ecole Polytechnique Federale de Lausanne.

MORTENSEN, N. G., LANDBERG, L., TROEN, I., and PETERSEN, E. L. (1987-2003). *Wind Atlas Analysis and Application Program (WAsP). Vol. 2: User Guide.* Riso National Laboratory, Denmark.

NEFF, D. E., and MERONEY, R. N. (1998), *Wind-tunnel modelling of hill and vegetation influence on wind power availability.* J. Wind Eng. Ind. Aerodyn. **74-76:** 335-343.

PANOFSKY, H. A. and DUTTON, J. A. (1984), *Atmospheric Turbulence.* Wiley-Interscience, New York.

RAITHBY, G.D., et al. (1987), *The Askevein Hill project:A finite control volume prediction of the three-dimensional flows over the hill.* Boundary-Layer Meteorology **39:** 247-267.

REHM, R. G., MCGRATTAN, K. B., BAUM, H. R., and SIMIU, E. (2000), *Large eddy simulation of flow over a building complex.* 3rd International Symposium on Computational Wind Engineering, University of Birmingham, 4-7 Sept. 2000.

SALMON, J.R., et al. (1988), *The Askevein Hill project: Mean wind variations at fixed heights above ground.* Boundary-Layer Meteorology **43:** 247-271.

SCHLICHTING, H. (1979), *Boundary Layer Theory*, 7th Ed. McGraw-Hill, New York.

SPERA, D.A. (ed.) (1994), *Wind turbine technology: fundamental concepts of wind turbine engineering.* AMSE Press, New York.

TAYLOR, P.A. and TEUNISSEN, H.W. (1983), Askervein '82: Report of the September/October 1982 Experiment to Study Boundary-Layer Flow over Askervein, South Uist. *Research Report: MSRB-83-8,* Atmos. Environ. Service, Downsview, Ont., Canada.

TAYLOR, P.A. and TEUNISSEN, H.W. (1985), *The Askervein Hill Project: Report of the Sept./Oct. 1983, Main Field Experiment.* Research Report: MSRB-84-6, Atmos. Environ. Service, Downsview, Ont.. Canada.

TAYLOR, P.A. and TEUNISSEN, H.W. (1987), *The Askervein Hill project: Overview and background data*. Boundary-Layer Meteorology **39:** 15-39.

TAYLOR, P.A. (1998) *Turbulent boundary layer flow over low and moderate slope hills*. J. Wind Eng. Ind. Aerodyn. **74-76:** (1998) 25-47

TROEN, I. (1990), *A high resolution spectral model for flow in complex terrain*. 9th Symposium on Turbulence and Diffusion, Roskilde, Denmark, April 30 - May 3. 1990, 417-420.

UTNES, T. and EIDSVIK, K. J. (1996), *Turbulent flow over mountainous terrain modelled by the Reynolds equations*. Boundary-layer Meteorology, **79:** 393-416.

VERSTEEG, H. K. and MALALASEKERA, W. (1995), *An introduction to Computational Fluid Dynamics: The Finite Volume Method*. Longman Group.

WALMSLEY, J. L., TAYLOR, P. A. and KEITH, T. (1986), *A simple model of neutrally stratified boundary-layer flow over complex terrain with surface roughness modulations (MS3DJH/3R)*. Boundary-layer Meteorology, **36:** 157-186.

WIERINGA, J. (1993), *Representative roughness parameters for homogenous terrain*. Boundary-layer Meteorology, **63:** 323-363.

WRIGHT, N. G., and EASOM, G. J. (1999), *Comparison of several computational turbulence models with full-scale flow around a building*. J. of Wind and Structures. **2**(4): 305-323

WRIGHT, S. D., ELLIOT, L., INGHAM, D. B., and HEWSON, M. J. C. (1998). *The adaptation of the atmospheric boundary layer to a change in surface roughness*. Boundary-layer Meteorology **89:** 175-195.

YING, R. and CANUTO, V. M. (1997), *Numerical simulation of flow over two-dimensional hills using a second-order turbulence closure model.* Boundary-layer Meteorology, **85**: 447-474.